Modulation of Calcium signalling by F-actin during maturation and fertilization of starfish oocytes

Thesis

UNRESTRICTED

"Modulation of Calcium signalling by F-actin during maturation and fertilization of starfish oocytes"

Agostina Margarita Puppo Studer

Licenciatura en Ciencias Biologicas

Universidad de la República - Uruguay

Thesis submitted for

Degree of Doctor of Philosophy

Sponsoring establishment:

Stazione Zoologica "A. Dohrn"

Villa Comunale, I-80121

Napoli, Italy

September 2009

DATE OF SUBMISSION: 30 SEPT 2009

DATE OF AWARD: 1 FEB 2010

Director of studies: **Dr. Luigia Santella**

Department of Cellular and Developmental Biology

Stazione Zoologica Anton Dohrn

Napoli, Italy

External Supervisor: **Dr. John Parrington**

Department of Pharmacology

University of Oxford

Oxford, UK

Acknowledgments

I want to thank my director of studies Dr. Luigia Santella with her endless enthusiasm for science, for finding new questions, in discussing hypotheses, and all the people in the Lab, Dr. Jong Tai Chun, Gianni Gragnaniello and Dr. Ezio Garante for helping me and sharing all these years. I would also like to thank my supervisor Dr. John Parrington for his suggestions and support during my PhD studies.

To my big Family. And to my friends and to Vasco, many thanks for your support, for such a great experience of life and for making my stay in Napoli, happy.

INDEX

Abbreviations

1-MA: 1-Methyladenine

ABP: Actin-binding protein

cADPr: cyclic adenosine diphosphate ribose

CCD: Charge coupled devise

CG: Cortical Granules

Cyto B: Cytochalasin B

EGTA: ethylene glycol-bis(2-aminoethyl)-N,N,N',N'-tetraacetic acid

ER: Endoplasmic Reticulum

FE: Fertilization envelope

FC: Fertilization cone

Fc: Follicle cells

GV: Germinal vesicle

GVBD: Germinal vesicle breakdown

IB: Injection buffer

$InsP_3$: Inositol (1,4,5)-trisphosphate

$InsP_3R$: Inositol (1,4,5)-trisphosphate receptor

JAS: Jasplakinolide

Lat-A: Latrunculin-A

MPF: Maturation/M-phase promoting factor

NAADP: Nicotinic acid adenine dinucleotide phosphate

PH: Pleckstrin homology domain

PIP_2: Phosphoinositol (4,5)-bisphosphate

PLC: Phospholypase C

PtdIns: Phosphatydil-Inositol

PTX: Pertussis toxin

RFP: Red fluorescent protein

RFU: Relative Florescence units

RyR: Ryanodine receptor

VLE: Vitelline layer elevation

ABSTRACT

The Calcium ion (Ca^{2+}) is a universal intracellular messenger that is implicated in the regulation of a great variety of intracellular processes. Among them, there is the meiotic maturation of oocytes from several species and their fertilization.

The cell model system chosen for the work of this thesis has been the starfish oocytes. They constitute an exceptional model to study the properties of the dynamic release of Ca^{2+}. First, the cells are large and nearly transparent, making them suitable for imaging experiments after microinjection of fluorescent markers. Immature oocytes extracted from the gonad are arrested at the prophase stage of the first meiotic division. Overcoming the meiotic arrest (maturation), is induced by the application of the maturing hormone 1-Methyladenine (1-MA), whose action involves intracellular Ca^{2+} transients. During the maturation process, the oocytes develop their ability to be successfully activated by a fertilizing spermatozoon by liberating higher levels of calcium. 1-MA also induces dramatic actin cytoskeleton rearrangements.

In the present work, the relevance of the actin cytoskeleton in the modulation of the Ca^{2+}signals generated by hormonal stimulation and by the sperm has been studied. For this purpose, actin-specific disrupting agents and a specific antibody targeting the actin binding protein depactin have been delivered into living cells by needle microinjection, to study their effects using confocal laser fluorescent microscopy. Thus, the Ca^{2+} increases induced either by 1-MA, by the fertilizing sperm or by the injection of exogenous $InsP_3$, which is the canonical Ca^{2+} mobilizer second messenger, have been monitored with video fluorescent microscopy.

The results described indicate that actin filaments play direct and indirect roles in modulating the intracellular Ca^{2+} mobilization induced by the maturation process triggered by 1-MA as well as in the Ca^{2+} responses induced by the sperm.

CHAPTER I

INTRODUCTION

1- THE STARFISH OOCYTE.

Starfish oocyte as an animal model.

The cellular model chosen for this work has been the starfish oocyte. Starfish are marine animals and their body present radial symmetry. They have five rays emerging from a central disk, with an oral surface exposed to the substrate and containing the mouth, and an aboral one exposed to the sea water where the madreporite is present, the entry site of the water-vascular system. Starfish are monosexual animals, but present no sexual dimorphism. The gametes are liberated from the gonads of males and females at the same time from gonopores at the base of each arm (Ville et al, 1978).

The two species used in our study are the *Asterina pectinifera* and the *Astropecten aranciacus* (Fig I 1), both of which belong to the phylum *Echinodermata*, class *Stelleroide*, subclass *Asteoidea*. The former, captured in Mutsu Bay, Japan, has its breeding season from September to October. The latter species lives in the bay of Naples, Italy, and reproduces from February to May.

Hence, the two species with two different breeding seasons gave us the possibility to have an access to the oocytes during a substantial fraction of the year. Moreover, by comparing two different species we are able to draw more general conclusions from our observations.

The two species display different morphological traits and live in slightly different environments. Living in shallow waters of stony sediments, *A. pectinifera* is green or bluish with orange spots on its skin and averages 15 cm in diameter. On the other hand, *A. aranciacus* can reach 50 cm in diameter, and in its dorsal surface is brown- grey. Each arm contains spines, which help it bury itself in the sandy bottoms 2-20m deep in the sea.

Despite these differences, the oocytes of the different species share certain characteristics that are useful for studying the meiotic cycle and the fertilization events. To start with, each of the tubular gonads is replenished with oocytes that can be obtained for experiments by simple operations. To obtain them, a small part of the gonads must be extracted from the animal and put into sea water, then the oocytes drop from the cut ends of the gonads; in this way the availability of the needed biological material is high. Importantly, the gametes go through oogenesis during the stages of leptotene, zygotene and pachytene, becoming synchronously arrested at the first meiotic division and staying arrested until the time of ovulation. The overcome of the arrest is triggered by the release of the hormone 1-methyladenine (1-MA) by the follicle cells surrounding the oocyte at

Fig I 1: The Japanese species *Asterina pectinifera* (on the left) and the Neapolitan *Astropecten aranciacus* (on the right).

the time of spawning. The hormone 1-MA can be applied *in vitro*, allowing the control and study of the maturation and the fertilization events in a population of synchronous cells. Another important feature is the dimension of the oocytes of about 300 μm in diameter for *A. aranciacus* and of 180 μm for *A. pectinifera.* The large size of the cells facilitates the microinjection procedures, which are among the most utilized techniques in this work. The transparent nature of the cytoplasm of the oocytes of both species has facilitated the observation of morphological traits as well as the localization of injected fluorescent proteins.

Oocyte morphology.

Starfish contain two tubular gonads per arm, located in the interambulacral area. Fully grown immature starfish oocytes arrested at the prophase I of meiosis have a large nucleus termed 'germinal vesicle' (GV). The diameter of the GV in the *A. aranciacus* oocytes is about 70 μm, and 50 μm in the case of *A. pectinifera.* The GV lies close to the plasma membrane on one side, confering polarity to the cell. The area containing the GV is called the 'animal pole', and the other, the 'vegetal pole'. In the GV, chromatin is distributed in a very decondensed fashion, and a prominent nucleolus is present. Throughout the cytoplasm, the endoplasmic reticulum (ER) distributes evenly (Jaffe and Terasaki, 1994). The cytoplasm is filled with other intracellular organelles, lipid droplets, yolk granules and cortical granules. Yolk granules contain phosphoglycoproteins that serve as nutrient during embryogenesis, and are distributed preferentially in the center of the oocyte.

The cortex is an important compartment in the oocyte (Sardet *et al*, 2002). It is composed of the plasma membrane and the subplasmamembrane cytoskeleton. Actin filaments are tightly packed in the subplasmalemmal region except for the area where GV is apposed to the plasma membrane at the animal pole, that serves as a 'corridor' through which the polar bodies are extruded. Organelles such as the cortical granules (CG) are also

present in the cortex. Each CG is 1 μm long and contain sulphated acid mucopolisaccharides which are exocytosed at fertilization from the entire cortical region.

Another polarized feature of the echinoderm oocytes is the presence of an astral microtubule scaffold sandwiched between the GV and the plasma membrane. This premeiotic aster is probably responsible for maintaining the eccentric localization of the GV at the animal pole, and contains a reticulated form of keratin filaments resembling a hair net, thus called a snood (Schroeder and Otto, 1991), and located at 1 μm from the plasma membrane.

The cell surface is covered with microvilli, tipically unbranched and straight structures. Microvilli contain an inner core of organized bundles of filamentous actin (F-actin) crosslinked by the action of actin-binding proteins. Observations by SEM indicate they measure 0.1 μm in diameter and 0.35 μm in length (Schroeder and Stricker, 1983).

The vitelline layer, a structure of glycoproteins 0.25 μm thick, surrounds the oocyte. The outmost structure is the jelly coat, an almost transparent fibrous matrix containing molecules that induce sperm agglutination and the acrosome reaction. A single sheet of follicle cells immersed in the jelly coat makes contact with the oocyte surface. Since they are distant 2 to 15 μm from the oocyte surface (depending on the species), each follicle cell projects cytoplasmic extensions in the jelly coat that make contact with the oocyte surface through desmosome-like attachments. Thus, 1-MA would be transported intracellularly along the follicle cell processes, and excreted in the desmosome gap. 1-MA receptors are likely to be located on the oocyte-side of the desmosome (Schroeder, 1981).

Oocyte maturation.

When exposed to the maturation hormone, the immature oocytes can restart meiosis. The hormone provokes two successive M-phases of the cell cycle without an intervening S-phase, bringing the oocyte to the pronucleus stage. This process is called "maturation". Fertilizability of the egg cell is acquired during the maturation process. As mentioned above, immature oocytes fail to show physiologically normal responses to the interacting sperm.

The receptor for 1-MA hormone has not been isolated or cloned yet, but is believed to be present on the cell surface because the maturation process can be initiated by the external incubation of the oocytes with the hormone, but not by its injection. The fact that oocytes from which the vitelline envelope had been removed could still respond to the 1-MA enforced the idea that the receptor was placed on the oocyte plasma membrane (Shida and Shida, 1976). Experiments by Doree and Guerrier (1975) have shown that 1-MA can still elicit its biological activity even if its uptake into the cells is blocked by its inactive analogue 1,9-dimethyladenine. Furthermore, mild treatment of the oocyte plasma membrane with Triton X-100 to extract proteins at the plasma membrane significantly impeded the response to 1-MA (Morisawa and Kanatani, 1978).

The concentration of 1-MA necessary for obtaining mature eggs with 100% frequency is above 10^{-7} M, and this dose is independent of temperature. For maturation to occur, the oocytes also have to be exposed to the hormone longer than the minimal contact time. The so-called 'hormone dependent period (HDP)' depends on temperature. It is defined as the length of time oocytes need to remain in contact with 1-MA to induce maturation in 50% of the oocytes (Nemoto, 1982), and it increases as the incubation temperature is lowered.

The environmental stimuli deciding the breeding season period are not identified yet. However, it is known that in order to coordinate gamete spawning between males and females, the radial nerves of the starfish should release the peptide neurohormone GSS

(Gonad-Stimulating Substance) (Kanatani et al, 1967). The GSS stimulates follicle cells to synthesize 1-MA, which is the maturation inducer for many starfish species (Kanatani et al, 1970). Moreover, 1-MA acts on the gonads of both males and females, and may have many other target sites, like the central nervous system, which may eventually help to coordinate the synchronous release of mature gametes.

Meiosis re-initiation.

Several lines of evidence have suggested that the receptor for 1-MA may be coupled to heterotrimeric G proteins (Shilling et al., 1989). As is well known, the α and βγ subunits are active when bound to GTP. Upon activation, the alpha subunit dissociates from the other two subunits (Gβγ), each subunit being now able to act on specific targets. Microinjection of pertussis toxin (PTX) (Shilling et al, 1989) or $G_i\alpha$ into oocytes prevented 1MA–induced maturation, supporting the relationship between 1-MA receptor and this G protein. Anti-Gβ subunit antibodies, have shown that the G proteins are localized throughout the plasma membrane (Chiba et al, 2000).

Dithiothreitol (DTT) induces maturation of starfish oocytes, although the specific identity of the target of the reducing action is unknown. Interestingly, while PTX inhibits 1-MA-induced GVBD, it has no influence on the DTT-induced maturation (Chiba, 2000). It has been suggested that Gβγ may target phosphoinositide-3 kinase (PI3K) (Sadler and Ruderman, 1998), which phosphorylates inositides to generate lipid messengers.

The meiotic dynamics depends on the activation of an M-phase regulator. Since the cytoplasmic extracts of the oocytes that had been hormonally stimulated can stimulate the progression of the cell cycle in non-stimulated cells, a cytoplasmic factor present in the hormone-treated cells appeared to be sufficient for inducing maturation (Masui and Markert, 1971). The molecular composition of this Maturation-Promoting Factor (MPF) is known to be cyclin B and Cdc2 kinase. In immature oocytes, the complex is already present but in an inactive phosphorylated form, thanks to the action of a Wee1-protein

kinase family member (Myt1), which has been identyfied in *A. pectinifera* starfish oocytes (Okumura et al, 2002). In the presence of 1-MA, the protein kinase Akt (protein kinase B, PKB) becomes activated, in turn directly phosphorylating and downregulating Myt1, contributing to Cdc25 activation (Okumura et al, 2002). Then, under 1-MA stimulus, cyclin B/Cdc2 is activated by the Cdc25 phosphatase which dephosphorylates Thr14 and Tyr15, independently of protein synthesis (Kishimoto, 1998). MPF is first activated in the cytoplasm, but undergoes further activation in the GV, supported by Cdc25 phosphatase (Kishimoto, 1999). As *de novo* protein synthesis is not necessary for maturation, protein phosphorylation plays a decisive role in the process. Apparently, Cdc2 directly phosphorylates many proteins, although multiple kinases may regulate substrate proteins during meiotic maturation. Our Lab has found that cytoskeletal elements such as actin filaments are also substrates of MPF (Lim et al, 2003).

Oocyte changes during oocyte maturation.

The earliest known response to 1-MA is the release of intracellular free Ca^{2+}: it occurs within minutes. The nature of this response will be discussed later in this chapter, in relation to the morphological changes that take place during maturation. When exposed to 1-MA, starfish oocytes undergo cytoplasmic restructuring as well as topological changes in the surface. The first detectable morphological change is the retraction of microvilli at the plasma membrane, and the subsequent formation of broad leaf-like projections as soon as 1 minute after 1MA addition. The desmosome-like attachments connecting the follicle cells to the oocyte disappear. As a result, the follicle cells detach from the single layer and accumulate against each other forming a clump at one side of the oocyte. Approximately 10 min after 1-MA addition, the leaf-like projections are transiently replaced by numerous 5 to 15 μm spikes, corresponding the number of follicle cell processes to the number of spikes that appear (Schroeder, 1981). These spikes contain F-actin, as shown by fluorescent NBD-phallacidin (Schroeder and Stricker, 1983), and by the sensitivity to

Cytochalasin B (Cyto B), which specifically disrupts F-actin based structures. Their formation was hypothesized to occur by *de novo* actin polymerization (Otto and Schroeder, 1984).

By 20 min after the first contact with the hormone, the spikes withdraw, and flaccid and curved projections appear instead. At this point, microvilli are present in less density than before the challenge with 1-MA, but the distribution becomes polarized. Hence, these results indicate that in addition to the changes in the cell surface and topography, the actin cytoskeleton present at the cortex undergoes extensive reorganization as an early response to 1-MA.

Heil-Chapdelaine and Otto (1996) have shown by quantitative estimates of fluorescent phalloidin-staining in fixed cells, that there are two cortical populations of F-actin during early maturation: (1) the stable, nonspike F-actin and (2) the rapidly polymerizing/depolymerizing actin in spikes. However, it is still not clear by which mechanism 1-MA triggers the polymerization of the actin cytoskeleton and subsequent formation of spikes.

Following treatment with 1-MA, the oocyte becomes less rigid (Nakamura and Hiramoto, 1978; Nemoto et al, 1980). Cyto B causes a dramatic decrease in stiffness of starfish oocytes (Nemoto et al, 1980), the resulting stiffness being comparable to that of mature oocytes. Hence, it has been suggested that the organization of F-actin is responsible for the stiffness of the oocytes (Heil-Chapdelaine and Otto, 1996).

During meiotic maturation, cortical granules (CG) translocate towards the egg surface, apposing themselves to the plasma membrane. The long axes of CG are often perpendicular to the oocyte's plasma membrane (Longo et al., 1995; Santella et al., 1999) awaiting for the calcium signals that trigger their exocytosis during fertilization.

1-MA also triggers ER reorganization. From a network of cisternae in immature oocytes, the ER acquires the form of interconnected spherical shells surrounding yolk granules (Jaffe and Terasaki, 1994).

During maturation, the chromatin starts condensing and the nuclear envelope disappears. This event is referred to as 'Germinal Vesicle Break Down (GVBD)' and begins 20-35 min after 1-MA addition for the *A. pectinifera* starfish and at about 60 min in the *A. aranciacus*. The nucleoplasm remains separate from the cytoplasm for 15 min following GVBD, due to the presence of the intact nuclear lamina, which dissociates only later, enabling the intermixing of the nuclear and cytoplasmic contents. Two meiotic divisions then ensue, and two polar bodies are extruded to form the female pronucleus, without the second metaphase arrest that occurs in vertebrate oocytes. The timing and patterns of the GVBD are affected by cytoskeleton-disrupting drugs. When the oocytes are pretreated with microtubule-specific drugs, the timing of GVBD is not affected. However, Cyto B, which affects the microfilament cytoskeleton specifically, reduces the number of oocytes starting GVBD within a normal time frame. Moreover, the Cyto B treatment diminishes the pre-GVBD changes in nuclear shape, like the widening of the nucleus that leads to a decreased length-to-width ratio (Stricker and Schatten, 1991). In these cells, an incomplete intermixing of nucleoplasm with cytoplasm was observed at the physiological time of GVBD. Therefore, microfilaments are thought to be instrumental in oocyte maturation events.

2-CALCIUM HOMEOSTASIS.

Multicellular organisms need information to flow among their cells. Since many extracellular signalling molecules are not membrane-permeant, signal transduction to the interior of the cell is required (Guse and Lee, 2008). The Calcium ion (Ca^{2+}), in addition to being a structural element present in bones and teeth, is active in its free form inside cells and tissues, carrying and transducing signals. It is a messenger that mediates biological processes as diverse as fertilization at the start of new life, to muscle contraction, secretion, gene transcription and eventually apoptosis at the demise of the cell (Carafoli, 2002). To decode an external signal, such as that of hormones, neurotransmitters, growth factors and sperm, and to effectively transduce it into the cell, the concentration of intracellular free Ca^{2+} needs to change rapidly. The physiological Ca^{2+} concentration in the cytoplasm is about 100 nM, and can rise to 1-10 μM under stimulation within seconds. The cytoplasmic Ca^{2+} concentration $[Ca^{2+}]_i$ is efficiently regulated so that cells manage to cope with abrupt changes in its concentration by modulating the interplay between Ca^{2+} release and Ca^{2+} re uptake processes. $[Ca^{2+}]_i$ augments by Ca^{2+} release from intracellular stores and by Ca^{2+} influx from the extracellular media, while it diminishes by the action of intracellular and plasma membrane Ca^{2+} pumps as well as by sequestration to Ca^{2+}-binding proteins.

Three compounds are known to elicit Ca^{2+} release inside cells. They are called second messengers: namely, D-*myo*-inositol 1,4,5-trisphosphate ($InsP_3$), cyclic adenosine diphosphoribose (cADPr), and nicotinic acid adenine dinucleotide phosphate (NAADP).

Animal cells are equipped with ion channels gated either by the membrane potential, by ligands or by the emptying of the Ca^{2+} stores. Receptor-channels located in the endoplasmic reticulum (ER) and in the nuclear envelope are opened by $InsP_3$ or cADPr. The channel opened by the latter is sensitive to ryanodine and is thus called Ryanodine Receptor (RyR). $InsP_3$ also mediates the exit of Ca^{2+} from the Golgi vesicles (Pinton et al., 1998). The rise of cytosolic Ca^{2+} is restored to the basal level by the energy-spending

action of the Ca^{2+} pumps present in the plasma membrane, in the Golgi, in the nuclear envelope and in the ER. They import Ca^{2+} into the lumen of the organelles or export it to the extracellular space. The inner membrane of mitochondria possess Ca^{2+} exchangers, usually Na^{+}/Ca^{2+} exchangers (NCX), a variant of which is also found in the plasma membrane. While Ca^{2+} pumps have high Ca^{2+} affinity but limited transport velocity, NCXs have the opposite characteristics, giving the cell adequate flexibility to cover all the demands necessary for Ca^{2+} homeostasis (Carafoli, 2002).

Once $[Ca^{2+}]_i$ increases in the cytosol by any of the means above, a number of proteins complex with it. These proteins buffer Ca^{2+} but several of them also decode the information it carries and further transmit it to the targets. They do so by changing conformation after Ca^{2+}-binding and thus acquiring the capacity to interact with their selected targets. Some of the better described of these Ca^{2+} modulated proteins are the EF hand proteins, the C2 domain containing proteins, gelsolin, annexins and others.

$InsP_3$-mediated Ca^{2+} release.

$InsP_3$, a water-soluble phosphorylated sugar, was the first Ca^{2+} mobilizer discovered and is more extensively studied than other Ca^{2+}-linked second messengers. It was first discovered as a Ca^{2+} mobilizer in permeabilized pancreatic acinar cells (Streb et al., 1983), and then shown to be a universal second messenger, releasing Ca^{2+} in a vast number of cell types from fungi to plants to animals.

$InsP_3$ is formed by hydrolysis of its precursor phosphatydilinositol-4,5-biphosphate ($PI(4,5)P_2$), a phospholipid present at the plasma membrane. The first changes in the turnover of membrane phospholipids were detected in hormone-stimulated exocrine tissues.

PIP_2 is generated by a two-stage phosphorylation of PtdIns. In the major metabolic pathway, PtdIns is first phosphorylated at the 4-position of the inositol head group by a phosphoinositide 4- kinase (PI 4-K) to form phosphatidylinositol 4-phosphate (PI(4)P).

The following step is the phosphorylation on the 5-position of the ring by a phosphoinositide 5- kinase (PI 5-K) to generate PIP_2. The PIP_2 turnover is tightly regulated and the transformation of PI $\leftrightarrow$ PI(4)P $\leftrightarrow$ PIP_2 is reversible. This is made possible by the concerted action of the kinases aforementioned and by the action of phosphomonoesterases that dephosphorylate the compounds. In this way, the concentration of PIP_2 is maintained at a steady-state level (Berridge, 2005).

There are several isoforms of enzymes that generate $InsP_3$ from PIP_2. PLC β involves the activation of G proteins-coupled receptors that activate the phospholipase. In contrast, PLCγ is activated by receptor-linked tyrosine protein kinases. The second pathway works under stimulation by growth factors, and is also involved in PI3 kinase and ras/raf/MAPK cascade stimulation.

At least six subfamilies of PLC have been identified including the β, γ, δ, ε and, more recently, the ζ and η isozymes (Nakahara et al., 2005; Rhee, 2001; Saunders et al., 2002). These isoforms contain a combination of various regulatory domains that include the pleckstrin homology domain (PH domain), the Src homology 2 domain (SH2), and the C2 domain. The PH domain is responsible for PIP_2 and PIP_3 targeting, and can also interact with the βγ subunits of heterotrimeric G proteins (Camps et al., 1992). The SH2 domains interact with tyrosine kinases (Noh et al., 1995; Weiss, 1993). The active site of the enzyme is composed of the X and Y domains, which associate to form the PIP_2 cleavage site. PLC β, γ and δ have been identified in sea urchin eggs (De Nadai et al., 1998), and PLC β and γ have been identified in those of starfish. In starfish eggs, the Ca^{2+} release at fertilization occurs via a PLC γ-SH2 domain-mediated mechanism (Runft et al., 2004).

Once $InsP_3$ is generated, it diffuses from the plasma membrane to the cytosol (Berridge, 1995), where it specifically binds to receptor-channels located in the membrane of intracellular Ca^{2+} stores (the ER and the Golgi), eliciting Ca^{2+} release to the cytoplasm. The $InsP_3$ receptor ($InsP_3R$) is a transmembrane protein with the $InsP_3$-binding site next to the N-terminal end that projects into the cytoplasm. Four subunits are necessary to build a

Ca^{2+} channel, which is submitted to dual regulation, by $InsP_3$-binding and by Ca^{2+} (Berridge, 1995).

$InsP_3$ is then rapidly metabolised by enzymes that either add or remove a phosphate group in order to silence the $InsP_3$-dependent response. This property, as well as others, are necessary for the second messenger to function.

PLC generates $InsP_3$ but also diacylglycerol (DAG), which functions as an intracellular messenger as well. It activates protein kinase C to phosphorylate specific proteins (Takai et al., 1979). Thus, the major role of PIP_2 is to be a precursor to these two important second messengers. However, PIP_2 also plays additional roles: it is a substrate for phosphoinositide kinases that produce $PI(3,4,5)P_3$, and it directly interacts with many cellular proteins, including those that specifically bind and regulate the actin cytoskeleton (Hilpela et al., 2004). Indeed, it has been shown that a pool of PIP_2 co-sediments with actin cytoskeletal elements (Hinchliffe et al., 1996). Also, vesicles containing PIP_2 induce actin assembly in Xenopus extracts indicating that it can induce actin polymerization *in vivo* (Ma et al., 1998). Surprisingly, the levels of PIP_2 in the inner leaflet of the plasma membrane are very low. PIP_2 comprises only the 1% of the total phospholipid content present in the membrane, corresponding to an effective concentration of about 10 μM (Hilpela et al., 2004). Featuring its local regulation at the restricted regions of the plasma membrane, PIP_2 was also shown to accumulate in membrane lipid rafts, creating a specialized domain for interacting with actin binding proteins and for regulating microfilaments (Hilpela et al., 2004). Interestingly, the actin cytoskeleton located under the plasma membrane is a matrix that contains the enzymes involved in PI metabolism (Payrastre et al., 2001). Thus, a fine interaction between PIP_2 turnover and actin dynamics appears possible.

cADPr as a second messenger.

The Ca^{2+} releasing action of cyclic ADP-ribose (cADPr) was first discovered in sea urchin egg homogenates (Clapper et al., 1987). cADPr is a low molecular weight metabolite of the pyridine nucleotide nicotinamide adenine dinucleotide (β-NAD^+), generated by ADP-ribosyl cyclases (ARCs) (Lee, 1999). Three homologues of the enzyme have been identified to date; one is the mammalian homolog glycoprotein CD38, identified as a lymphocyte antigen (States et al., 1992). Despite being discovered as an antigen and distributing extracellularly, CD38 is involved in the transport of cADPr accross the membrane (Franco et al., 1998). However, CD38 is not exclusively expressed on the cell surface but it is also present in the inner membrane of the nuclear envelope possibly to synthesize cADPr (Gerasimenko et al., 1995). The ARC isoforms β and γ are also located intracellularly in sea urchin eggs (Davis et al., 2008). They were found to be present and active inside acidic and exocytic vesicles, to where the ARC substrate is provided by means of transporters and from where the product (cADPr) is liberated (Davis et al., 2008).

cADPr induces the release of Ca^{2+} from ryanodine-sensitive, $InsP_3$-insensitive, intracellular stores in sea urchin eggs and other cell types. Thus, it has been suggested that cADPr-induces Ca^{2+} release by a ryanodine-sensitive channel (Galione, 1994; Sitsapesan et al., 1995), as judged by its inhibition with the antagonists of ryanodine receptors (RyR) e.g. ryanodine, ruthenium red, and procaine. Different experiments have shown that Ca^{2+}-induced and caffeine-induced Ca^{2+} release are potentiated by cADPr, while ruthenium red and high Mg^{2+} concentrations inhibited it, adding weight to the suggestion that the receptor involved in the cADPr response is the RyR (Guse, 2000). RyRs have some similarity to $InsP_3Rs$ in a sense that these two transmembrane proteins have a quatrefoil arrangement of four identical subunits. Like $InsP_3Rs$, RyRs are present in the ER membrane. Both channels display Ca^{2+}-induced Ca^{2+} release (CICR), which has been used in models to explain the complex cellular Ca^{2+} responses –in the form of oscillations and waves.

cADPr is converted into ADP-ribose (ADPr) to silence its signal. In turn, ADPr has been suggested to modulate ion channels in eggs and smooth muscle cells.

NAADP: the new entry in the field of Ca^{2+}-linked second messengers

Nicotinic acid adenine dinucleotide phosphate (NAADP) is the most recently discovered Ca^{2+}-linked second messenger which is synthesized by the conversion of the amide nicotinamide group of the common metabolite NADP to a carboxyl group. In chemical terms, NAADP is actually the most potent of all Ca^{2+}-releasing second messengers. A Ca^{2+} response inside cells requires only 10 to 100 nM NAADP (Clapper et al., 1987). Interestingly, also the enzyme responsible for NAADP synthesis is also CD38. The enzyme may also catalyze its hydrolysis assuring the rapid metabolization of NAADP. NAADP has now been involved in Ca^{2+} release in a vast number of cells, from plants to mammals.

The Ca^{2+}-mobilizing capacity of NAADP, as that of cADPr was first demonstrated in sea urchin egg homogenates. This cell system has been widely used since it contains a very abundant ER fractions that can be isolated, making it easy to study the cell Ca^{2+} stores. However, it was soon discovered that NAADP had a broader site of action than the ER. Stratification of cell homogenates showed that the type of organelle sensitive to NAADP might be distinct from the ER. It was later suggested that this Ca^{2+} store consisted of acidic lysosome-like organelles (Churchill et al., 2002). NAADP released similar amounts of Ca^{2+} as $InsP_3$ and cADPr, but its action was not inhibited by the pharmacological antagonists of the other two messengers, e.g., heparin and 8-NH2-cADPr (Lee et al., 1995), implying that its action is mediated by distinct receptor Ca^{2+} channels. Most recently, it has been suggested that NAADP releases Ca^{2+} from a pool in the nuclear envelope that is sensitive to thapsigargin, through the activation of RyRs (Gerasimenko et al., 2003; Gerasimenko and Gerasimenko, 2004). However, the NAADP-dependent Ca^{2+} response was blocked by L-type Ca^{2+} channels antagonists like verapamil and nifedipine,

which have no inhibiting effect on the $InsP_3R$ and RyRs (Genazzani et al., 1997). The suggested NAADP-sensitive Ca^{2+} store would take up Ca^{2+} by means of a bafilomycin-sensitive V-H^+-ATPase that creates an acidic lumen, and by a Ca^{2+}/H^+-exchanger that uses the proton gradient (Churchill et al., 2002). Lysosomotrophic agents that disrupted lysosomes, such as glycylphenylalanine 2-naphthylamide (GPN) eliminated the Ca^{2+}-releasing capacity of NAADP as they lysed and depleted its stores (Churchill et al., 2002), as shown from the reduced fluorescence of the dye lysotracker that localizes to lysosomes. The NAADP-dependent Ca^{2+} response can be auto-inactivated by sub-threshold NAADP concentrations (Aarhus et al., 1996). When this occurs, even supra-threshold amounts of NAADP do not trigger a Ca^{2+} response. It was suggested that high affinity-binding sites in the 'NAADP receptor' mediated channel inactivation, and low affinity sites would enable channel opening (Galione and Ruas, 2005). Important additional informations concerning the molecular mechanism of NAADP action has come from work on starfish eggs. The addition of NAADP to a mature egg induces a Ca^{2+} response that is restricted to the cortical domain of the cell (cortical flash). This cortical flash was found to be dependent on external calcium, an observation that has led to the discovery of an inwardly directed Ca^{2+} current (channel) gated by NAADP (Moccia et al. 2003). It was also found that the influx of Ca^{2+} was promoted by thapsigargin, i.e., by the emptying of the ER Ca^{2+} stores. The observation suggests that the NAADP gated Ca^{2+} current could be mediated by a SOC type Ca^{2+} channel. The suggestion was reinforced by the inhibition of the inward current by the SOC inhibitor SKF96356 (Lim et al 2001; Moccia et al. 2003). Interestingly, the work on starfish oocytes did not provide a clear indication of the existence of acidic organelles as a target for NAADP (Moccia et al 2006). More recently, two-pore channels (TPCs) have been proposed as the candidates for the long sought-after NAADP receptors (Calcraft et al., 2009). These channels comprise a family of voltage-gated and NAADP-sensitive receptors expressed in lysosomal and endosomal membranes (Calcraft et al., 2009). Finally, NAADP has been proposed to be responsible for priming the initial Ca^{2+} signals,

which would be further amplified by cADPr and/or $InsP_3$-dependent mechanisms through a CICR process (Guse and Lee, 2008).

3- CALCIUM IN THE HORMONE-INDUCED RESUMPTION OF MEIOSIS.

The signal that starfish oocytes receive to resume meiotic maturation is the hormone 1-methyladenine (1-MA). The role of Ca^{2+} in starfish oocyte maturation has been controversial. Moreau *et al* (1978) showed that prophase-arrested oocytes from *Marthasterias glacialis* preinjected with the Ca^{2+}-sensitive photoprotein aqueorin emitted fluorescent light within 2 seconds after external application of 1-MA. This occurred even in the Ca^{2+}-free sea water, indicating that the released Ca^{2+} came from intracellular stores. However, trials on other species, e.g. *Asterias forbesi* and *Asterina miniata*, failed to detect increases of aequorin or fura-2 fluorescence following hormonal stimulation (Doree et al., 1990). The importance of Ca^{2+} in triggering meiosis reinitiation was nevertheless favoured when the Ca^{2+} chelator EGTA was used: microinjection of EGTA suppressed GVBD in *Marthasterias glaciaris* oocytes, while no consequence was observed if EGTA was injected after the Ca^{2+} spike (Moreau et al., 1978). It was soon demonstrated that calmodulin (CaM), the universal Ca^{2+} sensor protein, is necessary for meiosis, since its inhibitors blocked the hormone-induced maturation (Meijer and Guerrier, 1981).

1-MA hormone acts on receptors located on the plasma membrane. Thus, the Ca^{2+} response was reduced and delayed if 1-MA was injected into the oocyte, instead of added to the sea water bath. The specificity of the Ca^{2+} response by 1-MA has been further supported *in vitro* by the promotion of a Ca^{2+} burst in isolated oocyte cortices by the physiological mitogen (1-MA) as well as by its active analogs, and by ditiothreitol, which matures the oocytes in the absence of 1-MA (Doree et al., 1978).

A detailed study in *A. pectinifera* oocytes has shown that 1-MA actually induces three Ca^{2+} waves, two in the cytoplasm and one in the nucleus (Santella and Kyozuka, 1994). Interestingly, the nuclear Ca^{2+} increase was relevant to the resumption of meiosis since maturation was blocked by the specific buffering of nuclear Ca^{2+} (Santella and Kyozuka, 1994).

The respective roles of the Ca^{2+} mobilizers $InsP_3$, NAADP and cADPr have been studied in starfish oocytes. At first, $InsP_3$ was not considered essential for meiosis resumption since the preinjection of a peptide containing the $InsP_3R$-binding site, called the $InsP_3$-sponge, did not affect the 1-MA-induced Ca^{2+} response (Iwasaki et al., 2002). Also, the injection of $InsP_3$ directly in the cytoplasm did not release the oocytes from the meiotic block in the absence of 1-MA (Picard et al., 1985). On the other hand, the activation of heterotrimeric G proteins led to PLCβ stimulation and $InsP_3$ production in response to 1-MA (Berridge, 2005; Clapham, 1995). Interestingly, liberation of the pre-injected caged $InsP_3$ in the nucleus provoked GVBD in 50% of the treated oocytes without stimulation with 1-MA (Santella and Kyozuka, 1997). The same effect was observed when caged cADPr was injected into starfish GV (Santella and Kyozuka, 1997). After UV photolysis, cADPr generated repetitive spikes of Ca^{2+} that triggered meiosis reinitiation in the absence of 1-MA, most probably activating RyRs in the envelope of the nucleus.

The uncaging of injected cADPr into immature oocytes of the *A. aranciacus* generates a Ca^{2+} release in the cortex. Initially, spots of Ca^{2+} are observed in the subplamalemmal area and then unify to spread from there centripetally to the entire cytoplasm of the cell. The release occurs from intracellular stores, as shown by its independence of external Ca^{2+} (Nusco et al., 2002).

Experiments with the caged NAADP in the cytoplasm of prophase-arrested starfish oocytes have shown that *A. aranciacus* oocyte is sensitive to this messenger. A lower Ca^{2+} signal was also generated in Ca^{2+} free sea water containing 2 mM EGTA, indicating the independence of the NAADP-response on the external Ca^{2+} at this stage of maturation (Santella et al., 2000).

In the presence of inhibitors of the $InsP_3$ (heparin) and cADPr (8-NH2-cADPr) pathways, the release of Ca^{2+} by NAADP was inhibited by about 50% (Santella et al., 2000). This suggested that the action of NAADP could involve the recruitment of $InsP_3$ and cADPr. It also indicated that the pathways triggered by the three messengers may be correlated.

Adaptation of the Ca^{2+}-releasing mechanisms during oocyte maturation.

The physiological significance of the maturation process is to prepare the oocyte for fertilization and for the ensuing developmental changes. One of the first responses generated by the sperm is the increase in intracellular Ca^{2+} in the egg. The characteristics of the Ca^{2+} response induced by the sperm are different when immature oocytes are fertilized (Chiba et al., 1990). This is due to the fact that the mechanism of intracellular Ca^{2+} release is remodeled and sensitized to the second messengers during maturation. The augmented Ca^{2+} release was first documented during the maturation of starfish oocytes (Chiba et al., 1990). $InsP_3$ has long been claimed to have a role in the generation of Ca^{2+} signals at fertilization in many species. In starfish, the amount of Ca^{2+}-released by a given amount of injected $InsP_3$ in immature oocytes has been found to be much lower than that generated in mature eggs. In mammalian oocytes this is in part due to the increased expression and redistribution of cortical $InsP_3R$ (Fujiwara et al., 1993), but no *de novo* protein synthesis in starfish oocyte has been detected during maturation. The higher Ca^{2+} response observed in starfish eggs is thus not due to the increased expression and redistribution of the $InsP_3$ receptors, (Iwasaki et al., 2002), nor due to the increased amount of Ca^{2+} storage in the ER (Chiba et al., 1990; Lim et al., 2003). In other species, however, the differential expression of several distinct $InsP_3R$ isoforms during maturation could explain the changes in the Ca^{2+} response at different stages of oocyte development (Parrington et al., 1998). In starfish, as well as in many other species, the changes in $InsP_3$ sensibility during maturation is paralleled with morphological changes of the Ca^{2+} stores. Confocal microscopy of immature oocytes has shown that the ER distributes homogeneously throughout the cytoplasm in the form of interconnected membrane sheets. After 1-MA treatment, however, the ER redistributes, vesiculates and forms shells around the yolk platelets (Jaffe and Terasaki, 1994). In other species including mammals, ER clusters with accumulated $InsP_3R$ are detected after hormonal stimulation (Kline et al., 1999). Since there is no cluster formation in starfish oocytes, it has been suggested that in

this species this could be a mechanism to prevent the generation of multiple spikes during fertilization (Kline, 2000). The redistribution of the ER has been shown to depend on the interaction with microtubules and its associated molecular motors (Whitaker, 2006), and with microfilaments (FitzHarris et al., 2007).

Moreover, a relationship between the activity of the maturation-promoting factor (MPF) and ER restructuring has been shown. MPF activity levels normally decline after fertilization, and it has been observed that when MPF is maintained elevated after fertilization in mammals by proteasome inhibitors or by excess cyclin B, the ER clusters persist, whereas the treatment of unfertilized eggs with the cdk inhibitor roscovitine, eliminates them (FitzHarris et al., 2003). It has been found that MPF associates with microtubules through microtubule–associated molecules (MAPs) (Ookata et al., 1993), and that MPF phosphorylation of the actin cytoskeleton is responsible for the ER redistribution (Lim et al., 2003).

The photoactivation of caged cADPr in mature oocytes provokes a Ca^{2+} signal that is larger than in immature oocytes, suggesting that the cADPr-dependent Ca^{2+} release mechanism is also sensitized during maturation. After UV release of cADPr, fewer Ca^{2+} patches form in the cortex than in immature cells, but then a clear cortical flash or ring of Ca^{2+} is formed at the cortical area, and the amount of total Ca^{2+} released is much higher (Nusco et al., 2006).

In the case of the NAADP, the Ca^{2+} response also evolves along with the maturation process. In mature oocytes, NAADP releases higher levels of Ca^{2+} than in immature cells, and it has been observed that the Ca^{2+} levels remain elevated and do not decay to the baseline at the re-uptake phase. In strong contrast with immature oocytes, the NAADP-induced Ca^{2+}-response in postmeiotic eggs is linked to external Ca^{2+}. Immature oocytes respond to NAADP even in the absence of external Ca^{2+}, while mature eggs do not. Moreover, the NAADP response in mature cells is more sensitive to L-type inhibitors than in immature cells.

4- CALCIUM AT FERTILIZATION.

Fertilization occurs as the result of the union of the female and male gametes, the egg and the sperm. In nature, starfish fertilization occurs at the end of Meoisis I, but mature eggs with a female pronucleous are still fertilizable.

When the sperm and egg encounter each other, there is an increase of intracellular free Ca^{2+} in the egg, relevant for inducing the re-start of metabolic activity and cellular divisions leading to embryonic development. These Ca^{2+} ions enter the egg cytoplasm from the extracellular media across plasma membrane channels and are also released through channels present in internal organelles that serve as Ca^{2+} reservoirs. The plasma membrane channels are thought to be activated by voltage changes produced in the plasma membrane by the fertilizing sperm, but the second messenger NAADP is involved as well. The second messengers cADPr and $InsP_3$ are fundamental for Ca^{2+} release from internal stores. The direct injection or photoliberation of their caged forms in the cells provoke cytosolic Ca^{2+} increase, although the specific action of each one on the Ca^{2+} stores is not clear. Further, they seem to be partially redundant or to have overlapping actions in the generation of the sperm-induced Ca^{2+} wave since specific antagonists of each of the Ca^{2+} mobilizers do not completely block the Ca^{2+} response. Then, it is clear that the mechanism regulating Ca^{2+} liberation is neither simple nor fully understood. Indeed, it is possible that some regulators of the pathway are still to be identified.

The importance of understanding how these second messengers are generated and the nature of the pathways leading to a coordinated action in order to generate the Ca^{2+} wave after sperm arrival, has prompted the execution of many experiments and ways of interpreting the mechanism. Three models have been proposed. One of these involves the direct entry of Ca^{2+} through the sperm and along a pore formed between the acrosomal process and the egg plasma membrane directly into the egg cytoplasm. Then, Ca^{2+} would continue to be liberated due to a Ca^{2+}-induced-Ca^{2+} release mechanism (CICR) (Jaffe,

1991). However, the direct injection of Ca^{2+} into the egg does not generate a Ca^{2+} wave, probably due to the high buffering capacity of the cytoplasm (Swann and Whitaker, 1986). Another theory proposes that the sperm activates an egg membrane receptor. Such a receptor would be associated with G-proteins that could activate PLCβ, since overexpression of G-protein linked receptors induce a Ca^{2+} wave similar to that observed at fertilization when triggered by ligand. Moreover, the non-hydrolysable GTP analog GTPγS causes Ca^{2+} increase and cortical granule exocytosis in echinoderms (Jaffe et al., 1988), and the non-hydrolysable GDP analog GDPβS inhibits the Ca^{2+} wave in rabbit (Fissore and Robl, 1994). The apparent contradiction when it was found that the pertussis and cholera toxin did not inhibit the Ca^{2+} response, was explained with the finding that in sea urchins the Gαq and Gαs subunits play a role in Ca^{2+} pathways, as well as being insensitive to the mentioned toxins (Voronina and Wessel, 2004).

In an alternative version of this hypothesis, the receptor sensing the arrival of the sperm might be linked to tyrosine kinases targeting PLCγ.

The PLCγ enzyme contains two SH2 domains that associate with the tyrosine kinases of the Src-family for activation. The injection of recombinant SH2 domains compete for this interaction thus affecting the Ca^{2+} signalling, and giving weight to the relevance of this pathway (Carroll et al., 1997; Giusti et al., 1999).

Finally, there is the sperm factor hypothesis that seems to have most validity for mammals (Parrington et al., 2007). A sperm-specific PLC isoform, PLCξ, is injected into the egg by the sperm, triggering Ca^{2+} release.

As we can see, most of the models indicate PLC activation and thus $InsP_3$ formation as responsible for the initiation of the Ca^{2+} release. The second messenger cADPr has been shown to increase the CICR sensibility in sea urchin (Galione et al., 1993), then it could contribute to the propagation of the Ca^{2+} wave once it has been initiated.

Starfish fertilization.

In starfish, the sperm triggers a localized increase of Ca^{2+} usually at the site where it binds to the egg and subsequently, a cortical release that takes the form of a ring is observed. Such a ring is called the "cortical flash". It is formed because the plasma membrane of the egg suffers a depolarization induced by the sperm (the fertilization potential) that changes the membrane potential to the level of activation of voltage-gated Ca^{2+} channels. This membrane potential change and the induced Ca^{2+} response have the important function of inhibiting polyspermic interactions, which would lead to abortive developmental programmes. After the cortical flash is formed, Ca^{2+} starts being released in the interior of the cell, being liberated as a wave front from the site of sperm interaction towards the antipode of the cell. In starfish eggs, one Ca^{2+} wave is generated in response to the sperm (contrary to the case of mammals for example, where oscillating levels of Ca^{2+} are detected for hours after the sperm arrival).

As already briefly mentioned, NAADP is thought to play an important role in generating the cortical flash in starfish oocytes. The uncaging of NAADP in mature eggs generates a Ca^{2+} release localized in the cortex that resembles very closely the cortical flash. Such response depends on the presence of extracellular Ca^{2+} and is inhibited by blockers of the L-type channels (Santella et al., 2004). Moreover, the photoliberation of preinjected NAADP in the presence of heparin and 8-NH2-cADPr (which block the $InsP_3$ and cADPr pathways respectively), do not block completely the Ca^{2+} release. Few cortical spots of Ca^{2+} are detected under such conditions, but they cannot propagate (Santella et al., 1999).

Then, the effects of NAADP are mostly observed in the subplasmalemmal region, where the cortical ring of F-actin is present. Indeed, the application of drugs that alter the actin cytoskeleton like Lat-A and JAS alter the NAADP-dependent Ca^{2+} response, diminishing it (Moccia et al., 2003).

The blockage of RyRs alone does not abolish Ca^{2+} release during starfish fertilization either; besides, the *A. pectinifera* species is not sensible to cADPr (Nusco et al., 2002), showing that this messenger may not be essential for Ca^{2+} release initiation in starfish. However, it has been proposed to contribute to the Ca^{2+} propagation along the cell enhancing the CICR mechanism.

The relevant role of $InsP_3$ has been largely proven, and several experiments carried out with heparin, monoclonal antibodies against $InsP_3Rs$ and inhibitors of PLC have been shown to strongly impair the ferilization-induced Ca^{2+} wave (Giusti et al., 2000; Iwasaki et al., 2002; McDougall et al., 2000).

In summary, it has been proposed that NAADP triggers the initial Ca^{2+} response in the egg at fertilization (Lim et al., 2001). Then, such Ca^{2+} increase would stimulate activation of PLCγ (Runft et al., 2004) and generate $InsP_3$, responsible for the Ca^{2+} wave front propagation along the egg's cytoplasm (Santella et al., 2008).

The cytoplasmic Ca^{2+} increase triggers the exocytosis of cortical granules. Such granules are relocalized during the maturation of the oocyte, migrating underneath the plasma membrane and with their long axes perpendicular to the surface thanks to rearrangements suffered by the actin cytoskeleton (Santella et al., 1999). The content of the cortical granules are distributed as an electron-dense material immersed in a granular material of lesser electron opacity (Longo, 1982) which have been described as containing calcium, serine proteases and mucopolysaccharides (Schuel, 1978). The release of the cortical granules content to the space between the plasma membrane and the vitelline layer provoke the entry of sea water and the swelling of such space, most probably due to the released mucopolysaccharides, that promote hydration of the lumen. The elevation of the vitelline layer due to cortical granule exocytosis represents the second block to polyspermy that eggs count on.

5- ACTIN CYTOSKELETON.

Actin is a 42 kDa protein that is highly conserved and abundant in all eukaryotic cells. Monomeric or globular actin (G-actin) has the ability to polymerize forming filaments (F-actin). Along with the microtubules and the intermediate filaments, actin filaments constitute the cytoskeleton. The actin cytoskeleton is a highly dynamic structure which plays roles in multiple cell functions: mechanical support, cell motility, intracellular transport, secretion, phagocytosis, and cytokinesis to name a few. Actin is present in the nuclear compartment as well, involved in gene expression and transcription regulation (Gieni et al., 2009).

Actin monomers bind to the divalent ions Ca^{2+} or Mg^{2+}, and incorporate either ADP or ATP. Actin monomers loaded with ATP undergoes hydrolysis after being incorporated into the actin filaments. Thus, F-actin is referred to as an ATPase. The rate of addition of the ATP-loaded monomers can be faster than the hydrolysis process, leaving an enriched ATP-loaded end in the fiber. At the opposite end of the fiber, ATP is more readily hydrolyzed giving rise to ADP-bound subunits, changing the conformation of the filament. Due to such conformational changes, ATP-G-actin preferentially binds to the ATP-rich end, instead of the ADP-rich end. The resultant F-actin filaments are polarized in a sense that the two ends show different dynamics of assembly and disassembly. The barbed (or plus) end is the one preferentially incorporating G-actin-ATP bound monomers, whilst the pointed (or minus) end undergoes a net loss of ADP-bound monomers. Chemically speaking, the critical concentration (equal to the the minimal G-actin concentration required for assembly) is nearly 20-fold lower at the plus than that at the minus end. This phenomenon and the hydrolysis of the ATP bound to the G-actin, rendering the filaments unstable, is the basis of the dynamic nature of the actin cytoskeleton. This dynamic regeneration process is called treadmilling. However, it is evident that treadmilling is not the only phenomenon regulating actin dynamics in living cells. The localization, as well as

the structures and networks formed by F-actin, needs to change rapidly in response to stimuli. Inside cells, G-actin is a few orders of magnitude more concentrated than the critical concentration. Hence, almost all the cellular actin pool would be incorporated into almost stable filaments if treadmilling was the only force at action, but this does not happen in cells. Moreover, the F-actin turnover rates *in vitro* are lower than those observed *in vivo*. These differences in actin remodelling are attributed to the action of actin-binding proteins (ABP). An array of ABPs bind to both G- and F-actin, regulating this two actin pools and the kinetics of actin polymerization. They carry the specific functions of monomeric actin binding, nucleation and formation of new filaments, the crosslinking of existing filaments, and the severing and the capping of actin fibers, among others. The role of the ADF/cofilin family of ABPs and its homologous protein in starfish, depactin, will be discussed more in detail, as it has been used in the present study.

Regulation of the actin cytoskeleton by ADF/Cofilin and Depactin.

The ADF (Actin Depolymerization Factor) family of ABPs are present in both plant and animal cells. The first protein found in this family was destrin, which was expressed in chick embryo brain. Cofilin is highly homologous to destrin, and was also reported to sever actin filaments (McGough et al., 1997). Depactin is the respective protein found in starfish oocytes, also carrying the role of cutting F-actin (Mabuchi, 1983). These family of proteins bind both G- and F-actin. The severing activity is a result of the binding between two actin subunits in F-actin. The cofilin binding is cooperative, and preferentially targets ADP-bound monomers instead of the ATP or ADP plus inorganic phosphate (Pi) (Ono, 2007). Under physiological conditions, F-actin presents a helical conformation. The cooperative cofilin binding induce changes in the helical turn of the actin fiber, causing its disruption. In addition to the severing activity, ADF/cofilins bind to the ADP-G-actin, inhibiting nucleotide exchange (Ono, 2007). Since the ATP-loaded monomers are more prone to polymerization, cofilin also affects actin polymerization at this level.

The ADF proteins are regulated by phosphorilation, pH conditions and by binding to PIP_2. The phosphorylation of cofilin is carried by LIM kinases, downstream effectors of the Rho family of small GTPases-activated signalling pathway. When phosphorylated in position Ser-3, cofilin is inactivated probably due to the electric change that repulses actin binding. The dephosphorylation and subsequent activation is mediated by conventional phosphatases PP1 and PP2A (Ambach et al., 2000), as well as Slingshot (Niwa et al., 2002). The ADF activities are then enhanced by basic conditions of pH, although depactin, the starfish cofilin, does not exhibit pH sensitivity (Mabuchi, 1983). Then, actin-binding is regulated by competition with all the other actin-binding proteins that are not described here.

PIP_2 modulates actin dynamics.

The actin cytoskeleton is also regulated by phospholipids. PIP_2 is present in the cell membranes, preferentially at the plasma membrane. It is synthesized mainly by PI4P-5 kinase and serves as a substrate for PLC and PI3K. Hydrolysis by PLC is highly relevant for Ca^{2+} signaling, since it forms DAG and the Ca^{2+} mobilizer $InsP_3$. On the other hand, PI3K converts PIP_2 into PI(3,4,5)P3 which further regulates the actin cytoskeleton dynamics. Many of the proteins capable of binding to PIP_2 contain distinct domains that bind the lipid, like the PH domain, ENTH and ANTH domains. The PH domains have been shown to be present in many cytoskeletal proteins such as Wiskott-Aldrich syndrome (WAS) family and ezrin-radixin-moesin (ERM) family (Sechi and Wehland, 2000). Others, are thought to bind the lipid by ionic interaction, between the clustered basic amino acid residues and the negatively charged head froup of PIP_2 at the inner leaflet of the membrane bilayer (Downes et al., 2005), as is the case for cofilin and profilin proteins among others. In summary, the possibility of PIP_2 binding to a plethora of actin-binding proteins enable it to regulate the actin cytoskeleton dynamics (Di Paolo and De Camilli, 2006).

Microvilli

Microvilli are finger-like extensions in the surface of the cells. The core of such structures is formed by a tightly and unidirectionally polarized array of F-actin, with the plus end of the filaments facing the plasma membrane. The actin filaments of microvilli from the intestinal epithelium in mammals are crosslinked by the actin binding proteins villin and fimbrin. Then, myosin I proteins associated with calmodulin are responsible for the binding of the actin filament to the plasma membrane. Microvilli maintain the same diameter along the entire strucuture, and finish in rounded and blunt ends. Although considered to be a conserved type of F-actin organization in many cellular types, they present differences. The microvilli constituting the brush border of the intestinal epithelium in mammals present homogeneous height and length. In the case of microvilli formed in the surface of fertilized sea urchin eggs, their height is not homogeneous, but they are usually longer than the ones from mammalian epithelial cells, and with fewer actin filaments as part of the internal core (Burgess and Schroeder, 1977).

CHAPTER II

MATERIALS AND METHODS

Preparation of oocytes.

A. aranciacus is captured in the Gulf of Naples during the breeding season in the months of February to May. *A. pectinifera* is collected in Mutzu Bay, Japan, during the month of September and then shipped to the Stazione Zoologica of Naples. In the Stazione Zoologica, they are kept in running sea water at 16°C.

The female gonads were dissected out by making a cut in one of the arms close to the central disc. The gonads are then put either in 'Neapolitan artificial seawater' (NASW, 490mM NaCl, 8mM KCl, 10mM CaCl2, 12mM MgCl2, 2.5mM, NaHCO3, pH 8.0 titrated with NaOH) or in filtered natural seawater (FSW). Immature oocytes (containing the germinal vesicle) were collected as they were released from the cut ends of the gonads, and kept in NASW or FSW at 16°C. Those oocytes that had spontaneously matured were discarded.

In order to obtain mature eggs, 1-methyladenine (1-MA, Sigma Chemical Co., St. Louis, MO) was added in a final concentration of 10 μM to immature oocytes. For *A. pectinifera* oocytes the incubation time with the hormone necessary for maturation was 30 min, while for *A. aranciacus* it was 70 min, both at 16°C.

The procedure employed to obtain male gametes was the same as explained for the female ones. They are not placed into sea water though, but kept 'dry', and stored at 4°C for the day. For fertilization experiments, 10 μl of the 'dry sperm' were put into 1 ml sea water. Then, 3-5 μl of such diluted sperm were added to the experiment-chambers containing eggs bathed in 2 ml of sea water.

Microinjection.

Delivery of dyes, drugs and proteins into the cells was performed using the microinjection technique. Substances were injected by air pressure (regulated by the Transjector 5246, Eppendorf) through borosilicate glass capillaries (O.D: 1.0 mm, I.D. 0.58 mm, Sutter Instrument, Novato, CA) prepared with the PN-30 puller (Narishige, Japan).

The volume of the injected material is estimated to be 1% of the egg's volume, and the final concentration of substance in the cytosol is 50 to 100 times lower than the concentration charged in the pipette.

F-actin staining in living cells.

Microinjection of Alexa Fluor 488- or 568-conjugated phalloidin (Invitrogen, Eugene, Oregon, USA), diluted to 50 μM in methanol was performed. After 10 min incubation, the living oocytes or eggs were mounted on an experiment-chamber bathed in seawater and analized by laser-scanning confocal microscopy.

F-actin observation in fixed cells.

Several fixation protocols were tried to supplement the *in vivo* labelling method. Firstly, I performed a method that was already published (Strickland et al, 2004). Egg cells were fixed for 30 min in 3% paraformaldehyde diluted in sea water at room temperature. Then, the cells were permeabilized in Wash Buffer (50 mM HEPES, 50 mM PIPES, 0.6 M mannitol, 3 mM $MgCl_2$, pH 7.0) containing 0.1% Triton X-100. After washing the cells in Wash Buffer, F-actin was stained using 3-10 U/ml of Alexa Fluor 488-conjugated phalloidin in PBS (137 mM NaCl, 2.7 mM KCl, 1.5 mM KH_2PO_4, 8 mM Na_2HPO_4, pH 7.2) plus 0.1% Triton X-100 for 30 min at room temperature.

Another set of five diverse fixation protocols were tested in order to find the one best preserving the actin cytoskeleton: (1) egg cells were fixed in 1% glutaraldehyde in sea

water over night, washed in PBS, and stained with 3-10 U/ml of Alexa Fluor 488-conjugated phalloidin in PBS with 0.1% Triton X-100 for 1hr at room temperature; (2) egg cells were fixed in 1% glutaraldehyde for 1hr and then washed and stained; (3) eggs cells were fixed in 0.5% glutaraldehyde for 1hr, then washed in PBS and phalloidin-stained; (4) eggs were treated with a mixture of fixatives, combining 3% paraformaldehyde and 1% glutaraldehyde for 1hr, and were washed and stained; (5) eggs were fixed in a cocktail of fixatives containing 3% paraformaldehyde and 0.5% glutaraldehyde for 1hr before being washed in PBS and stained. Following the F-actin staining, eggs were observed by laser-scanning confocal microscopy.

Laser-scanning confocal microscopy.

Two laser-scanning confocal microscopes have been used to analyze fluorescent-stained cells. One is the Olympus Fluoview 200, equipped with the UplanApo 20x/0.70, 40x/0.85 and 60x/1.20 (W) objectives, and used with the laser powered to the 50%.
The other one is the Zeiss LSM 510 Meta equipped with an 60x/1.20 (W) objective.

The software used has been the Fluoview Personal Microscope System, version 1.2.

Ca^{2+} imaging.

The calcium dye Calcium Green 488 conjugated to 10 kDa dextran (Molecular Probes, Eugene, Oregon) was microinjected in a 5 mg/ml concentration in Injection Buffer (IB, 10 mM Hepes, pH 7.0, 100 mM potassium aspartate). The cytosolic free Ca^{2+} changes have been monitored by a cooled CCD camera (MicroMax, Princeton Instruments, Inc., Trenton, NJ) mounted on a Zeiss Axiovert 200 microscope with a Plan-Neofluar 20x/0.50 objective. The excitation-emission filters were controlled by a shutter (Lambda 10-2, Sutter Instruments) managed by a computer.

Uncaging of $InsP_3$.

In order to activate the caged $InsP_3$ (Molecular Probes), oocytes were preinjected with Calcium Green and caged $InsP_3$ (50 μM, pipette concentration) and were irradiated with UV light (330 nm) for 25sec, using the computer-controlled shutter system Lambda 10-2 (Sutter Instruments, Co., Novato, CA). The subsequent changes in Ca^{2+} concentrations were captured by a CCD camera.

Data processing.

Fluorescent Ca^{2+} images obtained with the CCD camera as well as fluorescent images obtained by laser-scanning confocal microscopy were analyzed with the MetaMorph Imaging System (Universal Imaging Corporation, West Chester, PA, USA). The fluorescence augment captured by the CCD camera due to the Ca^{2+} release were normalized to the background, using the formula F_{rel}=[F-F0] /F0. Here, F corresponds to the average fluorescence measured in the entire cell, and F0 is the mean fluorescence obtained from 10 frames captured before the stimulus addition.

In order to analyze the instantaneous increment of fluorescence increase, the formula $F_{inst}=[(F_t-F_{t-1})/F_{t-1}]$ was applied. This type of analysis gave the information of the places where Ca^{2+} was being released in a certain frame or moment. The results obtained by any of the formula above, are expressed in relative fluorescence units (RFU). The numerical values of RFU are expressed as mean ± SD. The Student's t-test was used to determine the statistical significance of the differences found between control and experimental data; $P<0.05$ was considered significant.

Drug treatments.

U73122 (PLC inhibitor, Sigma-Aldrich) was diluted and stocked in DMSO. Then, it was added to the sea water bath in a final concentration of 10 μM and incubated for 30 min. The inactive analogue U73343 is added in the same amounts and times.

Heparin ($InsP_3R$ antagonist, Sigma-Aldrich) was prepared in IB and microinjected in all cases at 25 mg/ml or 50 mg/ml (concentration in the pipette). The same procedure was used for the inactive analogue De-N-sulphated heparin.

Neomycin (Sigma-Aldrich) has been prepared in IB before each experiment and solutions of 1 M, 500 mM and 10 mM (concentration in pipette) were microinjected in the eggs.

Ionomycin (Sigma-Aldrich) was prepared in DMSO and added to the eggs by bath incubation in sea water at a final concentration of 10 μM.

Experiments with actin-specific drugs jasplakinolide and latrunculin-A.

Jasplakinolide (JAS) and latrunculin-A (Lat-A) were purchased from Invitrogen, and dissolved in DMSO. Lat-A is added into the bath in a 3 μM concentration for 15 min, while JAS was incubated in a 12 μM concentration for 10 min.

Microinjection of proteins.

Several proteins were expressed in *E. coli* strain BL21 in collaboration with Dr. J.T. Chun at the Stazione Zoologica Anton Dohrn, and the purified proteins were microinjected into oocytes following dialysis in the injection buffer. The list of the bacterially expressed proteins include: the fluorescent G-actin-RFP and the control protein RFP, the PH-domain and the mutant R40A conjugated both to RFP or GFP. In addition, anti-depactin antibody, generously donated by Dr. Mabuchi was diluted in the injection buffer and microinjected into oocytes in the same manner. The concentration used in each experiment is indicated in the text and in the figures.

Sperm staining with Hoechst 33342.

Dry sperm (10 µl) was resuspended in 1 ml of sea water containing 1 µl of the DNA dye Hoechst 33342 (Invitrogen). After 5 min incubation at 4°C, eggs were inseminated by adding 3-5 µl of diluted sperm inside the experiment chambers containing 2 ml of sea water. The Hoechst dye is excited with UV light.

Transmission Electron Microscopy (TEM).

The samples prepared for TEM analysis were fixed in 1% glutaraldehyde in sea water for 1 hr. After being extensively washed in sea water, they were postfixed for 1 h in seawater containing 1% OsO4, and were subsequently dehydrated in a series of increasing concentration of alcohol and embedded in Epon 812. Sections of the oocytes were stained with 2% uranyl acetate and 0.2% lead citrate and examined with a LEO 912 AB energy filter transmission electron microscope.

CHAPTER III: The role of F-actin in modulating the Ca^{2+} signals during meiotic maturation.

Results.

Roles of the actin cytoskeleton during starfish oocyte Maturation.

Observations in our laboratory have shown that the addition of 1-MA to immature oocytes of the *A. pectinifera* species caused the formation of a Ca^{2+} wave that started always from a single point in the cell and spread towards the rest of the cytoplasm in the form of a half-moon. Further analysis of the Ca^{2+} wave showed that it always starts at the vegetal hemisphere (opposite to the Germinal Vesicle, GV), independently of the point at which the hormone was added or of the position of the oocyte in the observation camera. Moreover, the actual local release of Ca^{2+} took place predominantly at the cortex rather than from the entire cytoplasm (Kyozuka et al., 2008).

Then, the cortical area of the oocyte deserved further investigation in order to understand the mechanism of 1-MA-dependent Ca^{2+} release. As it may be recalled, Doree and collaborators had already found that isolated starfish cortices could release Ca^{2+} *in vitro* in response to 1-MA (Doree et al., 1978). Since the first responses to 1-MA addition are the intracellular Ca^{2+} burst and the reorganization of the actin-filled spikes, both taking place at around 2 minutes after 1-MA contact, it was interesting to explore the relationship between these two events during the maturation process. For this purpose, methodological ways to visualize the actin cytoskeleton were developed.

Microinjection of fluorescent phalloidin: a probe to visualize F-actin in *live* oocytes.

Phalloidin, a toxin isolated from the mushroom *Amanitas phalloides,* binds to polymeric F-actin. The microinjection of Alexa Fluor-conjugated fluorescent phalloidin was performed in live cells by delivering it from the pipette tip placed in the center of the cytoplasm. After ten minutes of incubation, the probe diffused to the entire cytoplasm and stained actin filaments in all the cell regions. As shown in Fig. III 1, immature oocytes microinjected with Alexa Fluor phalloidin displayed actin fibers throughout the cytoplasm. Filaments are located around the nuclear membrane, but almost no fluorescence was detected inside the GV. Under the plasma membrane, arrays of actin filaments forming a ring were heavily stained. The same distribution of the actin cytoskeleton was observed in both *A. aranciacus* and *A. pectinifera* oocytes (Fig III 1a and b). The same staining pattern was seen regardless of the nature of the fluorescent tag, e.g. Alexa Fluor 488 or the Alexa Fluor 568 on phalloidin.

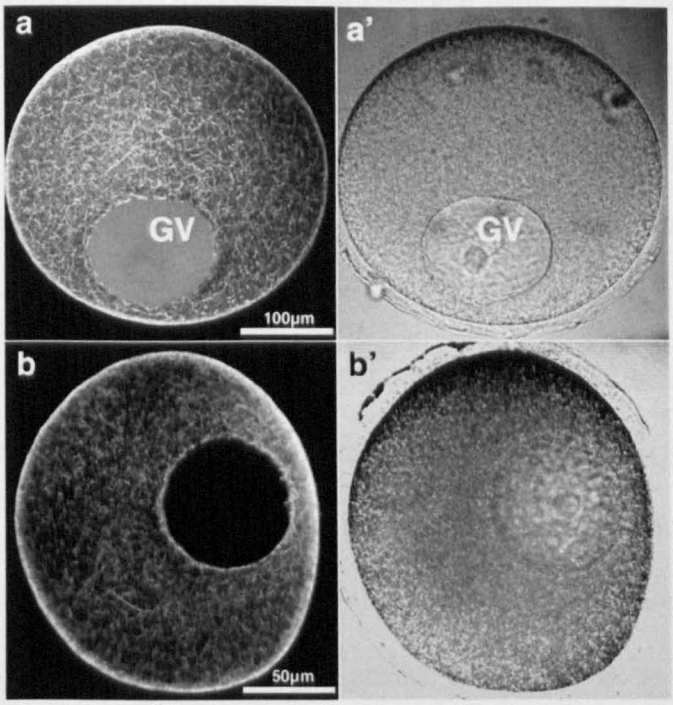

Fig III 1: Distribution of F-actin in living oocytes. Alexa Fluor 568-conjugated phalloidin (50 µM, pipette concentration) was microinjected into the live oocytes of starfish. Fluorescent filamentous actin is observed mainly under the plasma membrane, around the germinal vesicle (GV), and inside the cytoplasm. **a**, *A. aranciacus* oocyte. **b**, *A. pectinifera*. The distribution of the microfilaments is similar in both oocytes. **a'** and **b'**, the transmitted light images of the corresponding oocytes.

At higher magnification, the equatorial confocal plane displayed long filaments of actin running along the cortex and mingle in a continuous meshwork. The actin bundles in the cortex of the immature oocytes often displayed a morphology resembling a pearl necklace in the sense that the usual cord-like filament pattern is interrupted within regular intervals, resulting in the visualization of fluorescent dots on an invisible string (see arrows in Fig III 2a). In the interior of the cell, shorter fibers are seen in the background, round and dimly fluorescent. The latter could be due to the presence of very short actin fibers distributed around the ER contusions. Numerous thin fluorescent profiles are seen protruding from the plasma membrane, that correspond to the microvilli (Fig III 2a, arrowheads). In Fig III 2b the visible light profile of Fig III 2a is shown; the plasma membrane is focused at the equatorial plane. Confocal planes at the cell periphery showed the complexed and tangled tridimensional network of intracellular fibers that was hardly appreciated at the equator. When analysing an *en face* section, obtained by optically "cutting" the cell in a plane closer to the cell surface, a dense network of short actin fibers was observed. Among them, black holes deprived of fluorescence were found (Fig III 2 c). This structure non-permeant to the phalloidin could correspond to acidic and/or yolk granules, as well as to some cortical granules present in the subplasmalemmal region of the cell.

In Fig III 2d, the 'pearl necklace' distribution is visible again. Similar distribution of cytoskeleton has been described in immature starfish oocytes by immunostaining with cytokeratin antibodies (Schroeder and Otto, 1991). The resemblance to a "hair net"-like distribution gave them the name of snoods. They were detected in the cortex and reported to be associated with the animal pole, where the GV is present. Interestingly, we found the very similar pattern of F-actin staining with the use of phalloidin. Indeed, the actin-containing snood-like distribution in our live whole mount preparations was present in or near the cortex. Furthermore, as shown in Fig. III 3, the different confocal planes containing the GV showed the "phalloidin-snoods" around the GV.

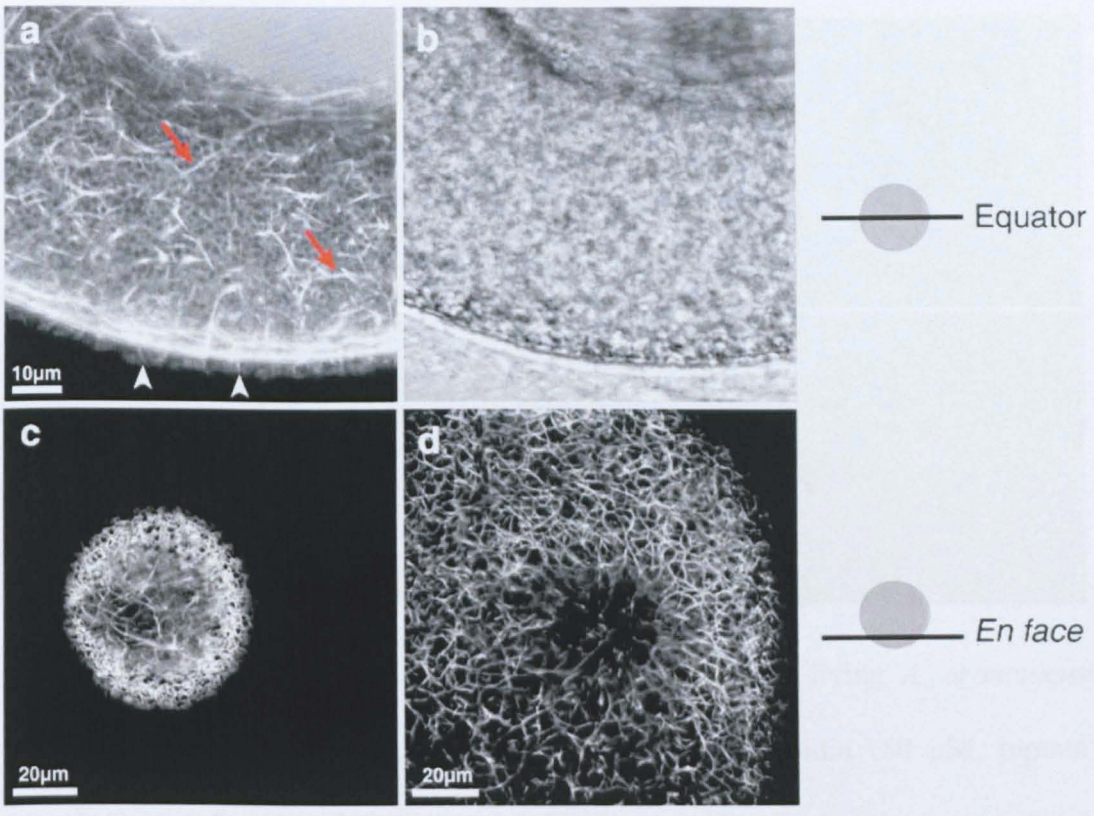

Fig III 2: Phalloidin-stained actin cytoskeleton in *A. aranciacus* immature oocytes (containing the germinal vesicle, GV). Oocytes were microinjected with Alexa-Fluor 488-conjugated phalloidin (50 µM, pipette concentration). **a,** the cortical actin fibers in the equatorial confocal plane. Actin fibers are often bundled in the cytoplasm (arrows), while they constitute microvilli in the egg surface (arrowheads). **b,** the transmitted light image of the oocyte depicted in a. **c** and **d,** actin fibers present in the *en face* sections. **c,** close to one hemisphere of the cell and in **d** close to the GV. In d the pearl necklace is again observed.

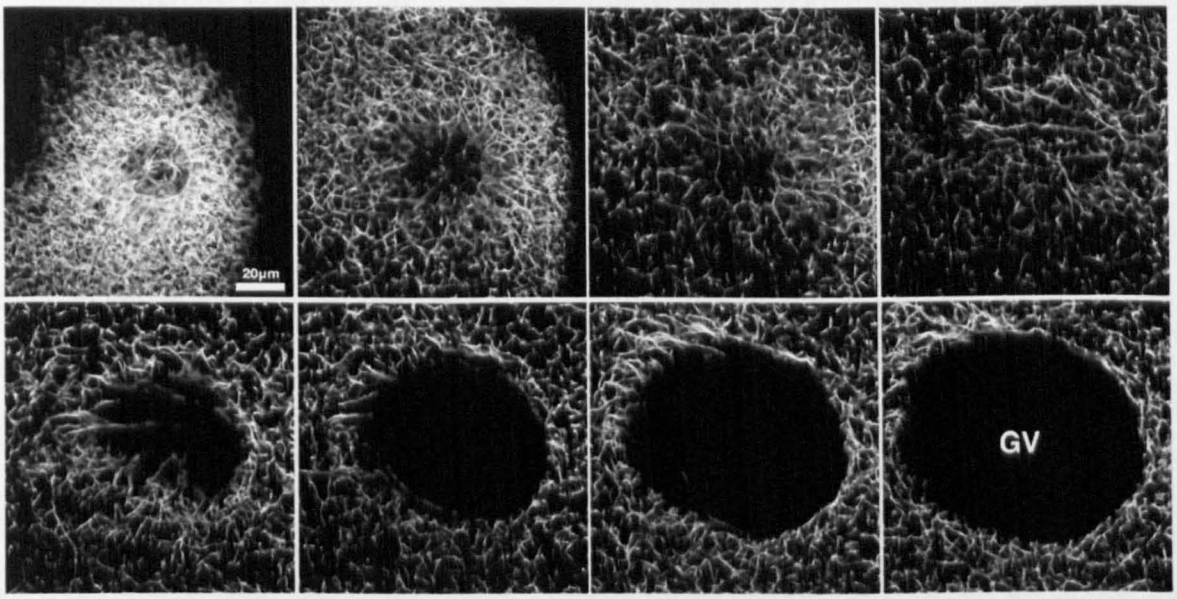

Fig III 3: F-actin distribution close to the germinal vesicle of a living *A. aranciacus* oocyte. The cell was microinjected with Alexa Fluor 488 phalloidin (50 µM, pipette concentration). Images from top left to down right correspond to the contiguous confocal planes along the Z axis covering the germinal vesicle (GV). Many of the fibers stained by the fluorescent phalloidin show the distribution like 'pearled necklace' around the GV area.

Phalloidins, however, are toxins. They have been reported to shift the monomer-polymer equilibrium of actin towards the polymer state (Cooper, 1987), thus interfering with some cellular activities such as cell locomotion and chromosome fetching (Lenart et al., 2005). Due to this reason, the "microfilament-stabilizing" effect of phalloidin had to be tested in our *in vivo* oocyte preparations. Injection of phalloidin in live oocytes of starfish did not exert an inhibitory effect to block the maturation process nor fertilization, as judged by the fact that characteristic cytological changes still take place in the presence of phalloidin in maturing and fertilized oocytes. However, after a long extended incubation, the actin cytoskeleton was considerably affected by phalloidin (Fig. III 4). As shown in Fig. III 4, the F-actin was fewer in number but thicker and shorter, and many fluorescent rods or spots are present in the cytoplasm.

F-actin staining in fixed oocyte.

In fear of any potential side effect of phalloidin, stabilizing and thereby creating actin fibers in live cells, the distribution of actin filaments was corroborated by staining the fixed eggs. However, new difficulties were expected: fixatives do not preserve the actin filaments well. Nonetheless, various fixation protocols were performed in order to find the optimal way to preserve the morphology of the actin cytoskeleton. The method by Begg (Begg et al., 1996) fixes the cells before the permeabilization step, thus particularly preserving the cortical cytoskeleton. Indeed, as shown in Fig III 5b, the cortical ring of actin filaments is still visible after fixation. In the center of the cell, the actin fibres appeared as shorter and less well defined than in the microinjected oocyte. In addition, we have performed alternative fixation protocols. Either glutaraldehyde was used as a fixative in different conditions and concentrations, or a mixture of paraformaldehyde and glutaraldehyde was tried. Following fixation, the permeabilization step and staining of the actin cytokeleton, always using phalloidin, was performed. The results obtained with the different protocols are summarized in Fig III 6. We observed that the extent of actin fibres

detected in the cytoplasm varied significantly depending on the composition of fixatives. Among the conditions tested, fixation with 0.5 to 1% glutaraldehyde produced the best results whereas paraformaldehyde-based fixatives failed to show the actin fibres in the interior cytoplasm (Fig. III 6). Hence, the choice of fixatives makes a big difference in detecting F-actin in fixed cells, and the method using no fixative (microinjection) actually produced the best results. Although more faint, the pattern of the F-actin distribution in glutaraldehyde-fixed oocyte was virtually the same as that in the oocytes microinjected with fluorescent phalloidin. Since F-actin is visualized within a few minutes and no actin filaments are created by phalloidin injection in the nucleus (despite the presence of the G-actin pool), it is not likely that the actin filaments visualized by fluorescent phalloidin represents an artifactually created structure.

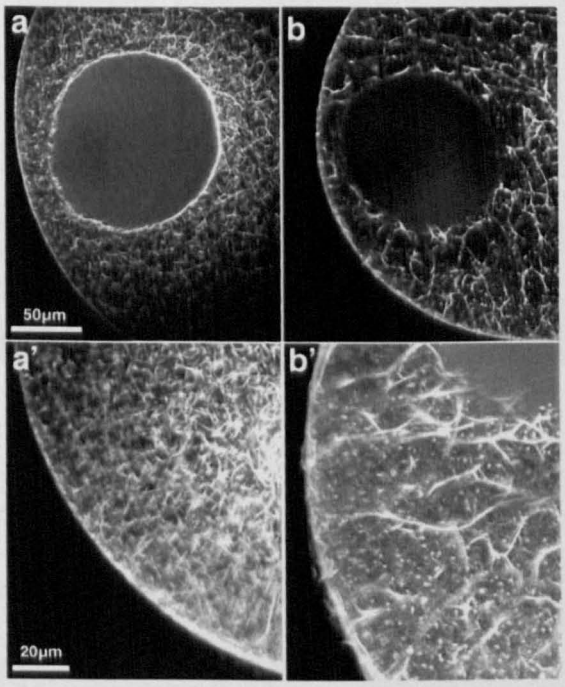

Fig III 4: Alexa Fluor 488-conjugated phalloidin injection affects the actin filaments in living oocytes after 3 hr incubation. **a,** *A. aranciacus* oocyte observed after 10 min of phalloidin injection (50 µM, pipette concentration). **a'** a high magnification image of the same oocyte. **b**, the oocyte incubated for 3 hrs after phalloidin injection. **b',** high magnification image of the oocyte in b.

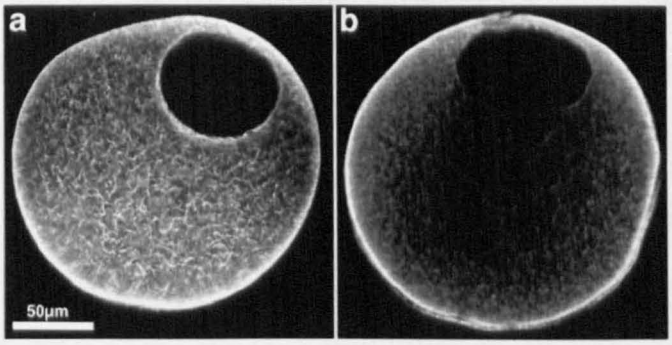

Fig III 5: Two methods for visualization of the actin cytoskeleton. **a**, Alexa Fluor 488-conjugated phalloidin was microinjected in the living oocyte (50 µM, pipette concentration). **b**, the phalloidin staining was performed in a fixed oocyte, following the protocol described by Strickland et al (2004).

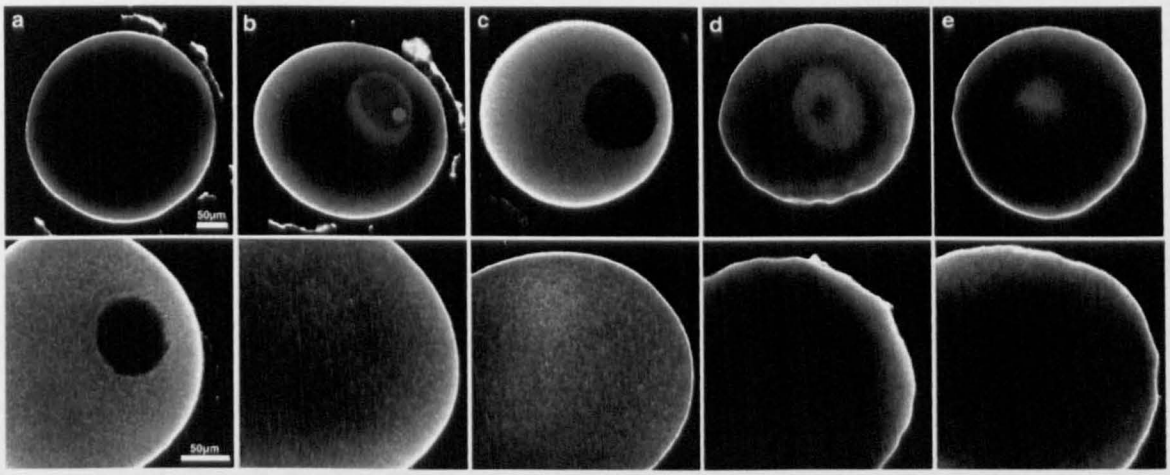

Fig III 6: F-actin visualization in cells fixed in different protocols. **a**, the oocyte was fixed in 1% glutaraldehyde in sea water overnight; **b,** oocytes incubated in 1% glutaraldehyde for 1hr; **c,** oocytes fixed with 0.5% glutaraldehyde for 1 hr; **d**, oocytes subjected to a mixture of 3% paraformaldehyde and 1% glutaraldehyde; **e,** oocytes fixed with 3% paraformaldehyde and 0.5% glutaraldehyde. After fixation, staining with Alexa Fluor 488-conjugated phalloidin (50 µM, pipette concentration) was performed in all the cases. For each condition, a whole cell view is shown on the top row and views with a higher magnification below.

In conclusion, F-actin is best stained in living oocytes by the direct injection of fluorescent phalloidin. Phalloidin may stabilize actin polymers, but it requires hours not minutes as observed in Fig. III 4. Hence, microinjected phalloidin is not likely to create new fibers within the timeframe of our study, and this method provides the additional advantage of real-time monitoring of the actin cytoskeleton in living cells.

F-actin changes during maturation.

The changes in the actin cytoskeleton were monitored by confocal microscopy after 1-MA addition. Since the microinjection of the dye has been performed in living cells, the effect of the hormone stimulation could be examined in single cells after phalloidin treatment. Starfish oocytes microinjected with phalloidin still undergo GVBD after 1-MA addition apparently in a normal way, respecting the physiological time schedule. Most importantly, the changes in F-actin distribution were not inhibited during the maturation process.

The changes in the actin cytoskeleton induced by 1-MA in an *A. aranciacus* egg are depicted in Fig III 7. After 15 minutes of incubation with 1-MA, little changes in the phalloidin distribution can be detected at this low magnification. In the cytoplasm the same dense network is seen 3 min after hormone addition, and the arrays of cortical actin fibers are still continuous in a ring shape. The size of the nucleus started to change at this time, slightly shrinking and possibly indicating the start of the intracellular F-actin changes. However, no F-actin fibers are seen inside the GV. When observed 36 min after the hormone treatment, the actin changes become evident inside the maturing oocyte. The cortical actin fibers look more disorganized, reducing the thickness of the cortical F-actin ring. Moreover, the actin fibers in the internal cytoplasm seem to be shorter and reduced in number, but more intense in fluorescence. The region immediately beneath the cortical ring conspicuously lacks staining of actin fibers, raising the possibility that the cortical ring and the intracellular pool of actin fibers present less interconnections after the hormonal

treatment. At 36 min, in the GV a fluorescent labeling delineating the nuclear membrane becomes evident, invaginating towards the inside of the GV, and probably indicating the initiation of dismantle of the nuclear membrane and start of GBVD. Indeed, the transmitted light image of this time point shows that the region of the GV closer to the plasma membrane, where the phalloidin fluorescent line is seen, the GV membrane has started to disrupt. Also, the GV continues shrinking, showing a smaller dimension than in the previous photo at 15 min, however, no visible actin fibers are present invading it.

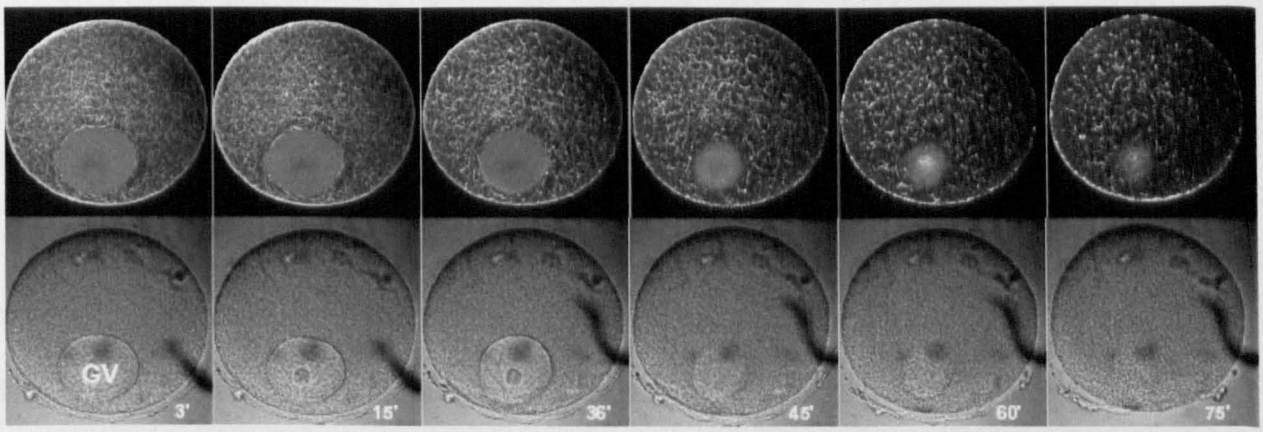

Fig III 7: Changes in the actin cytoskeleton in *A. aranciacus* oocytes during meiotic maturation. Oocytes were microinjected with fluorescent phalloidin (50 μM, pipette concentration) and monitored by confocal microscopy. The moment of 1-MA addition was set to 0'. In the top row, there are the fluorescent confocal images depicting F-actin, and in the lower row the corresponding transmitted light images. The cortical actin ring becomes disrupted and inner cytoplasmic fibers become shorter with the progress of meiotic maturation. The germinal vesicle (GV) breaks down and actin fibers become present in that area.

After 45 min, the cytoplasmic actin fibers are much shorter and the internal network appeared to have loosened. The membrane of the GV has already broken down, and many actin fibers have invaded the ex-GV area in its perimeter and in its central part. Although very much reduced in size, the nucleoplasm of the previous GV is still there, and has not fully mixed with the surrounding cytoplasm. The cortical fibers are also shorter and the cortical ring has lost its continuity. Cortical actin filaments are still apposed to the plasma membrane, but their disposition could be more perpendicular than parallel to the plasma membrane.

At 75 min, the cytoplasmic actin network seems to continue to reduce the number and the length of fibers, while the nuclear region is almost completely mixed with the surrounding cytoplasm. Similar results were obtained with *A. pectinifera* oocytes following 1-MA exposure (not shown).

The distribution of the actin fibers after 75 min incubation with phalloidin has not been affected by the presence of the toxin. Indeed, when the oocytes were incubated with 1-MA for 70 min and then injected with fluorescent phalloidin, the staining of actin fibers showed the same pattern as that displayed in figure III 7 at 75 min (not shown).

Once this new method for visualizing F-actin dynamics *in vivo* had been fully tested and proven to be valid and effective, it was used for analyzing the changes of Ca^{2+} release and the actin cytoskeleton.

Heparin and U73122 affect F-actin distribution.

The cortical Ca^{2+} burst generated in response to 1-MA in *A. pectinifera* oocytes was blocked when the cells were preincubated for 30 min in the presence of U73122, an inhibitor of the of the phospholipase C (PLC) family of enzymes. These enzymes are responsible for the hydrolysis of PIP_2 and generation of the second messenger $InsP_3$ at hormonal cues. Thus it was concluded that the $InsP_3$ formation was essential for intracellular release of Ca^{2+} during maturation. Moreover, the preinjection of oocytes with

the drug heparin, an antagonist of $InsP_3$ receptors, also resulted in the abolishment of the Ca^{2+} response (Kyozuka et al., 2008). While performing this experiment, though, we noted that the cytological morphology and the structure of the cytoskeleton were drastically changed by the two agents. These cells were still viable and functional in that they could respond with Ca^{2+} increase in response to $InsP_3$ injection that would lead them to undergo maturation and GVBD (Kyozuka et al., 2008). After heparin injection, the oocytes changed from the natural rounded shape to an irregular one, and become less transparent. These morphological changes could be a consequence of cytoskeleton alterations. It was then decided to test whether the actin cytoskeleton had been remodelled, as an indirect response to the heparin drug. After heparin injection into the cell and incubation for 15 minutes, phalloidin was microinjected in the cytoplasm of the same cell. As a result, the actin cytoskeleton had been changed by heparin. As shown in Fig III 8, the most affected area is the subplasmalemmal regions, which showed much strong fluorescent labelling when compared to the control.

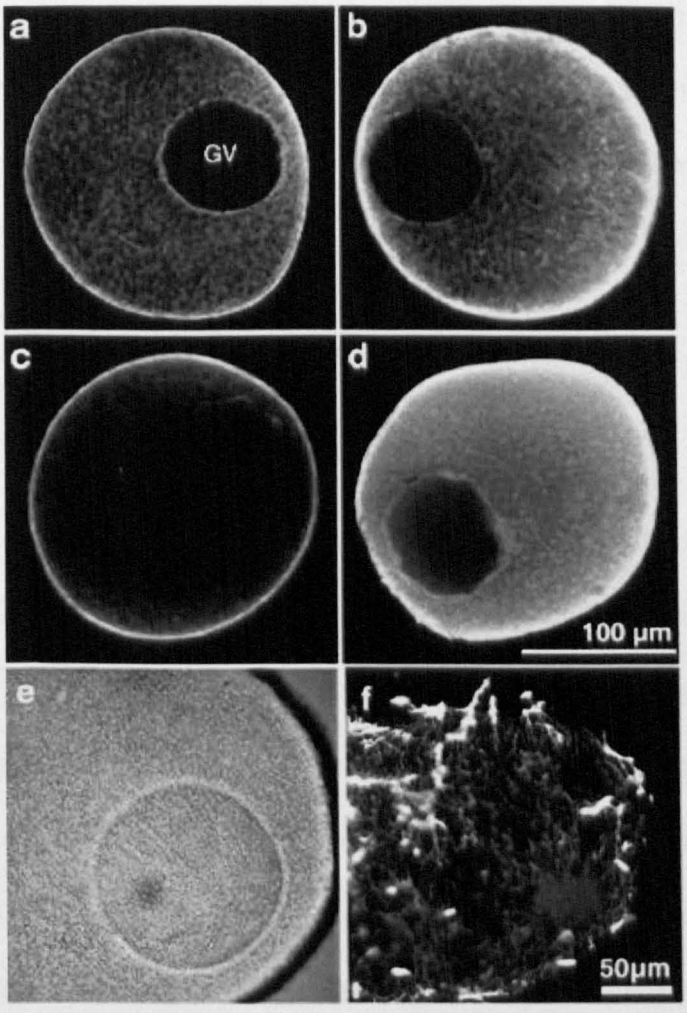

Fig III 8: Heparin-induced modifications of the actin cytoskeleton. **a,** F-actin distribution after phalloidin injection (50 µM in pipette) in a control living *A. pectinifera* oocyte. **b,** F-actin distribution in oocytes preinjected with heparin (50 µg/µl in pipette). F-actin staining by phalloidin in fixed oocytes either without (**c**) or with heparin (**d**) treatment. In both living and fixed cells, the cortical F-actin fibers were strikingly enhanced by heparin. **e** and **f,** an *A. aranciacus* oocyte treated with heparin (50 µg/µl in pipette) and then injected with fluorescent phalloidin (50 µM in pipette) is observed on an *en face* focal plane. The fluorescent image shows clusters of F-actin at the subplasmalemmal region (**f**). **e**, the corresponding transmitted light photo of the same oocyte shown in f.

When observed in *en face* sections, some clusters of phalloidin aggregation were seen under the plasma membrane (Fig III 8f), again suggesting that the cortical F-actin cytoskeleton is affected during heparin treatment. Likewise, the phalloidin staining in the post-fixed oocytes demostrated the same enhanced polymerization of cortical actin (Fig III 8c and d), confirming the results obtained in the living cells.

After obtaining the aforementioned results with heparin, a question emerged whether the PLC inhibitor U73122 provoked similar changes in the F-actin cytoskeleton. When oocytes were microinjected with phalloidin after U73122 treatment, at the same concentration and time incubation necessary for 1-MA-induced Ca^{2+} release inhibition, the actin cytoskeleton presented considerable extent of modifications (Fig. III 9). The actin filaments present in the cortex were much more enhanced than in the control cells. Moreover, the inner cytoplasmic changes were greater than after heparin treatment. After U73122 incubation, not only the cortical but also the cytoplasmic actin filaments were found to be increased in number, creating a more fluorescent and dense internal network of F-actin. Two different controls were done; one incubating with DMSO, the medium in which U73122 is diluted, and the other one is U73343, an inactive analog of U73122. The incubation with both these substances did not change the normal distribution of the actin cytoskeleton, as depicted in Fig III 9.

The changes in the actin cytoskeleton provoked by heparin and U73122 raised a question on how Ca^{2+} is released during the maturation process. These two drugs are reported to have specific effects on the $InsP_3$-dependent pathway, and thus their influence on the actin cytoskeleton came as an unexpected result.

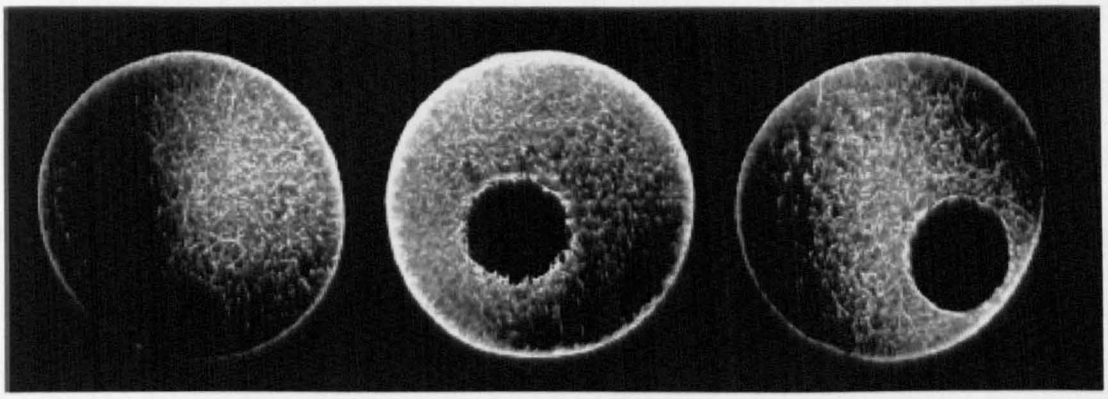

Fig III 9: Changes in the F-actin distribution after treatment with the PLC inhibitor U73122. *A. pectinifera* oocytes incubated in DMSO (n = 4) or in U73343 (an inactive analog of U73122, 10 μM for 10 min, n = 9) presented normal F-actin distributions as shown by fluorescent phalloidin injection (50 μM, pipette concentration). In the case of incubation with U73122 (10 μM for 10 min, n = 15) though, the cortical ring of fibers is visibly enhanced.

The actin cytoskeleton and Ca^{2+} signalling are influenced by heterotrimeric G proteins.

As mentioned in Introduction, 1-MA is thought to act on plasma membrane receptors associated with heterotrimeric G proteins. Indeed, maturation of starfish oocyte is induced by injection of βγ subunits of G-proteins (Jaffe et al., 1993). Moreover, experiments carried out in our laboratory microinjecting the nonhydrolizable analog of GTP, GTPγS, mimicked the Ca^{2+} response generated at maturation of *A. pectinifera* oocytes (Kyozuka et al, 2009). This goes in line with the canonical model proposing that the G-protein subunits could activate PLC and generate $InsP_3$ under the hormonal stimulus, creating the observed Ca^{2+} burst (Berridge, 2005). This Ca^{2+} burst is blocked if the G-proteins are repressed, as showed by preinjecting GDPβS (Kyozuka et al, 2009).

When considering the canonical model, the presence of GDPβS should not interfere with the Ca^{2+} signal if $InsP_3$ is provided by microinjection. However, when caged $InsP_3$ was photoliberated in the presence of GDPβS, the $InsP_3$-induced Ca^{2+} signal was affected. The amplitude of the Ca^{2+} peak was significantly reduced, but the kinetics of the Ca^{2+} rise were much faster than in control cells (Fig III 10a). Moreover, when the localization of the Ca^{2+} release was analyzed, it was clear that the patterns observed in GDPβS-containing oocytes also differed from those of the control. In immature oocytes, uncaging of $InsP_3$ usually provokes a Ca^{2+} release that initiates in the animal pole, close to the GV, and propagates along the cortex. When the oocyte was pretreated with GDPβS, the polarity of the first Ca^{2+} spot is no longer detectable, and instead, Ca^{2+} is observed to be homogeneously distributed in the cell, even without any preference for propagating along the cortical region (Fig III 10 b and c).

After obtaining these results, the actin cytoskeleton was analyzed in GDPβS-preinjected oocytes. As shown in Fig III 10e, GDPβS induced a drastic change in the microfilaments of live oocytes. The cortical filaments showed a new disposition, changing from the continuous ring alongside the plasma membrane (Fig III 10d) to long fibers disposed perpendicular to the surface and projecting to the inner cytoplasm (Fig III 10e). In this latter region, the observed effect is the partial depletion of actin fibers, implying depletion of the cytoplasmic actin pool because of the drastic cortical hyperpolymerization.

Maturing oocytes undergo a series of morphological and physiological changes. As mentioned in Introduction, $InsP_3$ receptors are sensitized after 1-MA treatment, and a greater amount of Ca^{2+} is released in response to the same concentration of $InsP_3$. It could be then hypothesized that if the same amount of $InsP_3$ is liberated in mature oocytes in the presence of GDPβS, its effects over the $InsP_3$ signalling pathway could be overcome by the major Ca^{2+} response produced. In the Fig III 11a we can observe that indeed the $InsP_3$-induced Ca^{2+} dynamics were not as much affected by the presence of GDPβS as in immature oocytes. Conversely, the actin cytoskeleton was still changed by the GDPβS

presence in the cell. In mature control oocytes, actin is disposed in the cortex in the form of short fibers perpendicular to the plasma membrane (Fig III 11b). In the case of GDPβS injected cells, some longer fibers were detected, but most importantly, the whole cortical region shows an increase of fibers, creating a ring that displays hyperpolymerized actin filaments, although not continuous under the surface (Fig III 11c).

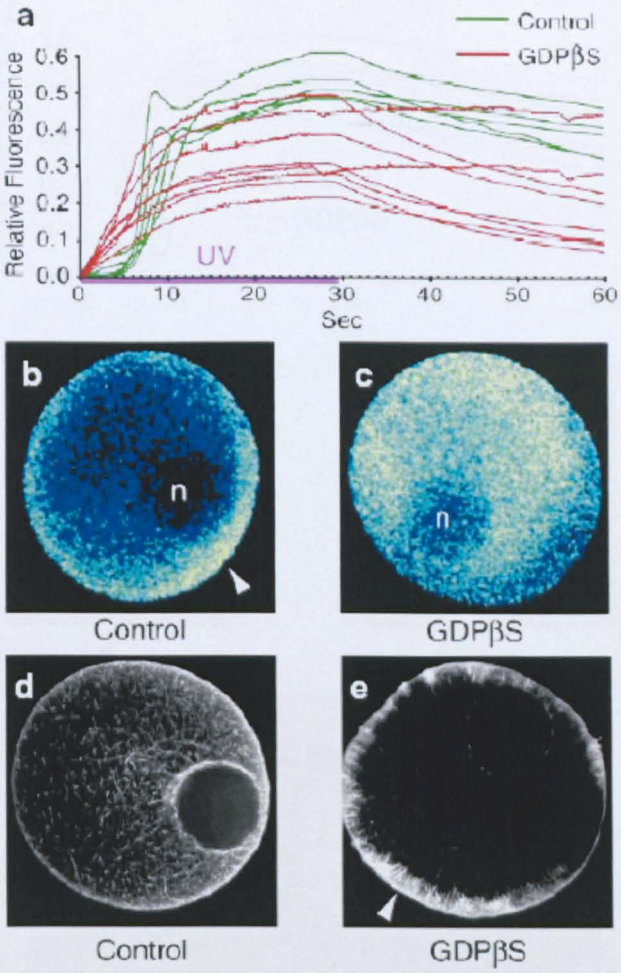

Fig III 10: GDPβS injection changes $InsP_3$–dependent Ca^{2+} signalling and the actin cytoskeleton. Immature oocytes of *A. pectinifera* were injected with Ca^{2+} dye and caged $InsP_3$ (50 μM, pipette concentration), and then with GDPβS (100 mM in injection pipette). After 20 min incubation, the UV uncaging was performed and the dynamics of Ca^{2+} release were examined. The moment of the first detectable Ca^{2+} signal was to t = 0. **a**, the kinetics of Ca^{2+} rise induced by $InsP_3$ uncaging. The brown curves (n = 8) correspond to cells containing GDPβS, and the green curves (n = 5) the control. The duration of UV irradiation is marked with the violet bar. **b and c**, relative fluorescence images 7 sec after $InsP_3$ uncaging. Ca^{2+} is relased from the animal hemisfere close to the GV or nucleus (n) of the control cell (**b**). In the oocyte preinjected with GDPβS, this polarity is lost (**c**). **e,** GDPβS drastically changes F-actin organization. Compared with the control (**d**), GDPβS injection induces enhancement of cortical F-actin fibers.

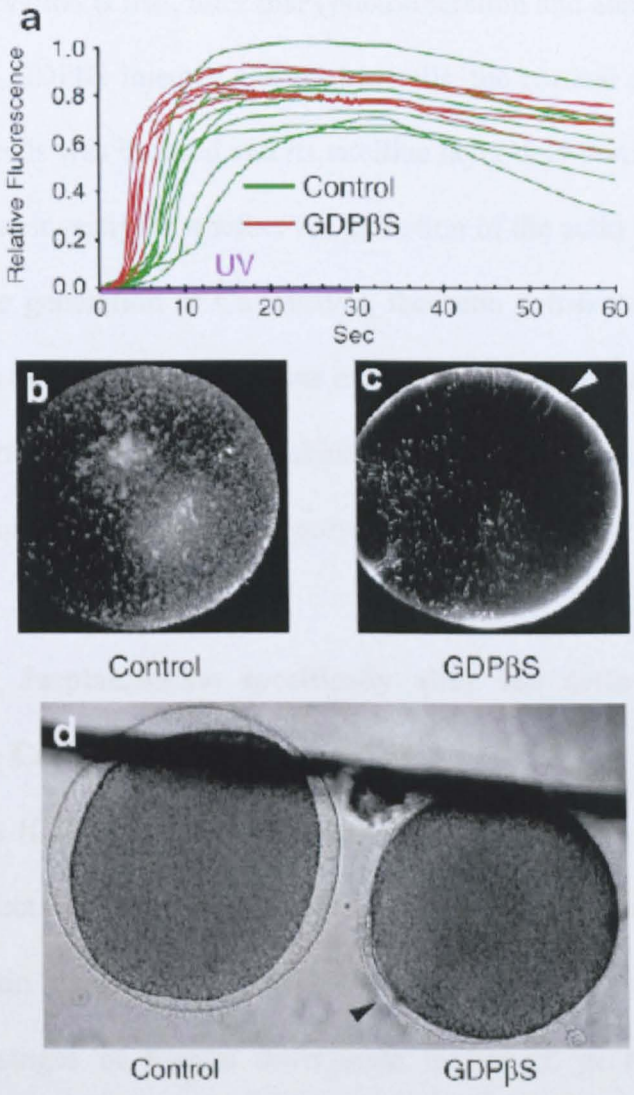

Fig III 11: GDPβS injection changes the actin cytoskeleton and $InsP_3$-dependent Ca^{2+} signals. *A. pectinifera* oocytes injected with Ca^{2+} dye and caged $InsP_3$ were matured with 1-MA for 1hr and subsequently injected with GDPβS (100 mM in pipette). After 20 min, $InsP_3$ was photoactivated in the presence (brown curves, n = 6) or absence (green curves, n = 9) of GDPβS (**a**). The cortical actin fibers have been enhanced by GDPβS, as judged by the visualization of F-actin with Alexa Fluor 568-conjugated phalloidin in control (**b**) and GDPβS-preinjected eggs (**c**). **d,** the GDPβS-containing eggs elevate the vitelline layer only partially after InsP3 uncaging.

Another observation is that, after $InsP_3$ photoliberation and almost equal amounts of Ca^{2+} release between GDPβS injected and control cells, the cortical granule exocytosis of the former group of cells was blocked and its vitelline layer only partially elevated (Fig III 11d). Then, in order to investigate whether the alteration of the actin cytoskeleton had any relevant effect on the generation of Ca^{2+} waves, the actin cytoskeleton was deliberately modified and its effect on Ca^{2+} signalling was examined after hormonal stimulation. These experiments were performed using the Japlakinolide and Latrunculin-A, which specifically bind actin proteins and change the status of polymerization.

Latrunculin-A and Jasplakinolide specifically alter the actin cytoskeleton, with consequences on the Ca^{2+} signalling at maturation.

Latrunculin-A (Lat-A) is a drug that specifically binds to G-actin (Spector et al., 1989). Under the effect of Lat-A, there is no G-actin available for polymerization and *de novo* formation of actin filaments, thus the net effect of this drug is depolymerization of the actin fibers. The changes of F-actin distribution in live *A. pectinifera* oocytes after applying this drug are shown in Fig III 12. Lat-A is membrane-permeant and is applied to the oocytes by bath incubation in seawater. The first changes detected were in the cortical region. After 15 min incubation, the cortical ring of actin fibers lost its continuity and showed only some patches of F-actin, or even dots (probably composed of very short fibers). The effect of the drug is progressive, and more drastic effects are seen after 30 min incubation when the cortical filaments are completely disassembled and the cortical ring is no longer visible. Comparable results were obtained when cells were fixed after Lat-A treatment (Fig III 12).

In the case of jasplakinolide (JAS), the effect is the opposite: it favours actin polymerization. Being isolated from marine sponge *Jaspis johnstoni*, it specifically binds to F-actin and stabilizes the filaments. The phalloidin microinjection of oocytes pretreated

with JAS, show very much enhanced phalloidin-staining in the cortical region (Fig III 13), indicating that F-actin hyperpolymerization has indeed taken place in the cortical area.

The cortical actin cytoplasm has been affected by the use of these two actin-specific drugs. Interestingly, Lat-A and JAS had parellel effects on Ca^{2+} signalling. In Lat-A incubated cells, the amount of Ca^{2+} released was less than in control cells, and the effect was time-dependent, implying that the Ca^{2+} signalling is modulated by the extent of actin depolymerization (Kyozuka et al., 2008). Oocytes incubated wih JAS also presented a deregulated Ca^{2+} response to 1-MA, inhibiting the Ca^{2+} wave in a dose-dependent manner (Kyozuka et al., 2008). The two graphs shown below have been extracted from the paper published by Kyozuka et al., 2008 and illustrate the latter mentioned results, showing that there is a close relationship between the actin cytoskeleton and intracellular Ca^{2+} signalling during maturation.

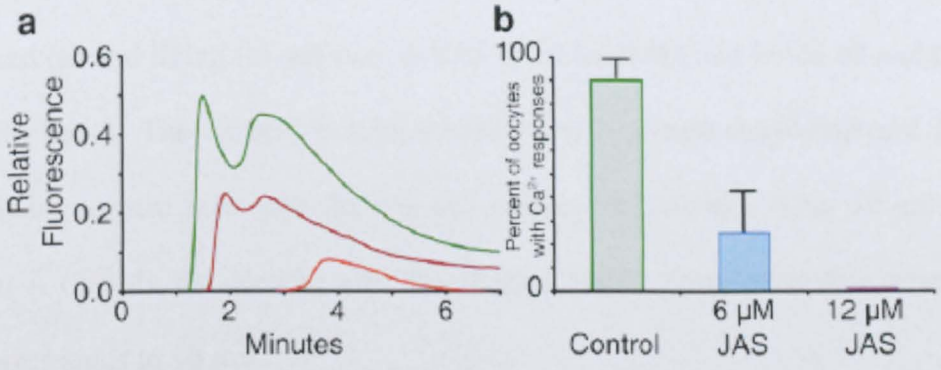

Graph "**a**" shows the Lat-A inhibition of the 1-MA-induced Ca2+ signaling in a time-dependent manner, since oocytes pretreated with Lat-A 0.5µM for 10 min (brown curve) and 15 min (red curve) generate a lower and delayed Ca^{2+} response to 1-MA than control cells (green curve). Graph "**b**" indicates the 1-MA-induced Ca2+ signaling inhibition by JAS in a dose-dependent manner. In the absence of JAS, 92% of cells responded to 1-MA with Ca^{2+} release, while only 25% respond in the presence of 6µM JAS and none of the cells respond after 12 µM JAS treatment. This graphs have been reproduced from Kyozuka et al, 2008.

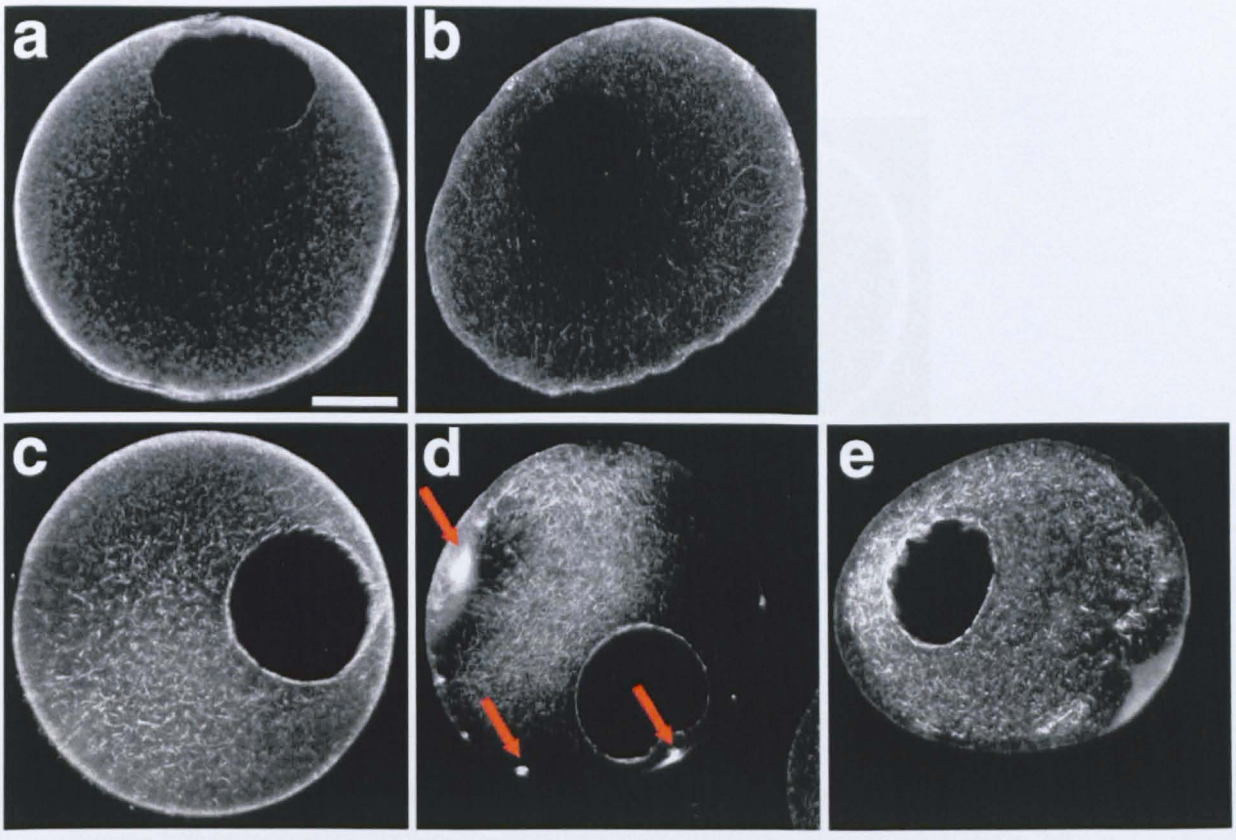

Fig. III 12: Lat-A induces structural changes in the cortical actin cytoskeleton. Alexa Fluor 488-conjugated phalloidin (50 µM, pipette concentration) stained F-actin in control fixed (**a**) and living (**c**) oocytes, as well as in fixed (**b**) and living (**d** and **e**) oocytes treated with Lat-A. The cortical F-actin cytoskeleton has been depolymerized giving place to a thinner cortical actin network (**b**) and patches (**d**, arrows). After 30 min incubation with Lat-A (3 µM), the cortical actin fibers have almost completely disappeared (**e**). Scale bar corresponds to 50 µm.

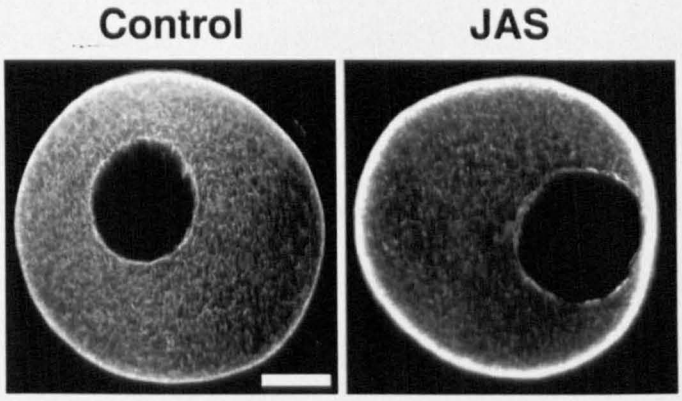

Fig. III 13: JAS incubation enhances the cortical actin cytoskeleton. F-actin was visulaized by preinjected Alexa Fluor 488-conjugated phalloidin (50 µM, pipette concentration). **a**, control oocyte. **b**, Incubation of the oocytes (*A. pectinifera*) with 12 µM of JAS strongly hyperpolymerized cortical actin within 10 min. Scale bar = 50 µm.

Discussion for Chapter III.

When immature oocytes of starfish are stimulated with 1-MA, the first changes detected are the intracellular Ca^{2+} release and the alteration of actin filaments in the cell. The relationship between these two changes, which occur two minutes after addition of the hormone, have not yet been much studied. In general, the intracellular Ca^{2+} release is due to the action of second messengers that activate Ca^{2+} channels principally on the ER. Early studies suggested that the effect of 1-MA is mediated by heterotrimeric G-proteins, which in turn activate the phospholipase C, the enzyme synthesizing $InsP_3$ by means of PIP_2 hydrolisis. $InsP_3$ would then open $InsP_3R$ located on the ER and and release Ca^{2+} to cytosol. In support of this idea, it was shown that blockage of heterotrimeric G-proteins with PTX toxin inhibited the meiotic maturation and actin spike formation (Sadler and Ruderman, 1998).

To monitor the dynamic changes of the actin cytoskeleton in living cells, we developed a method to visualize F-actin by using microinjection. The fluorescent phalloidin microinjected into living cells provided real-time information of the actin cytoskeleton, which was similar to the distribution of F-actin in the fixed cells. Although phalloidin is known to be an F-actin inducer, we have shown that its presence in the cell does not interfere with the maturation process and GVBD timing (Fig III 7). Moreover, experiments applying the same technique in the eggs of sand dollar demonstrated that phalloidin did not affect the elevation of the fertilization envelope nor other fertilization processes up to 50 μM of cytosolic concentration (equivalent to 100-fold higher than the dose used by us) (Hamaguchi and Mabuchi, 1982). By using the microinjection method, we were able to study the distribution of microfilaments in the resting conditions and in response to 1-MA. As showed in Fig III 8 and 9, we observed that treatment of the oocytes with the $InsP_3$-pathway altering drugs heparin and U73122 not only abolished the Ca^{2+} responses but also altered the actin cytoskeleton. These two drugs enhanced the cortical F-

actin in the immature oocytes. The changes in the actin cytoskeleton induced by the aminosteroid U73122 could be explained since U73122's known role is to block PIP_2 hydrolysis. PIP_2, apart from being the substrate for $InsP_3$ formation, also binds to actin-binding proteins (ABPs) regulating F-actin dynamics. The inhibition of PIP_2 hydrolysis would alter its turnover dynamics, thus affecting the PIP_2/ABPs relationships and modifying the microfilament cytoskeleton. Hence, shifting the equilibrium of PIP2 metabolism by inhibiting the resting activity of PLC might explain the unexpected actin-hyperpolymerizing effect of U73122.

In the case of heparin, the reasoning is not so straight-forward, since it is supposed to specifically affect $InsP_3Rs$. In light of the fact that heparin is a polymer of highly-sulfated glycosaminoglycan, it is conceivable that the high density of negatively charged residues might interact with actin-binding proteins, and thereby modulate their activities to change the status of actin polymerization (Kyozuka et al., 2008; Puppo et al., 2008). As $InsP_3Rs$ are in close association with actin filaments (Bose and Thomas, 2009; Fujimoto et al., 1995; Turvey et al., 2005), alteration of the cytoskeletal environment of InsP3Rs by heparin might contribute to the modulation of Ca^{2+}-releasing activities.

Since the drug-induced actin changes were dramatic in the cortical area of the cell, in close proximity to the plasma membrane where the 1-MA receptors are presumably located, the upstream components of the $InsP_3$ pathway were studied. Based on the literature, the 1-MA triggers the $InsP_3$ pathway via heterotrimeric G-proteins. The nonhydrolyzable analogs of GTP and GDP, which respectively stabilize the active and inactive forms of the G-proteins, provoked modifications in the actin cytoskeleton in immature and mature eggs (Figs III 10 and 11). Such effects could be ascribed to heterotrimeric G-proteins, as suggested in the work where PTX inhibited spike formation (Sadler and Ruderman, 1998), or also to deregulation of small G proteins like the Rho family, which are known to modulate the actin cytoskeleton. Since *Clostridium difficile* toxin B, a specific blocker of the Rho G-proteins did not alter the 1-MA induced Ca^{2+}

dynamics, the Rho family might not play a role in this process (Kyozuka et al., 2009). In parallel to the cytoskeletal changes, the kinetics of the Ca^{2+}-release evoked by exogenously provided $InsP_3$ were significantly affected by GDPβS. Hence, it is shown that G-proteins may play a role not only in activating PLC necessary for $InsP_3$ formation, but also in modifying the actin fibers, and demonstrated that the changes of actin cytoskeleton led to the modification of the Ca^{2+} signalling pattern.

Electron microscopy studies using heparin showed that the over-polymerization of cortical actin dislodged the cortical granules and organelles from their normal subplasmalemmal location (Kyozuka et al., 2008). In addition, mature eggs injected with GDPβS failed to elevate the vitelline layer (Fig III 11d). Since G-proteins of the Arf, Arl and Rab families contribute to docking and several other steps leading to vesicle fusion and exocytosis (Di Paolo and De Camilli, 2006), the effect of GDPβS could be attributed to the inhibition of this type of G-proteins. However, cortical F-actin is visibly modified after GDPβS teatment as well, and actin filaments are also known to be relevant to exocytosis. Hence, further investigation is required to resolve the exact mechanism of cortical granule exocytosis involving G-proteins and the local actin cytoskeleton.

As already mentioned, 1-MA-induced Ca^{2+} release appears always in the vegetal hemisphere. Since 1-MA receptors are thought to be evenly distributed in the entire surface of the oocytes and $InsP_3Rs$ were reported to be homogeneously distributed along the starfish oocyte cytoplasm (Iwasaki et al., 2002), the origin of the polarity in the generation of the Ca^{2+} wave is not easily comprehensible. $InsP_3$-dependent Ca^{2+} channels become sensitized with the progress of meiotic maturation of the oocytes, releasing more Ca^{2+} in response to the same amounts of $InsP_3$ (Chiba et al., 1990). Such changes may be due to diverse reasons in diverse organisms, from increased Ca^{2+} loading in the ER of mouse oocytes, to the increased expression or changed distribution of $InsP_3Rs$ in Xenopus and mouse oocytes (Carroll et al., 1996). Furthermore, during the maturation process, changes in the ER morphology are detected in starfish, mouse and hamster oocytes (Carroll et al.,

1996; Jaffe and Terasaki, 1994). As $InsP_3$ receptors reside on ER, such reorganization might in part contribute to the sensitization of the intracellular Ca^{2+} releasing mechanisms. As far as Ca^{2+} signalling at meiotic maturation is concerned, however, such changes involving ER, $InsP_3R$ or $InsP_3$-pathway are not likely to be influential in shaping the Ca^{2+} response, for this Ca^{2+} response occurs within 2 min after 1-MA addition while the detectable changes in the ER structure take place much later. Taking the data obtained from studies using U73122, heparin and the modulators of the heterotrimeric G-proteins (Fig III 8, 9, 10 and 11), it is clear that their effect over $InsP_3$ is not the only one exerted, and that the actin cytoskeleton is in all the cases altered as well.

Structural differences *inherent* to immature oocytes could be the basis for the generation of Ca^{2+} signal polarities. It has been suggested that Ca^{2+}-releasing channels might be regulated by the association with cytoskeletal proteins like ankyrin and FK-506-binding protein (Carroll et al., 1996). Furthermore, 1-MA receptors are supposedly present in the post-junctional densities in the oocyte surface, which is rich in cytoskeletal proteins. These junctional sites between the oocyte and the follicle cells (Fc) are reminiscent of neuronal synapses in that the post-junctional density of the egg is connected to the pre-junctional densities of the Fc. The two surfaces are connected via desmosome-like connections, which are are built by cadherins that mediate the intercellular binding. In the cytoplasmic side of each of the two connecting cells, cadherins bind desmoplakin, which in turn anchores keratin filaments to the desmosome. One of the known proteins that link keratin filaments with the actin cytoskeleton in cells is ankyrin. After Fc provides 1-MA and detach from the oocyte, an actin-filled spike is formed at every junctional contact present in the cell surface (Schroeder, 1981). Thus, 1-MA-induced actin reorganization could be transmitted by the changes of the keratin filaments and ankyrin. However, this intriguing possibility that ankyrin-mediated modifications of cytoskeleton could influence F-actin and Ca^{2+}-releasing channels would still not explain the polarization of the generation of the Ca^{2+} wave.

Interestingly, immunocytochemistry experiments have shown the periodic presence of the heterotrimeric G-protein subunits β and γ over intermediate filaments in starfish oocytes (Chiba et al., 1995). The filaments with a 'pearl necklace' appearance were identified as cytokeratin filaments, and given the name of 'snoods' (Schroeder and Otto, 1991). The network of Gβγ-containing keratin filaments have been detected in the cortical region as well as around the GV in their studies. Moreover, the cytokeratin filaments disappeared during maturation (Schroeder and Otto, 1991). As shown in the Results section of this chapter, phalloidin microinjection in immature oocytes revealed the existence of dotted-strings, strikingly resembling the Gβγ-containing keratin filaments (Fig III 2). Also, such phalloidin-positive dotted-filaments have been detected under the plasma membrane and around the GV (Fig III 2 and 3), but were absent in mature eggs (not shown). The similar filament distribution stained by anti-cytokeratin antibody and phalloidin raises the possibility that decoration of actin and intermediate filaments with regulatory proteins may be common in the eggs of starfish. If both filament networks coexist in the cortical region, the presence of Gβγ subunits in the cytokeratin or actin filaments, which have been the ones activated during 1-MA-induced maturation, point to a complex structural regulation of the 1-MA-dependent pathway. Relevant to our studies, snoods have not been detected within 20 μm from the animal pole (Schroeder and Otto, 1991). Hence, in a way, the cytoskeletal features define cell polarity of oocytes, and might in part explain the polarity of the 1-MA-evoked Ca^{2+} waves that are specifically generated at the vegetal hemisphere.

Specific actin-targeting drugs Lat-A and JAS affect the cortical actin cytoskeleton either hypo or hyper-polymerizing the fibers, respectively. Studies of the Ca^{2+} dynamics with this drugs showed that the 1-MA-triggered Ca^{2+} response was diminished in both cases, implying that the two opposite extremes have deleterious effects (Fig III 12 and 13). Hence, what is crucial may not be the net polymerized or depolymerized state of the actin cytoskeleton, but its dynamic modulation at the time of physiological Ca^{2+} responses.

CHAPTER IV: Deregulated actin cytoskeleton alters Ca^{2+} signals and several crucial aspects of fertilization in starfish eggs.

Results

The dynamics of the sperm-induced Ca^{2+} release in the starfish egg.

The dynamics of the Ca^{2+} signals generated in the egg during the fertilization were studied by microinjecting the cells with the fluorescent Ca^{2+} dye, Calcium Green 488. As shown in Fig IV 1a, few seconds after the sperm arrives at the surface of the egg (considered as time 0:00), the cortical flash of Ca^{2+} signal was detected and immediately disappears. Subsequently, a Ca^{2+} spot was visible at the site of sperm interaction (at 30 sec). From that spot, the Ca^{2+} wave expanded towards the opposite side of the egg in the form of a half moon. At 3:03 sec, the wave reached the opposite side and covered the entire of cytoplasm. At this time point, exocytosis of the cortical granules was evidently taking place since the vitelline layer started to elevate, forming the fertilization envelope. As the free cytosolic Ca^{2+} remains elevated for some minutes, the vitelline layer continued to elevate and the fertilization cone was now visible. Following that, the Ca^{2+} levels began to decay (from time 4:42 on), and the fertilization cone was reabsorbed. However, the vitelline layer continued to elevate (13:53).

This pattern of Ca^{2+} release during fertilization is well known and studied in detail. However, we have simultaneously analyzed the fine subcellular relationship of sperm interaction and the egg Ca^{2+} reponse. Taking advantage of the large dimension of the acrosomal reaction that starfish sperm need to generate in order to traverse the jelly coat and reach the egg surface, it was possible to study the spatiotemporal dynamics of the sperm entry. By comparing Fig IV 1a and b, it is clear that at the time point when the first Ca^{2+} response to the fertilizing sperm occurs, at 0:26 sec, the sperm is still *outside* the

oocyte. Indeed, it remains in the outside even after 3:03, when the massive Ca^{2+} wave has swept away.

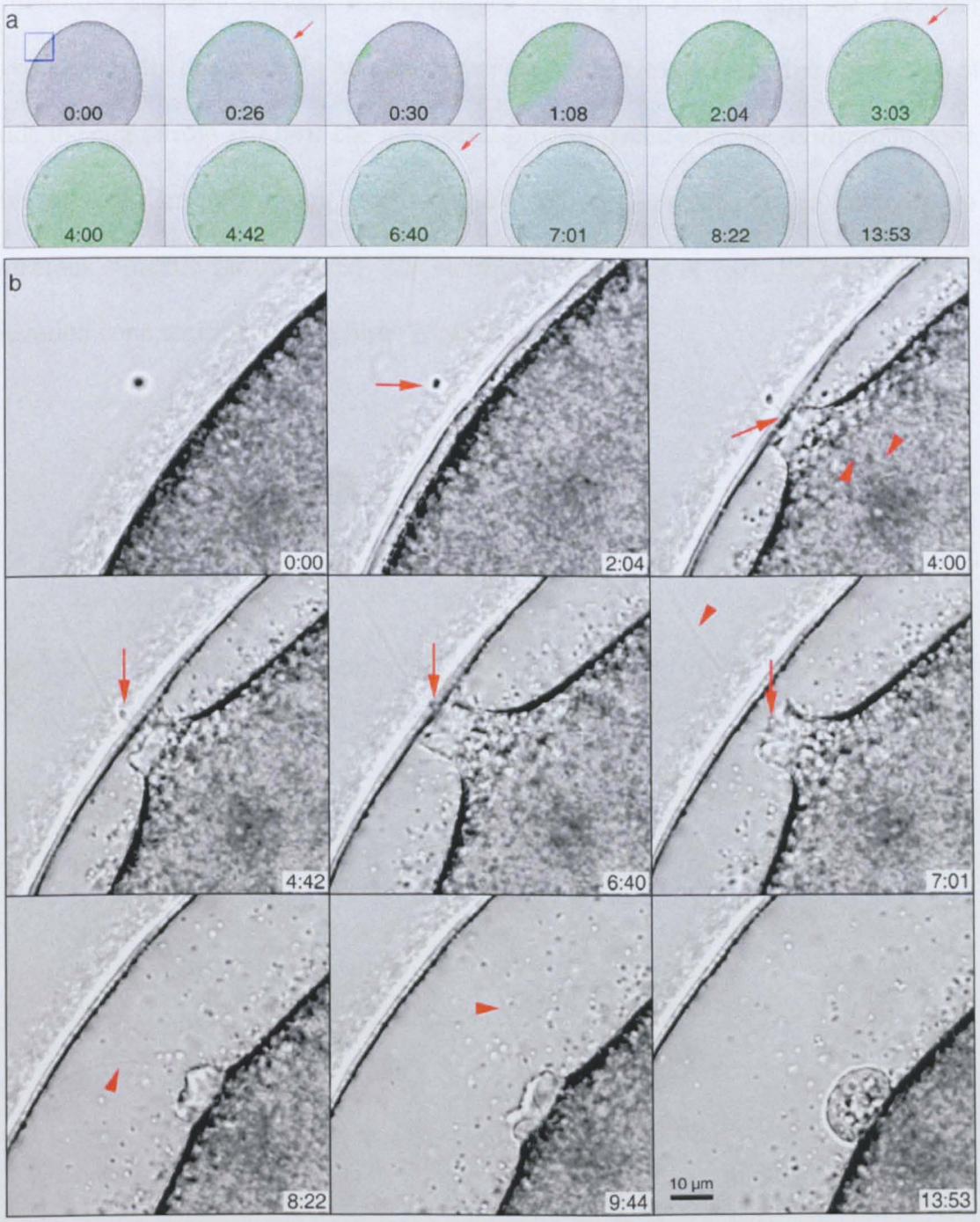

Fig IV 1: Spatiotemporal analysis of Ca^{2+} signals and the morphological changes of the egg at fertilization. *A. aranciacus* oocytes were loaded with the Ca^{2+} dye and matured by 1-MA for 1hr. **a**, merged images of the bright filed view of the egg and the pseudo-coloured Ca^{2+} signals. The time of sperm arrival at the jelly coat was set to t = 0 (min:sec).

At 0:26, a cortical flash was observed, which was followed by a Ca^{2+} spot at the site of sperm interaction at 0.30 sec. From that point, the Ca^{2+} wave front was generated and propagates to the rest of the egg and reaches the anitpode by 3:03. At this time point, the vitelline layer started to elevate. **b**, an enlarged view of the sperm entry site. The sperm arrived at the jelly coat, and the vitelline layer started to elevate while the sperm was still outside the egg (arrow at 2.04). The acrosomal process penetrating the fertilization cone is visible at 4:00. Inside the egg, the acrosomal process appeared to be extended to a filamentous structure (arrowheads). The sperm tail is visible at 7:01, 8:22 and 9:44. The fertilization cone seals in a round bleb (13:53).

When the Ca^{2+} wave travelled half the way into the cytoplasm at 2:04, the sperm head traversed the jelly coat and the vitelline layer started to elevate (Fig IV 1a). At 4:00, the fertilization cone is seen. Also in this image, the acrosomal process was in the plane of focus, which traversed the vitelline layer and reached the fertilization cone. In the cytoplasm beneath the fertilization cone, a long filament obliquely connecting to the acrosomal process was observed (arrowheads in Fig IV 1b at 4:00), suggesting that the acrosomal process might be associated with filamentous structures of the egg cytoplasm, which may help the entry of the sperm. At 6:50, much later than the Ca^{2+} signal had invaded the entire cytoplasm of the egg, the sperm traversed the vitelline layer to enter the domain of the egg. When the sperm head entered the fertilization cone, it starts to retract by separating itself from the vitelline layer (Fig IV 1b at 7:01). The tail of the fertilizing sperm also entered the vitelline layer (visible at 8:22 and 9:44). Between the vitelline layer and the plasma membrane, many rounded-shaped profiles are visible, corresponding to the contents of the cortical granules. The fertilization cone finally retracts and closes into the form a round bleb (13:53).

As discussed in the previous chapter, the antagonist of the $InsP_3$ receptors, heparin, blocked the 1-MA-induced Ca^{2+} response, but also had a dramatic effect on the actin cytoskeleton of premeiotic oocytes. Thus, it was interesting to know the effect of this drug in the Ca^{2+} dynamics generated by fertilization, as well as its effects on the actin cytoskeleton of the mature egg. Indeed, the fertilization of mature eggs preinjected with heparin produced multiple Ca^{2+} spots, instead of one. Each Ca^{2+} spot is released by interaction with a different sperm, indicating that the heparin induced polyspermic egg interaction. As seen in Fig IV 2a, the first Ca^{2+} spot was generated at 0:17 secs, but it fails to block interaction of supernumerary sperm; a second and even third spot were detected at 0:43 and 0:47. Subsequently, the Ca^{2+} signals merged to form a wave to propagate to the entire egg cytoplasm.

Compared with the control eggs, several abnormalities are found during the fertilization of heparin-preinjected eggs. To begin with, the first Ca^{2+} spot observed appears much later than in the control egg. In the control egg, the first Ca^{2+} response is in the form of the cortical flash, as early as 0:01 sec after the sperm arrival to the surface of the egg. In the egg treated with heparin, the cortical ring was not often detected, and the first Ca^{2+} spot appears at 0:17. Such difference is observed in the graph as well, where the small peak at the beginning of the Ca^{2+} curve corresponding to the cortical flash (arrow) is missing or substantially reduced in heparin-preinjected eggs.

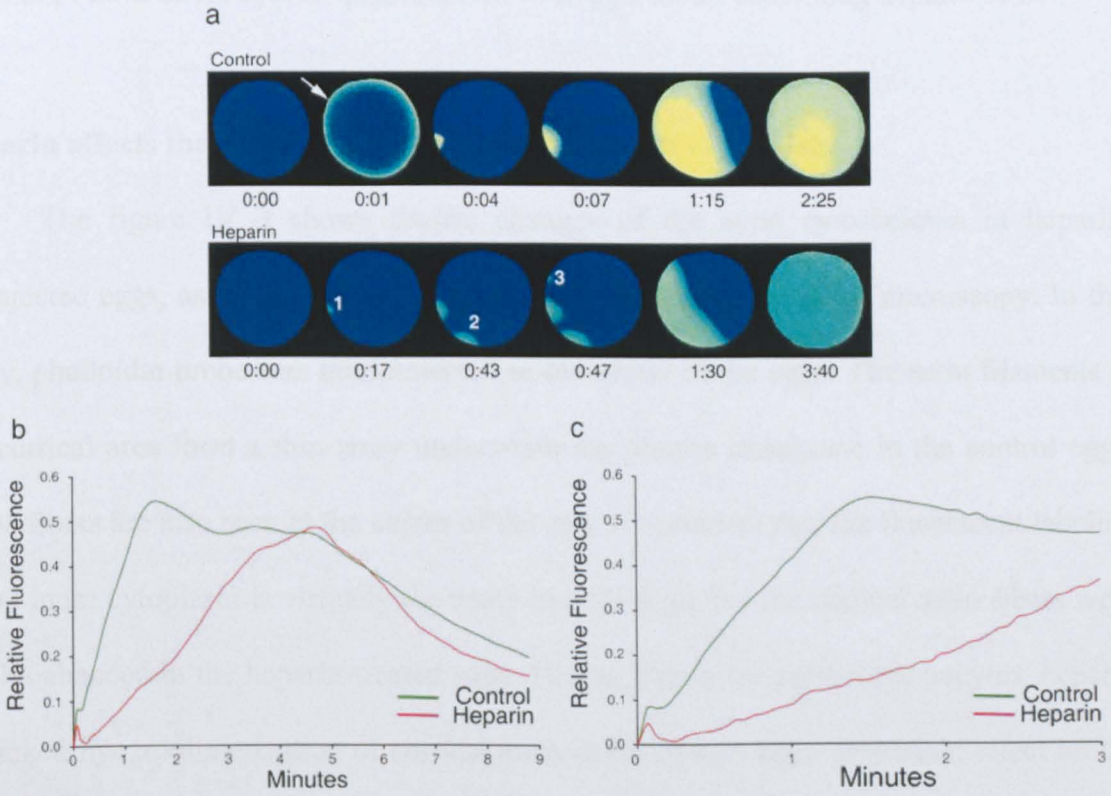

Fig IV 2: Heparin affects the Ca^{2+} release at fertilization. *A. aranciacus* oocytes were injected with Ca^{2+} dye, matured and directly fertilized (control) or preinjected with heparin (50 µg/µl) and then fertilized. **a**, In the control egg, a cortical flash (arrow) was evident and the ensuing Ca^{2+} signal originated from one single spot at the site of sperm interaction. In the heparin-preinjected egg, there is often no cortical flash, and multiple initial Ca^{2+} spots are observed, implying multiple sperm-interactions. **b**, Heparin delayed and reduced the magnitude of Ca^{2+} release as expected. **c**, The graph shown in **b** is plotted in a shorter time scale in order to show the delayed kinetics of the Ca^{2+} response in heparin-treated cells.

The amount of released Ca^{2+} also differed between both cases. Heparin, as expected from an inhibitor of $InsP_3$ receptor, reduced the amplitude of the Ca^{2+} peak. In the control egg, the amplitude of the Ca^{2+} response was 0.83 ± 0.03 RFU, and for heparin-treated cells the peak was 0.55 ± 0.12 RFU. The kinetics of the response was altered further. The Ca^{2+} transient peaked at the average of 70 sec in the control eggs, but the eggs pretreated with heparin reached the maximum Ca^{2+} amount at 272 sec, implying that heparin delayed the release or propagation of intracellular Ca^{2+}. However, no previous study has analyzed heparin's influence on the microfilament cytoskeleton of fertilizable eggs. To face this question, I have microinjected phalloidin in live eggs, either containing heparin or not.

Heparin affects the cortical actin pool in mature eggs of starfish.

The figure IV 3 shows drastic changes of the actin cytoskeleton in heparin-preinjected eggs, as visualized by fluorescent phalloidin and confocal microscopy. In this study, phalloidin probe was microinjected in the center of the eggs. The actin filaments in the cortical area form a thin array underneath the plasma membrane in the control eggs. Some fibers are also seen in the center of the cell. It is evident that the fluorescent labeling in the inner cytoplasm is virtually the same in both eggs, but the cortical actin fibers were much enhanced in the heparin-treated eggs. Hence, like in the premeiotic oocytes, heparin provoked hyperpolimerization of cortical actin in the mature eggs. Heparin's effect on the cortical actin pool was confirmed in the eggs fixed with glutaraldehyde. The eggs preinjected with heparin displayed much enhanced F-actin-staining in the cortex when compared with control eggs preinjected either with the injection buffer or with the inactive analog De-N-sulfated heparin (Figure IV 4). Reflecting remarkable changes in the cortical actin cytoskeleton, the shape of the heparin-treated cell is also strikingly affected, and the filaments in the inner cytoplasm appeared to be depleted.

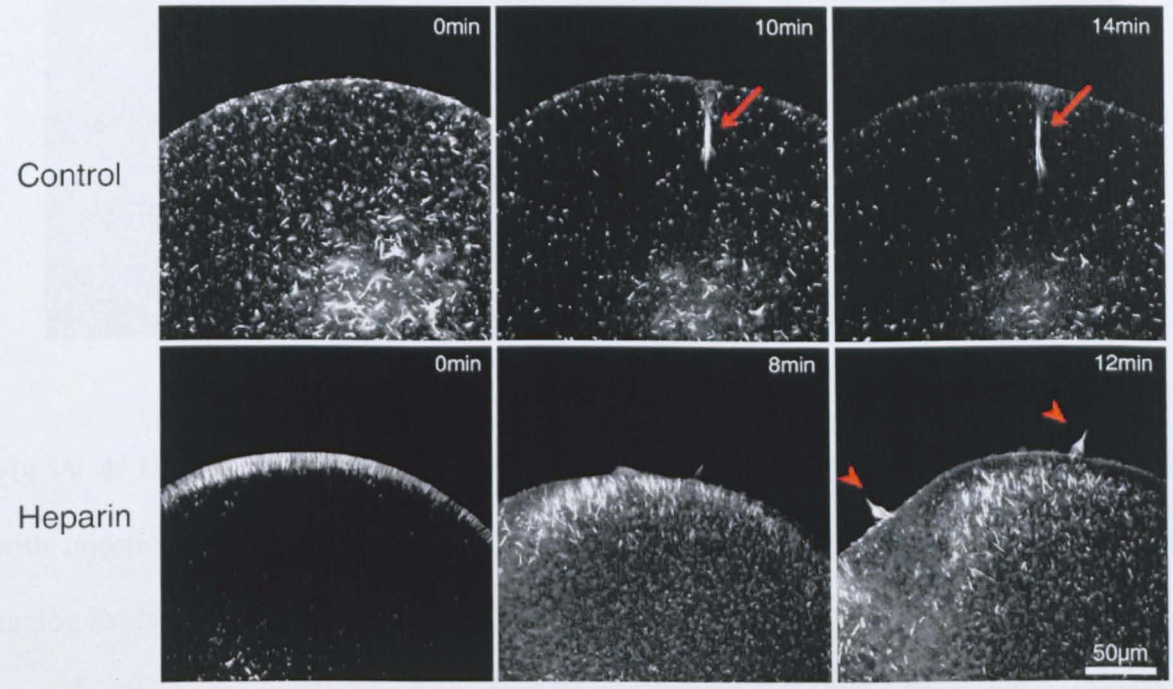

Fig IV 3: Effects of heparin on the cortical F-actin organization and its dynamics during fertilization. Phalloidin-stained (Alexa Fluor 488-conjugated phalloidin, 50 μM in pipette) F-actin was visualized by confocal microscopy in the presence or absence (Control) of heparin (50 μg/μl, concentration pipette) preinjection. Eggs treated with heparin displayed hyperpolimerization of cortical actin. After sperm addition, heparin-preinjected eggs often formed multiple fertilization cones (arrowheads). Arrow: phalloidin-positive actin bundles associated with the penetrating sperm.

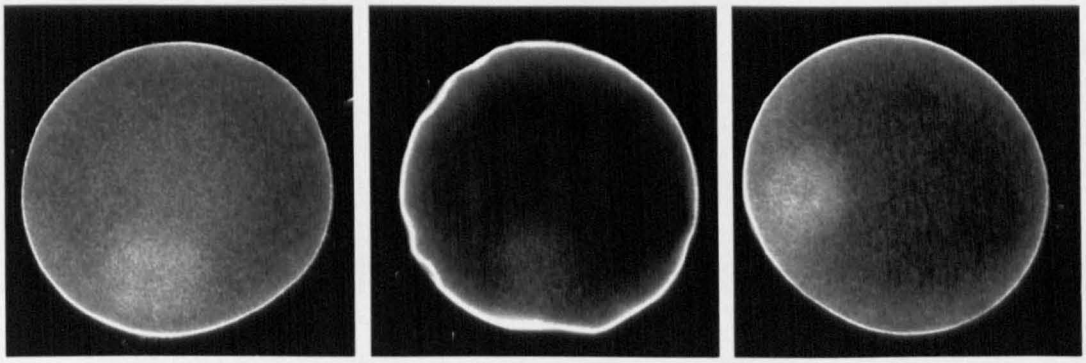

Fig IV 4: Heparin hyperpolymerizes cortical actin. *A. aranciacus* eggs were preinjected with Injection Buffer (Control), Heparin (50 µg/µl, concentration pipette), or an inactive analog De-N-Heparin (50 µg/µl, concentration pipette). Following 15 min incubation, eggs were fixed with glutaraldehyde 0.5% for 1 hr and stained with Alexa Fluor 488-conjugated phalloidin incubation.

Heparin affects vitelline layer elevation and thus fertilization envelope formation.

When phalloidin-stained F-actin was visualized in live eggs at fertilization under confocal microscopy, the cortical actin filaments undergo relocation. After sperm-egg interaction, the cortical ring of fibers move towards the interior of the cell, almost depleting the suplasmalemmal area of actin fibers (Fig IV 5b). In parallel, the vitelline layer elevates due to the exocytosis of the cortical granules, and the fertilization envelope forms. In 6 out of 10 heparin-treated eggs, the enhanced actin cortex does not change homogeneously in the entire surface during fertilization. Actin filaments often fail to disperse towards the interior of the cytoplasm, as was shown in one part of the egg (Fig. IV 5b). Evidently, cortical granule exocytosis and the resultant vitelline layer elevation took place only in the region of the cortex where the actin filaments have been rearranged.

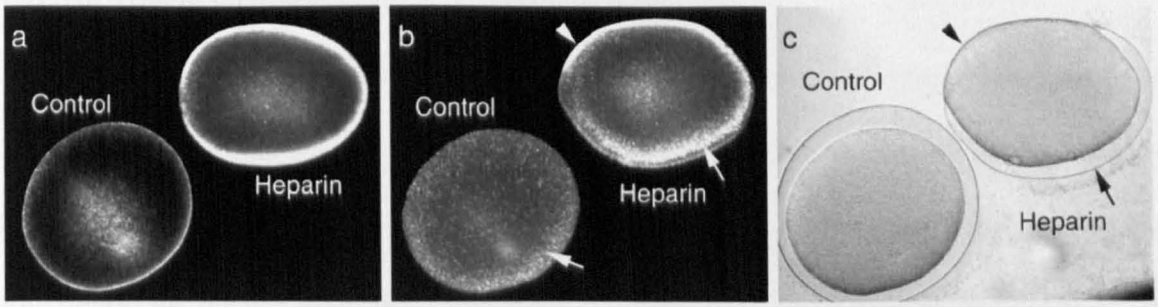

Fig IV 5: Heparin changes the actin cytoskeleton and affects vitelline layer elevation at fertilization. The heparin-injected egg (25 μg/μl) presents an enhanced cortical actin ring when compared to buffer-injected control (**a**), as observed by microinjected fluorescent phalloidin. After sperm addition to the same eggs, the actin filaments migrate centripetally in both control and heparin-preinjected eggs (**b**, arrows), but the dispersing movement of actin filaments was often blocked in one part of the heparin-preinjected egg (**b**, arrowhead). In the transmission light images, vitelline layer elevation takes place only at the side where F-actin has redistributed (arrow) but not in the area where the filaments are still apposed to the plasma membrane (**c**, arrowhead).

Heparin affects formation of the fertilization cone.

After the observation that heparin induces polyspermy and partial vitelline layer elevation, we decided to study whether fertilization cone formation was deregulated by heparin. Fig. IV 6a shows the phalloidin-stained actin fibers inside the fertilization cone. Underneath the plasma membrane, the actin filaments have already been mobilized by the fertilizing sperm and migrated centripetally, depleting the cortex of actin filaments. On the surface, some short and pointed filaments are observed, representing actin spikes or microvilli. In the corresponding transmission light photos (Fig IV 6b) the fertilization cone has sealed after the sperm entry, forming a round bleb. In the heparin-preinjected eggs, however, multiple fertilization cones are seen. This was expected since, as mentioned above, heparin induces supernumerary sperm interaction in starfish eggs. In fact, the average number of fertilization cones detected in a given focal plane in heparin-injected eggs was 6.4 per egg (n = 10) compared to 1.6 (n = 10) in the control. The fertilization cones of the heparin-treated eggs, like the control ones, contained actin filaments. However, their shape was noticeably different. Instead of showing a rounded bleb profile, these took piriform or conical shapes (Fig IV 6b arrowheads). The presence of phalloidin seems not to be responsible for the shape differences since fertilization cones in the eggs not microinjected with phalloidin were of the same characteristics. On the surface of the plasma membrane, weak fluorescent profiles of spikes and microvilli were present (Fig IV 6a). In the cortical region of the cytoplasm, heparin hyperpolimerized actin, and the filaments have only partially migrated following fertilization.

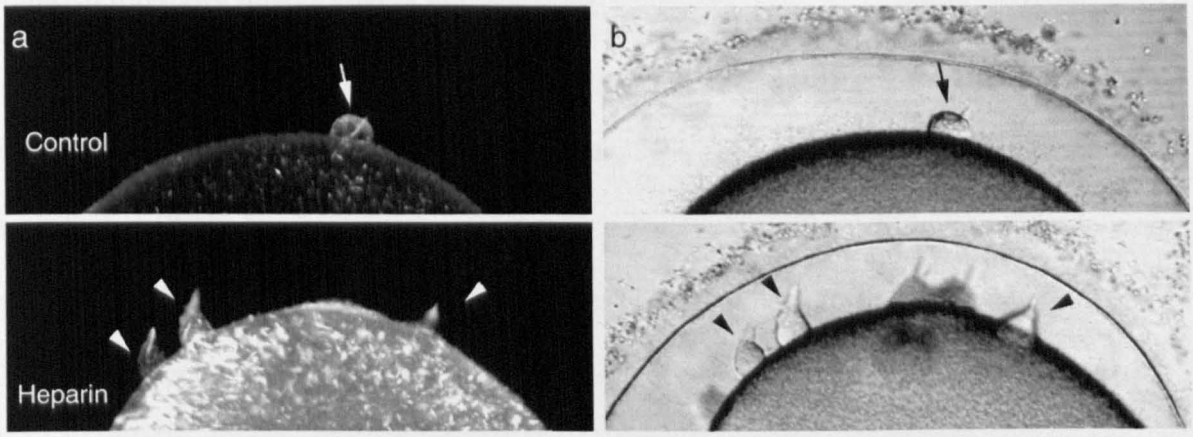

Fig IV 6: Heparin induces aberrant fertilization cone formation. Starfish eggs preinjected with phalloidin were fertilized in the presence or absence of heparin treatment. **a**, In control eggs (without heparin), a single fertilization cone filled with actin filaments is formed 9 min after sperm addition (**a**, arrows). In heparin-pretreated eggs, multiple fertilization cones are formed (arrowheads). **b**, the corresponding transmitted light images.

Heparin partially blocks sperm entry.

Heparin was demonstrated to promote polyspermy and form multiple amorphous fertilization cones. Nonetheless, it was not clear if the supernumerary sperm inducing Ca^{2+} spots and multiple fertilization cones actually enter the egg. Two different methods were applied in order to answer the question. Staining sperm cells with the membrane-permeant DNA-dye Hoechst 33342, we first observed that not all the fertilization cones generated in heparin-treated eggs contained DNA corresponding to the sperm head (not shown). A successful entry of sperm into the fertilized egg was able to be monitored by CCD video camera as well. In the control eggs, the sperm creating a fertilization cone entered the egg 9 times out of 10 tested. In heparin-treated eggs, only 14 out of 28 fertilization cones examined in 8 eggs (polyspermy) showed successful sperm entry. The fast transmission light images taken with the CCD camera at short intervals during fertilization enabled us to study the dynamics of the sperm entry. When analyzing these photos, it was evident that the sperm triggered the formation of a fertilization cone but then often remained outside apparently being 'bounced back' to outside. Figure IV 7 shows some moments of the abortive fertilization process. After the arrival of the sperm on the surface of the egg (considered t = 0:00), it starts to penetrate the jelly coat (time 2:51), but was unable to manage to penetrate the jelly coat and stay outside the egg (time 3:19). However, the fertilization cone continues developing under the elevating vitelline layer (time 5:20), while the sperm is still seen on the extracellular surface of the cell. Once the fertilization envelope has formed, the distorted 'empty' fertilization cone took conical shape (time point 7:52).

In summary, heparin affected many aspects of the fertilization. It provoked polyspermy, deregulated the formation of fertilization cones, and blocked the sperm entry process. In the literature, heparin has been defined as an $InsP_3R$ antagonist; however this work has found that heparin also has a secondary or indirect effect, modifying the actin cytoskeleton in both immature and mature oocytes. Then, its deleterious effects on

fertilization could be also attributed to its activity to modify F-actin. For this reasons, the result was corroborated with the specific actin-targeted drugs, JAS and Lat-A.

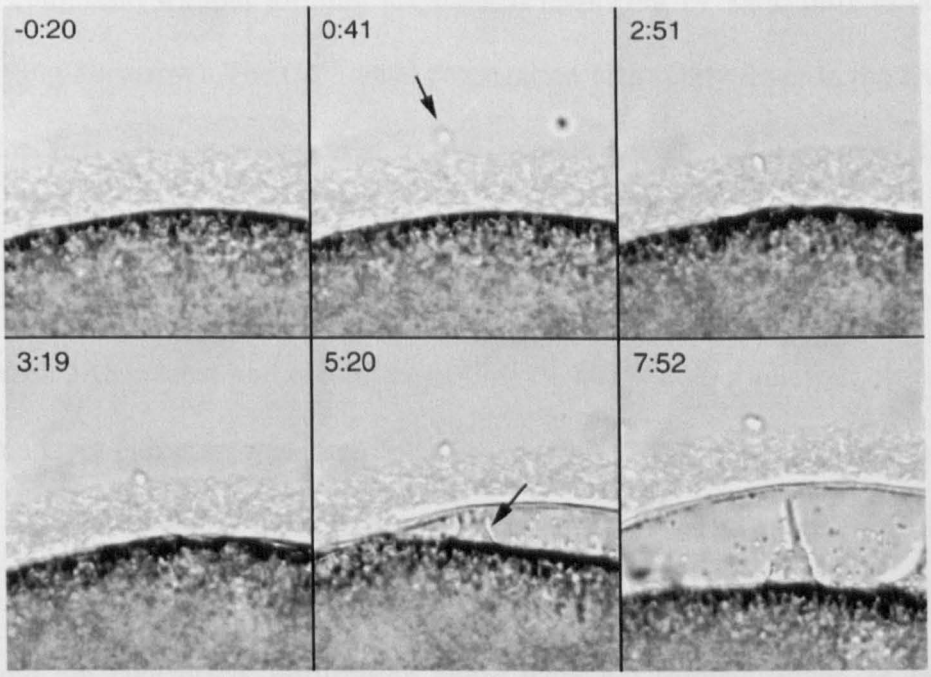

Fig IV 7: Heparin impedes sperm entry into the fertilized egg. Transmission light images of the heparin (25 μg/μl)-injected eggs were examined by CCD camera. Sperm arrived to the jelly coat (time 0:00) and started penetrating the egg. A fertilization cone started to be formed (arrow at 5.20) but then the sperm bounced back to the jelly coat instead of entering the cytoplasm of the egg.

JAS and Lat-A induce polyspermy and affect vitelline layer elevation by directly affecting the cortical F-actin structures.

As previously mentioned, the net effect of JAS is actin hyperpolymerization near the plasma membrane. When fertilized in the presence of JAS, many Ca^{2+} spots were observed per egg, implying that JAS also provoked polyspermy as heparin did. The three polyspermic Ca^{2+} spots in JAS-treated eggs merged to form a wave that extended to the rest of the cytoplasm without forming the cortical flash (Fig IV 8a at 0:01 in the control egg, arrow; Fig 8b, arrow). The Ca^{2+} wave propagation was subtly faster in the JAS treated eggs, as the first Ca^{2+} spot appeared at 0:01 and the Ca^{2+} wave covered the entire cytoplasm at 1:00. The control egg reaches the maximum Ca^{2+} value later, as can also be observed in the graph of the figure. The amount of Ca^{2+} released, however, did not differed much between JAS-treated and control eggs (Fig IV 8b). Another relevant observation is that vitelline layer elevation was interrupted by the JAS treatment. At variance with to the case with heparin in which the vitelline layer partially elevated after fertilization, JAS incubation completely blocked vitelline layer elevation (Fig IV 9a). As the vitelline layer elevation did not take place, fertilization cones were not formed, either. Moreover, the surface of the egg had a corrugated appearance, indicating that the mechanical property of the cytoplasm had changed inside the egg.

Then, *in vivo* phalloidin staining of mature eggs was performed in order to analyze the changes of F-actin distribution in the JAS-treated eggs. In the control eggs, the actin cytoskeleton is prominent in the cortex with some short fibers distributed in the cytoplasm. In the eggs treated with JAS, the cortical F-actin was hyperpolimerized with occasional long fibers posed perpendicularly to the plasma membrane. The pool of cytoplasmic F-actin seems to have disappeared though, probably due to depletion of monomeric actin necessary to enhance the cortical fibers. These specific alterations of cortical F-actin produced by JAS are strikingly similar to those induced by heparin during fertilization.

On the other hand, Lat-A produced the net opposite effect in that actin was hypopolymerized. Diverse experiments using different concentrations of Lat-A in the medium were used, since the Ca^{2+} and morphological responses at fertilization were very sensitive and greatly changed during this narrow range of treatments. Incubation with as little amount as 0.5 µM of Lat-A was sufficient for altering the Ca^{2+} response during fertilization.

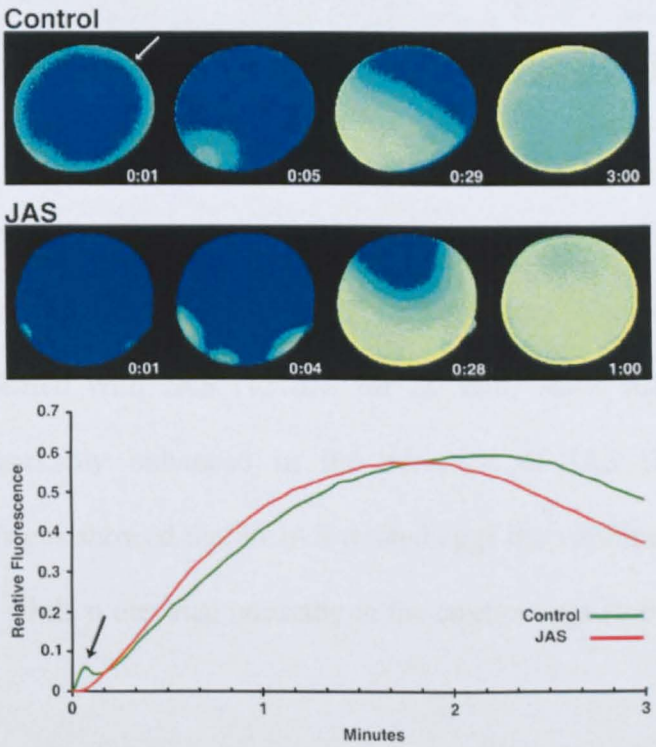

Fig IV 8: JAS incubation induces polyspermic egg interaction and deregulated Ca^{2+} response. Pseudo-coloured fluorescence images of Ca^{2+} release at fertilization of control (top panel) and JAS-treated (12 µM for 20 min, lower panel) eggs. The JAS-treated eggs often lacked the cortical flash (arrow) despite multiple Ca^{2+} spots indicating polyspermic egg interaction. In the graph, the amplitude and the kinetics of Ca^{2+} rise are shown, which were similar for control and JAS-treated eggs.

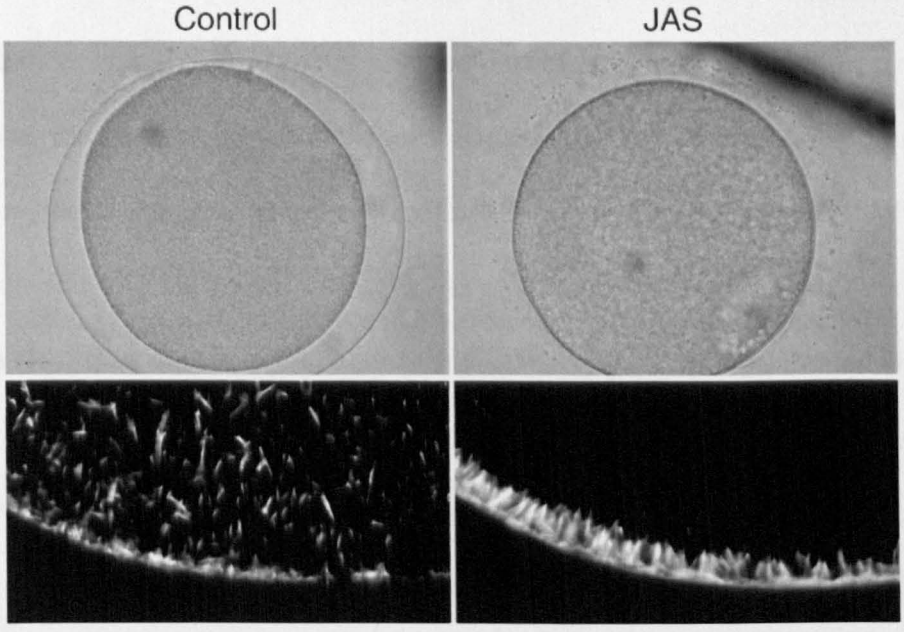

Fig IV 9: JAS hyperpolymerizes cortical actin in mature eggs and blocks vitelline layer elevation at fertilization. Confocal images of mature eggs injected with fluorescent phalloidin and incubated with JAS (12 μM for 20 min) show that the cortical actin filaments were remarkably enhanced in the presence of JAS (lower panels). The transmission light images showed that in JAS-treated eggs the vitelline layer elevation was completely blocked, while it elevated normally in the control eggs (top panels).

In Fig IV 10 the graph shows that the amount of Ca^{2+} released at fertilization following Lat-A-incubation is lower than in normal fertilization in sea water. Moreover, at this concentration, the surface of the cell looks corrugated, and the vitelline layer has only partially elevated creating a polarized fertilization envelope (Fig IV 10b). When Lat-A concentration was slightly raised to 1 μM, the egg could still be fertilized, the total Ca^{2+} released was less than the control but not much different from the eggs treated with 0.5 μM Lat-A (Fig IV 11a). However, unlike the eggs treated with 0.5 μM Lat-A, vitelline layer elevation was completely blocked (Fig IV 11b), and the fertilization cone was absent. Such results indicate that although Ca^{2+} was present in the cell and even reached the cortical region, appropriate changes of the local actin cytoskeleton is necessary for normal cortical granule exocytosis and vitelline layer elevation to occur.

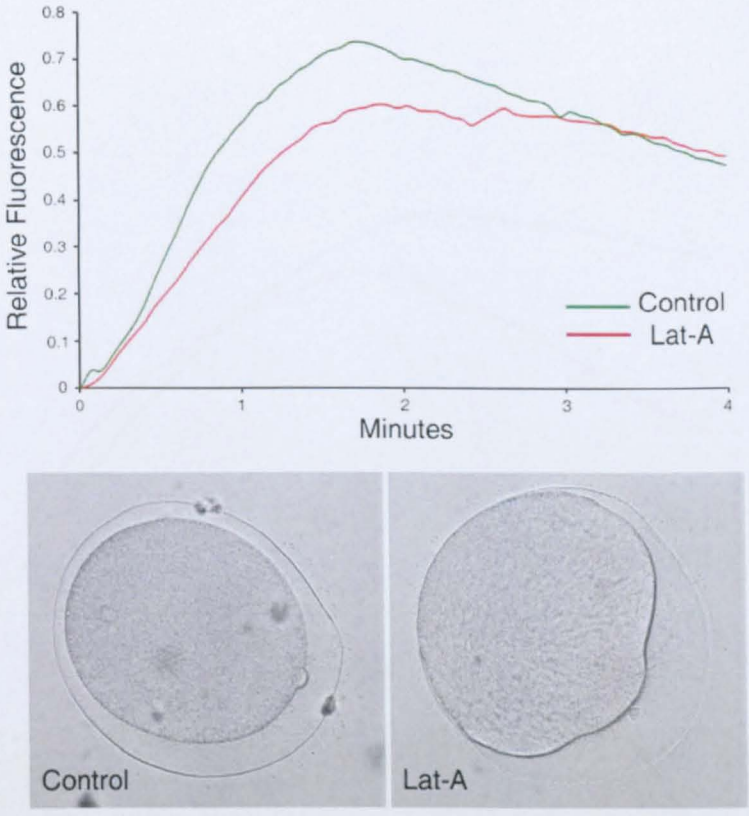

Fig IV 10: Dose-dependent effects of Lat-A treatment (0.5 μM, 15 min) on Ca^{2+} signalling and the elevation of the vitelline layer at fertilization.

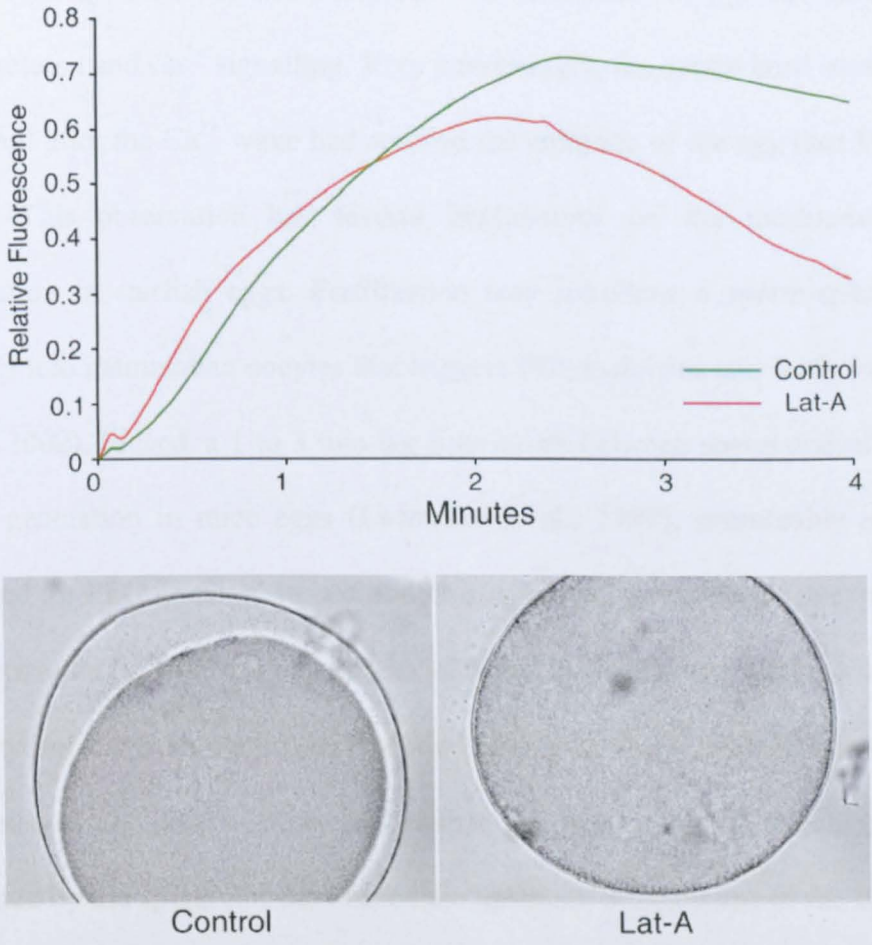

Fig IV 11: Lat-A incubation at higher dose (1 μM, 15 min) provokes significantly lower Ca^{2+} response at fertilization, but enhances the cortical flash. The vitelline layer elevation is blocked after fertilization in the Lat-A treated egg.

Discussion for Chapter IV.

The present section addressed the fertilization-triggered changes in the actin cytoskeleton and Ca^{2+} signalling. Very interestingly, the sperm head started penetrating the egg well after the Ca^{2+} wave had reached the antipode of the egg (see Fig. IV 1a and b at 6:40). This observation has several implications for the mechanism of Ca^{2+} wave generation in starfish eggs. Fertilization may introduce a sperm-specific PLC isoform (PLCξ) into mammalian oocytes that triggers PIP_2 hydolysis and $InsP_3$ formation (Saunders et al., 2002). Indeed, a 1 to 3 min lag time exists between sperm arrival and the first Ca^{2+} wave generation in mice eggs (Lawrence et al., 1997), presumably reflecting the time required for PLC infusion. In echinoderms, however, it is difficult to expect the same thing to happen during fertilization. Echinoderm sperm have a very long acrosomal process and PIP_2 hydrolysis is thought to be provided mainly by PLCs contained in the egg, like PLCγ (Santella et al., 2004). However, neither the exact way in which these enzymes are activated by the sperm nor the immediate upstream components of the PLC pathway in the egg side have been clearly resolved. Despite this fact, most of the studies have pointed to PLC activation, and consequently to a necessary role of $InsP_3$, to explain the the Ca^{2+} waves generated at fertilization.

During the course of studying the ability of heparin to block $InsP_3$-dependent Ca^{2+} signalling, we have found that heparin has a profound effect on the actin cytoskeleton of the starfish eggs. Since the actin cytoskeleton in part regulates intracellular Ca^{2+} signalling (Santella et al., 2008), the inhibiting effect of heparin cannot be solely ascribed to its antagonistic effect on $InsP_3$ receptors. It is not surprising that that heparin diminished the Ca^{2+} released and impaired the wave propagation in light of the fact that it is a widely used inhibitor of $InsP_3$ receptors. However, heparin failed to completely block fertilization-induced Ca^{2+} signalling even at the dose that would completely abolish $InsP_3$-dependent Ca^{2+} release, raising the possibility that $InsP_3$-dependent pathway may not be the only

mediator of Ca^{2+} releasing. Although heparin binds Ca^{2+}, as well as other divalent cations like Mg^{2+}, under physiological cytosolic conditions monovalent sulfate groups on heparin tend to complex monovalent salts (Mohri et al., 1995). Hence, the possibility of a direct buffering effect of heparin on the released Ca^{2+} is not likely to be an alternative way to suppress Ca^{2+} signals. In support of this idea, the delivery of the same concentration of the inactive antagonist De-N-Heparin did not diminish the Ca^{2+} response nor change the actin cytoskeleton.

In this study, it was found that heparin induced polyspermic interactions during fertilization of starfish eggs. Such observations have been published in echinoderm and *Xenopus* eggs using electrophysiological measurements or DNA-fluorescent dyes, e.g. Hoescht (Mohri et al., 1995; Nuccitelli et al., 1993; Santella et al., 1999). In this dissertation, increased frequency of polyspermy was demonstrated by the detection of multiple initial Ca^{2+} spots under the CCD camera. During the polyspermic fertilization of heparin-preinjected eggs, the cortical flash (CF) was very much reduced or even absent.

The CF is thought to be triggered by the opening of voltage-gated channels at the plasma membrane of eggs; thus it occurs simultaneously or as a consequence of sperm-triggered changes in the membrane potential (fertilization potential) of the egg plasma membrane. Heparin has been reported to change the electric properties of the plasma membrane (Moccia et al., 2004; Mohri et al., 1995). On the other hand, the cortex of the cell is characterized by a ring-shaped array of F-actin, and the relationship between the CF and the cortical F-actin has been already reported (Moccia et al., 2003). With no aid of exogenous Ca^{2+}-releasing second messengers or sperm, the depolymerization of the cortical F-actin by Lat-A provokes the generation of the CF, just as it happens in the sperm-induced response (Lim et al., 2002). Furthermore, results from the previous chapter indicated that heparin injection provokes changes in the actin cytoskeleton of immature oocytes. Heparin also affects the cortical actin cytoskeleton in living and fixed mature eggs, and it was linked to deregulation of many aspects of fertilization, such as vitelline

layer elevation, fertilization cone formation and sperm entry. The cortical granule exocytosis and vitelline layer elevation are known to depend on elevation of cytoplasmic free Ca^{2+}. In the presence of heparin, the Ca^{2+} augment was lower than in control situation, although not abolished. The compromised release of intracellular Ca^{2+} could be the cause of impaired vitelline layer elevation. However, the elevation is not blocked in the entire egg surface. While the reduced amount of Ca^{2+} propagated along the entire cell (Fig IV 2), the vitelline layer elevation took place only in the regions where the cortical F-actin cytoskeleton was reorganized (Fig IV 5). Then, other effects of heparin such as the extensive reorganization of the cortical actin cytoskeleton might be responsible for impeding or suppressing sperm-induced structural changes leading to the gamete fusion and cortical granules exocytosis. Such an interpretation was substantiated by the experiments with the actin-polymerizing drug JAS. In the presence of JAS, the cortical actin of mature eggs is hyperpolymerized, and the CF, which is specifically taking place in the subplasmalemmal region, is selectively absent in the fertilized eggs (Fig IV 8). In addition, JAS also induced polyspermic interaction, similar to heparin. The F-actin depolymerizating drug Lat-A was also used. Opposite to JAS, Lat-A depolymerized the actin cytoskeleton, but the effect was more readily observed in the cortical actin filaments. Similar to JAS, Lat-A had a deleterious effect on the vitelline layer elevation. Treatment of *A. aranciacus* eggs for 10 min with 1 μM Lat-A blocked the vitelline layer elevation at fertilization, although the Ca^{2+} liberated was only slightly reduced. The same effect was observed after treatment of *A. pectinifera* eggs with Lat-A 3 μM for 30min (Puppo et al., 2008). Taken together, these results suggest that the adequate fine regulation of the cortical actin network is critical in generating Ca^{2+} responses, especially CF, and cortical granule exocytosis.

The number, shape, and functionality of the fertilization cones generated were also influenced by the changes of the actin cytoskeleton after the treatment of the eggs with heparin, which produced multiple fertilization cones with the irregular shapes (Fig IV 6).

Intuitivelly, the formation of the fertilization cone is expected to be more depent on structural changes than because of ion-conducting function of $InsP_3R$. Although cytoskeletal changes by JAS suppressed some aspect of Ca^{2+} signalling, i.e. CF, our experiment with the JAS could not settle this issue on fertilization cones since the vitelline layer elevation in JAS-treated eggs was completely blocked (Fig IV 9), and no fertilization cone was formed. Such was also the case with the fertilized eggs pretreated with Lat-A (Fig IV 11). Finally, it was observed that not all polyspermic interactions resulted in sperm entry. Most of the irregular fertilization cones formed in heparin-containing eggs failed to bring the interacting sperm into the egg (Fig IV 7). As a result, most of the fertilization cones in heparin-treated eggs were empty without a sperm inside.

Actin serves as a crucial strategy in fertilization of echinoderm eggs. As demonstrated in Fig IV 1, starfish sperm extends a long acrosomal process (up to 20 μm in length), which is filled with actin filaments. Apparently, the initial Ca^{2+} burst in the egg was triggered by the acrosomal process that formed *de novo* and came into contact with the egg surface. During the initial part of the massive Ca^{2+} release, the sperm itself was clearly outside. Interestingly, the egg seem to employ the cytoskeletal system to bring the sperm in. The fertilizing sperm appeared to be associated with a long fibrous structure in the cortex of the egg (see Fig IV 1b at 4:00) that was connected with the acrosomal process. Thus, such cortical fibers were thought to provide mechanical leverage to mediate sperm entry. The notion that sperm entry depends on cytoskeleton has been proposed in several species. The sperm acrosomal process interacts with actin-filled microvilli present on the surface of the egg (Foltz and Lennarz, 1993; Runge et al., 2007). The binding could be important for triggering downstream effects rearranging the cortical actin cytoskeleton that permits sperm entry and guiding monospermy. Regarding this, experiments using Calyculin-A (Cal-A) in sea urchin eggs showed interesting results. Cal-A-treated eggs are prone to polyspermy, just as seen after heparin treatment (Tosuji et al., 2000). Cal-A is an inhibitor of serine/threonine phosphatases 1 and 2, and it plays a role in translocating

already existing cytoplasmic F-actin to the cell cortex. In this way, cortical F-actin is enhanced (Rosado et al., 2000). Here again, alteration of the cortical F-actin resulted in polyspermy. Moreover, Cal-A inhibited sperm penetration and vitelline layer elevation (Tosuji et al., 2000), a result strikingly reminiscent of our finding. TEM images showed that CGs in Cal-A treated eggs were detached from the plasma membrane and displaced into the inner cytoplasm, just as observed for CGs in starfish eggs in response to heparin microinjection (Kyozuka et al., 2008; Santella et al., 1999). Furthermore, studies in mouse eggs concluded that "cytochalasin D-treated eggs had an impaired ability to establish a block to polyspermy at the level of the plasma membrane" (McAvey et al., 2002).

It is interesting to consider that the two drugs having opposite effects but targeting the same actin subcellular pool had comparable results in Ca^{2+} modulation and vitelline layer elevation. JAS and Lat-A produced similar effect on fertilization by blocking cortical granule-exocytosis and thus vitelline layer elevation. Indeed, it is clear that while incubation with JAS blocks the generation of the cortical flash at fertilization, the CF observed after Lat-A treatment is enhanced (Fig. IV 11). Hence, it may be argued that depolymerization, in general, is permissive to Ca^{2+} signalling, while polymerization may 'buffer' its propagation. Whether the subtle difference between JAS and Lat-A on Ca^{2+} signalling could be explained by the specific changes of the local actin cytoskeleton awaites further investigation. In the case of heparin-treated cells, cortical F-actin is hyperpolymerized in living cells, no CF is observed at fertilization and the eggs present polyspermy, all traits shared with the JAS-treated eggs. Contrary to what was observed with JAS, however, the sperm-Ca^{2+} release is diminished and its dynamics are affected in heparin-pretreated eggs. This result is not surprising considering that heparin suppresses the activity of $InsP_3$ receptor. Then, the other common effects of heparin and JAS might be attributed to the changes of the cortical actin cytoskeleton: the reduced CF formation, deregulated or abolished formation of the fertilization cone, failed sperm entry, and impaired elevation of the vitelline layer.

The CF may involve the participation of the second messenger NAADP. This messenger elicits a response very much like the CF when is uncaged in mature cells, and has been shown to start the Ca^{2+} response at starfish fertilization in an F-actin dependent mechanism (Moccia et al., 2004; Moccia et al., 2003). The generation of the CF and the ensuing global propagation of Ca^{2+} may induce further actin reorganization, enabling a physiological block to polyspermy, fertilization cone formation, sperm entry and posterior vitelline layer elevation. The cortical actin pool (Heil-Chapdelaine and Otto, 1996) is in the vicinity of the plasma membrane, where an array of actin-binding proteins (ABP) are recruited and anchored through the interactions with phospholipids. As the activity of some ABP are regulated by Ca^{2+}, e.g. gelsolin, while PIP_2 hydrolysis may serve as a general mechanism of liberating the plasma membrane-bound ABP, the hydrolysis of PIP_2 (accompaying Ca^{2+} release) may have a comprehensive impact on actin reorganization near plasma membrane. And this issue will be the main focus of the following chapter.

CHAPTER V: PIP_2 dynamics at fertilization and the regulation of Ca^{2+} signalling and F-actin polymerization.

Results.

This section addresses the spatiotemporal changes of PIP_2 (Phosphatidylinositol 4,5-bisphosphate) at fertilization. PIP_2 is enriched in the plasma membrane of the cells, and is the precursor for $InsP_3$ formation under the hydrolyzing action of PLC. Moreover, PIP_2 has been identified as a modulator of actin-regulatory proteins including gelsolin (Sun et al., 1999), profilin (Janmey, 1998), the Arp2/3 complex and the Wiskott-Aldrich syndrome protein (Higgs and Pollard, 1999), as well as cofilin (Yonezawa et al., 1990). To visualize the PIP2 at the plasma membrane, we used the RFP or GFP-tagged fusion proteins containing the pleckstrin homology (PH) domain of rat PLC-δ1. This PH domain (1-140 aa) has been demonstrated to bind to the PIP_2 molecule with high affinity and specificity both *in vitro* (Lemmon et al., 1995) and *in vivo* (Stauffer et al., 1998; Varnai and Balla, 1998). Hence, this PH domain has been used as a molecular marker to delineate or block PIP_2 at the plasma membrane (Halet et al., 2002; Stauffer et al., 1998).

It has been known that the PH domain of PLC-δ1 can bind to $InsP_3$, the product of PIP_2 hydrolysis, with higher affinity than to PIP_2. While PIP_2 is bound to the plasma membrane, $InsP_3$ diffuses freely in the cytoplasm. Hence, the production and augmented levels of $InsP_3$ in the cytosol can be indirectly assessed by the decreased PH-GFP labeling at the plasma membrane (Hirose et al 1999; Nash et al, 2001). We used PH-GFP and RFP-PH to examine the timing of PIP_2 hydrolysis at the time of Ca^{2+} signalling at fertilization. In addition, it is interesting to understand whether the specific binding and sequestering of PIP_2 affects the Ca^{2+} signals at fertilization. Moreover, by sequestering PIP_2 and inhibiting

its interaction with actin-binding proteins, the PH domain would affect the actin cytoskeleton dynamics.

The PH domain of PLC-δ1 preferentially localizes in the plasma membrane of starfish oocytes.

To begin with, the distribution of injected exogenous fluorescent PH domain was studied in starfish living oocytes. Two types of bacterially expressed PH fusion proteins were used for this investigation. Each of them contained either the red fluorescent (RFP) or green fluorescent protein (GFP) tag ligated to the PH domain peptide (designated RFP-PH and PH-GFP, respectively). Since the PH domain of PLC-δ1 is used as a molecular marker for PIP_2, we have tested if it effectively visualizes the PIP_2 in starfish oocytes when delivered by microinjection.

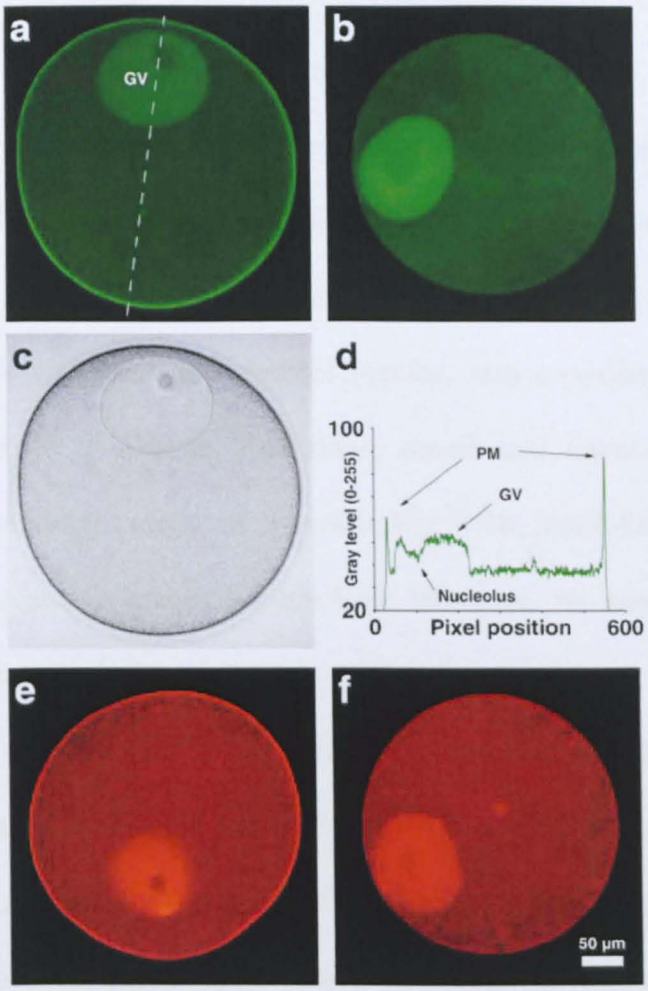

Fig V 1: The PH domain of rat PLC-δ1 preferentially binds the PIP_2 in the plasma membrane of starfish oocytes. PH-GFP or RFP-PH (9 µg/µl, pipette concentration) fusion proteins were injected in *A. aranciacus* oocytes and observed by scanning-laser confocal microscope. In 10 min, the fusion proteins localizes to the plasma membrane and germinal vesicle (GV) as expected (**a** and **e**). **b**, the distribution of R40A mutant of PH-GFP. **c,** the transmission light image of the oocyte shown in **a** is shown. **d,** the line scanning of the fluorescent intensities on the confocal plane of the oocyte in **a. f**, the distribution of the mutant R40A-RFP.

In Fig V 1, PH-GFP mainly stained the plasma membrane of the cell readily (within 5 min) and strongly, forming a continuous fluorescent ring (Fig V 1a). As shown in Fig. V 1d, the maximum levels of fluorescence were detected in the plasma membrane, where PIP_2 are preferentially located. The nucleus or GV is also green-stained, but it may have nothing to do with PIP_2 because R40A, which does not bind to PIP_2, also accumulated in the GV. Here, R40A was used as a control peptide, also conjugated to RFP or GFP. Substituting arginine 40 to alanine, this single amino-acid mutation is sufficient for impairment of PIP_2 binding. Indeed, as shown in Fig V 1b, R40A-GFP evenly stains the cytoplasmic domain, and it enters the nucleus. However, no specific localization is observed in the plasma membrane.

The RFP and GFP tag did not make any difference in reproducing the characteristic localization at the plasma membrane, although the RFP and GFP tags are added at different ends of the protein (N versus C terminal). Thus, both types of constructs can be used interchangeably, as needed, e.g. in combination with other fluorecent probes such as Ca^{2+} dye of Alexa Fluor-tagged phalloidin.

When the oocytes microinjected with PH-GFP or RFP-PH were examined by confocal microscopy at higher magnitude, numerous filamentous structures were detected on the surface of the cell (Fig V 2). These are short microvilli-like projections protruding from the plasma mambrane into the jelly coat. Although the probe has reached the plasma membrane, it does not instantly stain microvilli on the surface. Some minutes later, the filaments start to be stained and visible on the surface. This event occurs in parallel with the entry of the PH probe into the nucleus, indicating that the protein is still distributing inside the cell and reaching its targets. The PH-GFP-stained microvilli continually changed their length, indicating that the underlying structure is at dynamic equilibrium (Fig V 3).

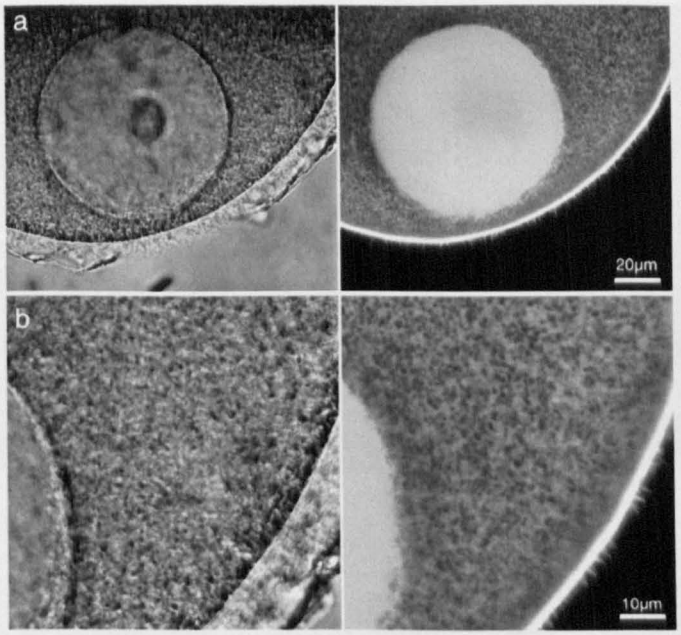

Fig V 2: PH-GFP visualizes filaments PIP_2 at that plasma membrane and delineates microvilli on the surface of starfish oocytes. *A. aranciacus* oocytes were injected with PH-GFP protein (9 μg/μl, pipette concentration) and observed with confocal microscope. Filaments are observed emitting from the surface.

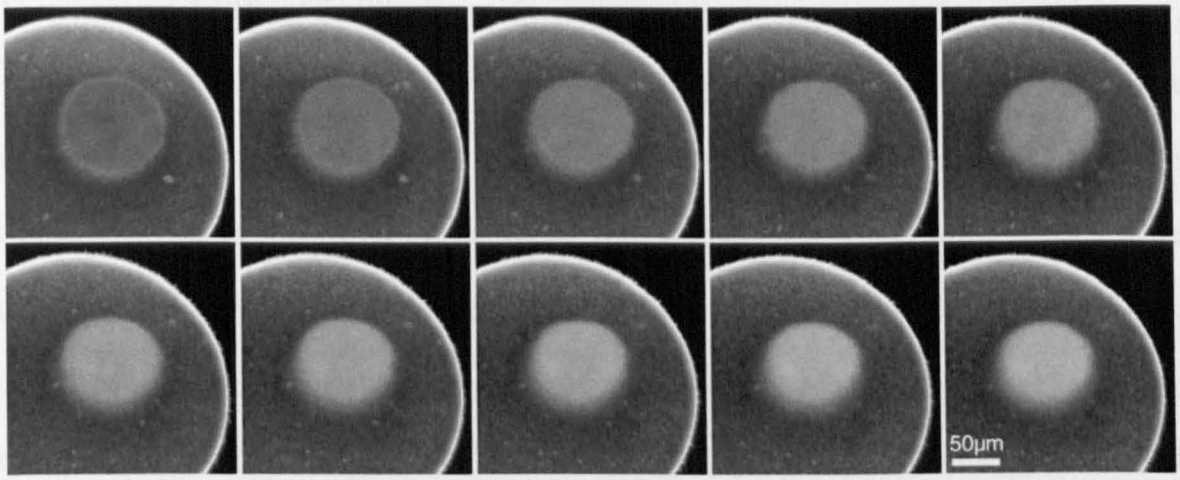

Fig V 3: PH-GFP stains dynamic filaments in the surface of the oocytes. *A. aranciacus* oocytes were microinjected with PH-GFP (9 µg/µl, pipette concentration) and immediately observed by confocal microscopy. Images were taken every 45 sec. The probe immediately reaches the plasma membrane and gradually enters the germinal vesicle. At 1.5 min, PH-GFP-positive filaments started to be visible in the surface of the oocyte.

The changes of PIP_2 at fertilization.

In order to monitor the dynamics of $PIP_2/InsP_3$ metabolism and Ca^{2+} response at fertilization, I have microinjected the RFP-PH inside mature eggs along with Calcium Green. The images obtained while analyzing with a CCD camera are shown in Fig V 4. In the column **a**, RFP-PH staining changed after fertilization. In **b**, the transmission light images were merged with the Ca^{2+} responses. In the first row of the panel, the fertilizing sperm has arrived at the surface of the cell (set to 0:00). The release of Ca^{2+} was first detected 0:27, while the sperm was still outside the jelly coat. Also, the RFP-PH staining was not changed at all when the Ca^{2+} burst first appeared. It is only at 0:36, while the Ca^{2+} wave is propagating towards the opposite pole of the cell, that an augment of RFP-PH signal was detected at the plasma membrane level in the region where the Ca^{2+} wave has already passed. The RFP-PH signal continues to increase in the areas of the plasma membrane that have been already swept by the Ca^{2+} wave (time 0:40). The RFP-PH augment occurs even before the vitelline layer elevation takes place (at times 0:36 and 0:40). Even after the vitelline layer has started to elevate, the PH-RFP signal increase is observed in the plasma membrane (time 1:44), specially in the spot where the sperm is making its entry.

There are two periods of PIP_2 elevation following fertilization. The first increase takes place 10 sec after the onset of the Ca^{2+} signals (Fig V 4c). The rise is brief and immediately followed by the decline. Soon after, synchronized with the elevation of the vitelline layer, the PIP_2 level at the plasma membrane is elevated for a prolonged period (asterisk in Fig V 4). Hence, it appeared that the PIP_2 increase may have two distinct physiological significances at fertilization.

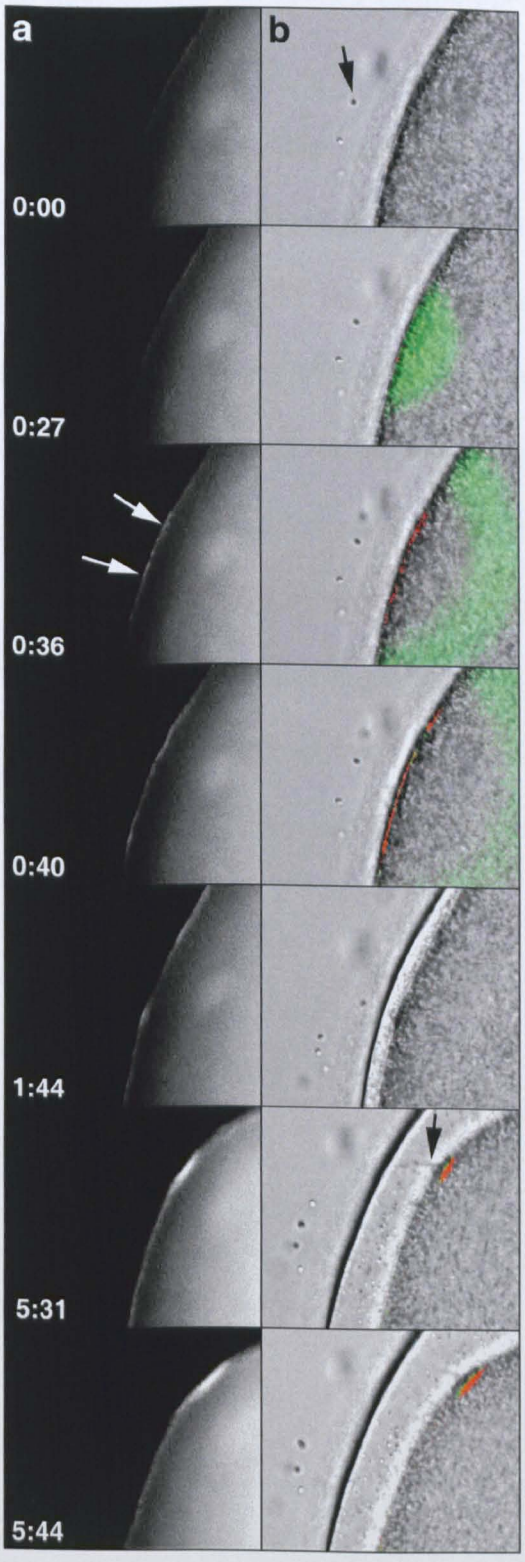
a
b
0:00
0:27
0:36
0:40
1:44
5:31
5:44

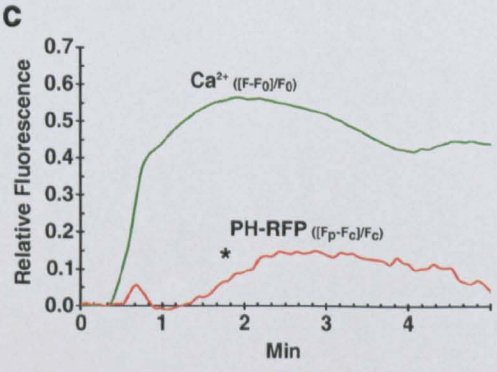
c
Relative Fluorescence
0.7
0.6
0.5
0.4
0.3
0.2
0.1
0.0
0
1
2
3
4
Min
Ca2+ ((F-F0)/F0)
PH-RFP ((Fp-Fc)/Fc)
*

Fig V 4: PH domain signal augments in the plasma membrane at fertilization. A mature egg preinjected with Ca^{2+} dye and RFP-PH (9 μg/μl, pipette concentration) was fertilized while monitoring under the CCD camera. The sperm arrival to the jelly coat was considered as time 0:00. **a**, changes in the RFP-PH localization. **b**, Ca^{2+} signals merged with the bright field view of the oocyte. At 0:27, the sperm triggered the Ca^{2+} wave. After the Ca^{2+} wave swept away, an increase in the PH-RFP signal is observed in the plasma membrane (arrows, time 0:36). At time point 1:44 the vitelline layer starts to elevate. **c**, Temporal relationship between sperm-induced Ca^{2+} wave ($F_{rel}=[F-F_0]/F_0$; green curve) and the relative fluorescence ($F_{rel}=[F_{pm}-F_{ct}]/F_{ct}$; red curve) for plasma membrane PIP_2 labelling. The F_{rel} value for RFP-PH changes 10 sec after the beginning of the Ca^{2+} release. The plasma membrane RFP-PH F_{rel} values first augments but falls 10 sec later, indicating translocation into the cytosol. Then, it rises again (asterisk).

RFP-PH stains spikes formation on the egg surface after fertilization.

In order to better analyze the subcellular changes in the RFP-PH distribution after the arrival of the sperm, I have performed confocal microscopy experiments. As already described, the confocal distribution of RFP-PH is preferentially at the plasma membrane level (Fig V 5a). In this region of sperm interaction, the continuity of the RFP-PH signal was lost as spikes projecting from the plasma membrane began to appear (arrow) when the vitelline layer started to elevate at 2 min. At 4 min, the fertilization cone started to form, presenting a very strong RFP-PH staining (arrow). At this moment, the sperm began to penetrate the egg and the fertilization envelope formed. From this time point on, the numerous fluorecently labelled spikes grew in length. At 11 min, the fertilization cone is well developed and strongly stained, enabling the sperm entry. The fertilization cone then retracts and seals in the plasma membrane, and spikes are still present from the plasma membrane to the vitelline layer (arrow at 20 min). When R40A-RFP was preinjected, it did not localize at the plasma membrane. After fertilization and the fertilization cone formation, no filaments were observed emitting from the surface (4 min) towards the perivitelline space. At 5 min, the start of the fertilization cone formation is visible, and stains very strongly with R40A-RFP. The staining disappears after the cone has been engulfed (at 11 min).

The RFP-PH-stained spikes in the perivitelline space contain F-actin.

By preinjecting phalloidin in the eggs and performing fertilization it was studied whether these fibers were actin-containing. The results obtained by confocal microscopy are shown in Fig V 6. The sperm already entered the egg, the FC retracted, and the FE was fully elevated. In panel **b**, the phalloidin stained image shows that the cortical actin fibers were rearranged after sperm entry, and that the spikes were extended from the surface of the egg towards the vitelline envelope (arrowheads). This suggests that the same RFP-PH positive filaments are F-actin-containing (arrowheads). In addition, many long and thick

actin bundles were associated with the penetrating sperm (arrow). This kind of structure probably helps sperm entry into the egg, and resembles the filamentous structure detected under CCD camera in Fig IV 1 (in the previous chapter).

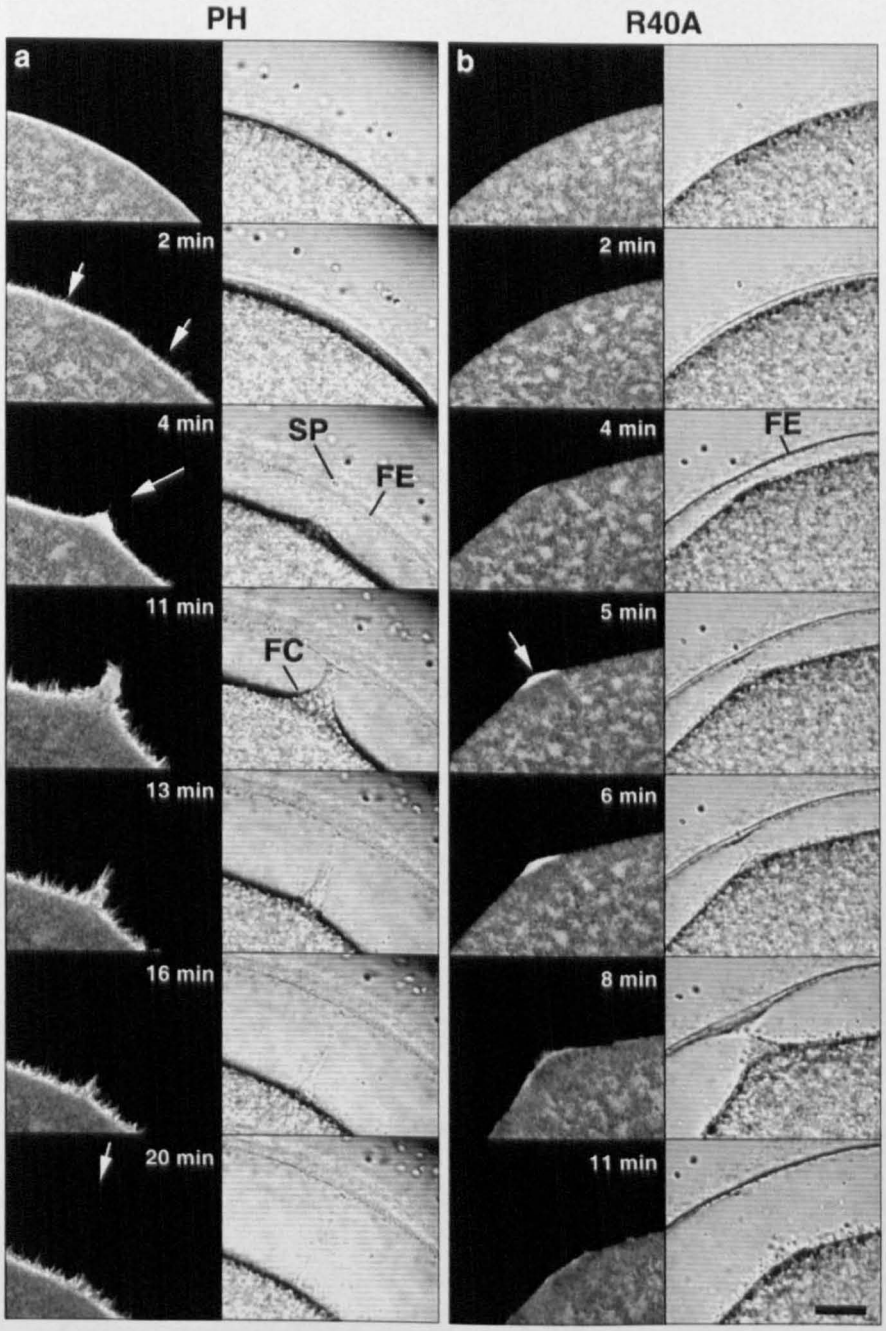

Fig V 5: The increase of PIP_2 at the plasma membrane during the later stage of fertilization is associated with the spike formation and elevation of the fertilization envelope. *A. aranciacus* eggs preinjected with RFP-PH (9 μg/μl) were fertilized and examined by confocal microscopy. **a**, In the left panel, the RFP-PH fluorescent images are shown; and in the right, the corresponding bright field view. At 2 min the RFP-PH signal increased at

the plasma membrane, and spikes appeared (arrows), while the vitelline layer started to elevate. At 4 min, the fertilization cone stained by RFP-PH is visible (arrow). In the bright field image the fertilizing sperm (SP) is in the focal plane, and the fertilization envelope (FE) is forming. At 20 min the fertilization cone has disappeared but two groups of filaments are seen, of shorter length and longer (arrow). **b**, Images of the control egg preinjected with R40A-RFP. Scale bar: 20 μm.

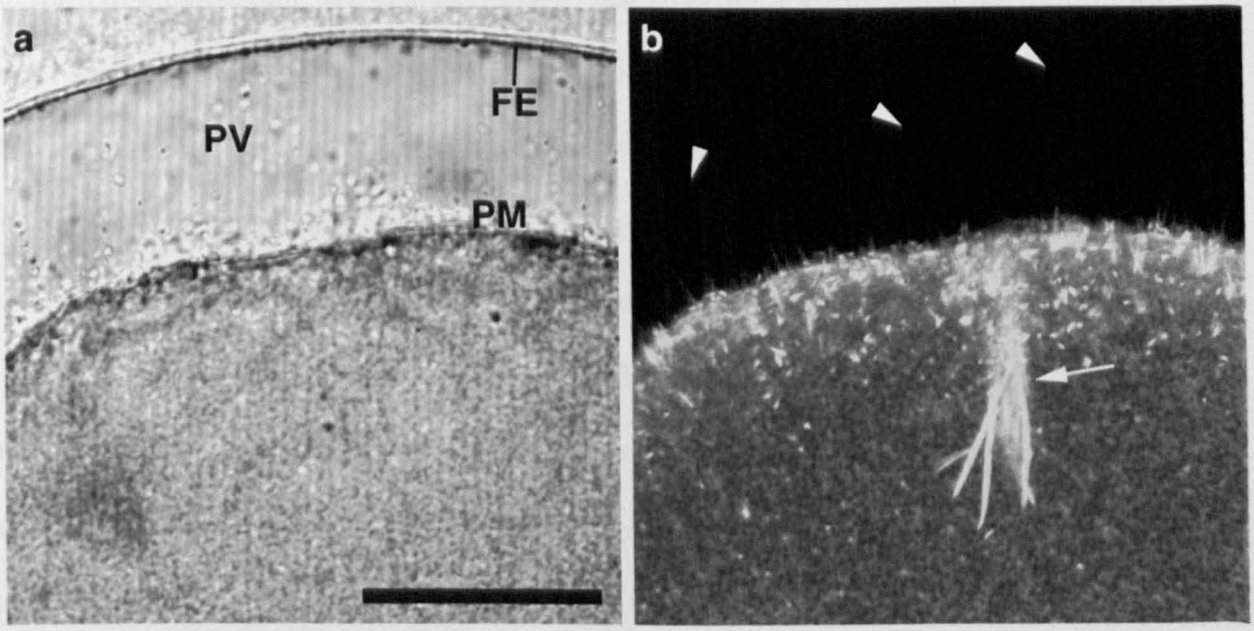

Fig V 6: The spikes formed in the perivitelline space during fertilization contain actin filaments. *A. aranciacus* eggs loaded with fluorescent phalloidin were inseminated. **a**, a transmitted light image after 10 min. **b**, the corresponding confocal images showing fluorescent phalloidin. After vitelline layer elevation, phalloidin-positive filaments were observed to emit from the plasma membrane (PM) and to reach the fertilization envelope (FE) (arrowheads). Inside the egg, long and thick F-actin bundles were detected at the sperm site entry (arrow). Scale bar. 50 μm.

Sequestration of PIP_2 with RFP-PH affects Ca^{2+} signalling at fertilization.

RFP-PH, by binding to PIP_2, could mask the substrate necessary for $InsP_3$ production. If this is the case, the Ca^{2+} signalling during fertilization could be influenced by the presence of RFP-PH. We have then performed co-injection of the RFP-PH (or the mutant analog R40A-RFP) along with the Ca^{2+} indicator dye and analyzed the Ca^{2+} pattern generated during fertilization under a CCD camera. Fig V 7a shows the spatiotemporal properties of the Ca^{2+} signals. The spatial component does not differ much between the RFP-PH and the control (R40A-RFP), since in both cases we observe a cortical flash and then a Ca^{2+} spot that from the point of sperm interaction, expands to the rest of the cell in the form of a half-moon. We can see though, that at 91 sec Ca^{2+} has been liberated in the whole surface of the egg injected with R40A-RFP. However, at the same time point, the Ca^{2+} is still being liberated and diffusing along the RFP-PH containing cell, showing that the temporal component has been altered. This is better depicted in the graph of Fig V 7b. RFP-PH microinjected cells reaches its maximum at 190.4 ± 85.0 sec (n = 18), later than the control cell containing R40A-RFP (134 ± 38.7 sec, n = 19). Furthermore, the Ca^{2+} amount liberated is also less than in the control egg. The average amounts of Ca^{2+} concentration released in PH-RFP microinjected cells is 0.87 ± 0.21 RFU (n = 18), slightly lower than in R40A-RFP-treated eggs, where the values reached 1.0 ± 0.15 RFU (n = 19).

Moreover, the occasions of polyspermic interactions increased in the PH-RFP-preinjected eggs. In the table of Fig V 7c, the number of interacting sperm with the RFP-PH- preinjected eggs is significantly higher than in the control (containing just Ca^{2+} dye) or in R40A-preinjected eggs. The question whether RFP-PH affects Ca^{2+} release during fertilization by a mechanism other than simply blocking PIP_2 access to PLC could be answered by uncaging of $InsP_3$ in the eggs preinjected either with RFP-PH or R40A-RFP. In this way, $InsP_3$ is already supplied to the cell so that PIP_2 hydrolysis is not necessary.

The eggs preinjected with RFP-PH displayed other abnormalities at fertilization. Those cells containing RFP-PH showed a big percentage of partial and even blocked vitelline layer elevation.

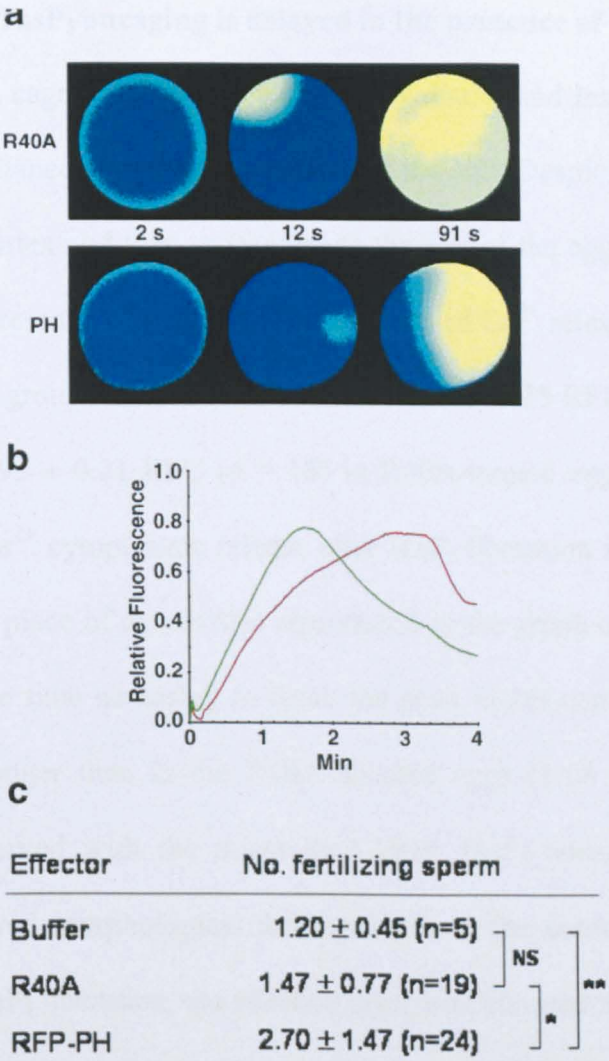

Fig V 7: RFP-PH attenuates the Ca^{2+} signalling at fertilization and induces polyspermy. **a**, Pseudo-coloured images showing the intensities and distribution of Ca^{2+} release in R 40A-RFP (9 µg/µl, top panel) and RFP-PH (9 µg/µl) preinjected eggs at fertilization. **b**, both the R40A-RFP (green curve) and RFP-PH (red curve) show the small increase in the beginning of the plot corresponding to the cortical flash, and the maximum relative fluorescence values was slightly lower in the eggs preinjected with RFP-PH. The Ca^{2+} rise in the RFP-PH eggs reaches the maximum significantly later than the control. **c**, Eggs were loaded with Ca^{2+} dye and injected with the injection buffer, R40A-RFP or RFP-PH. The number of initial Ca^{2+} spots was counted as an index of polyspermy. *P<0.01, **P<0.001, NS = non-significant.

The Ca^{2+} response to $InsP_3$ uncaging is delayed in the presence of RFP-PH.

After injection, caged $InsP_3$ is homogeneously distributed inside the cell, and UV-liberation occurs simultaneously in all the regions of the cell. Despite this, Ca^{2+} is released preferentially in the cortex and then propagates to the rest of the egg. This feature has not been changed by the presence of RFP-PH. The amounts of Ca^{2+} released were virtually the same between the two groups of cells with values of 0.97 ± 0.25 RFU (n = 15) in RFP-PH treated cells versus 0.93 ± 0.21 RFU (n = 15) in R40A-treated eggs (Fig V 8a). On the other hand, the fast Ca^{2+} cytoplasmic release after $InsP_3$ liberation is delayed in RFP-PH preinjected eggs. This piece of data is also reproduced in the graph of Fig V 8a. The mean values indicate that the time necessary to reach the peak in PH-containing eggs is 1.77 ± 1.03 sec (n = 15), longer than in the R40A-injected eggs (1.18 ± 0.63 sec, n = 15). Moreover, when observed with the transmitted light, $InsP_3$ uncaging in the RFP-PH-preinjected eggs showed morphological differences from the control. After the massive Ca^{2+} release due to $InsP_3$ liberation, the vitelline layer was elevated normally in the control eggs containing R40A-RFP. However, the eggs preinjected with RFP-PH showed impaired vitelline layer elevation (Fig V 8). In some cases the cortical granule exocytosis occurred all along the surface of the cell, but the vitelline layer did not elevate enough as the control (R40A-RFP) eggs, remaining at a closer distance from the plasma membrane. In other cases, the vitelline layer did not elevate at all in one hemisphere of the cell (Fig V 8b). The percentages of vitelline layer elevation after $InsP_3$ uncaging in the presence of injection buffer, R40A or RFP-PH are shown in figure V 8c.

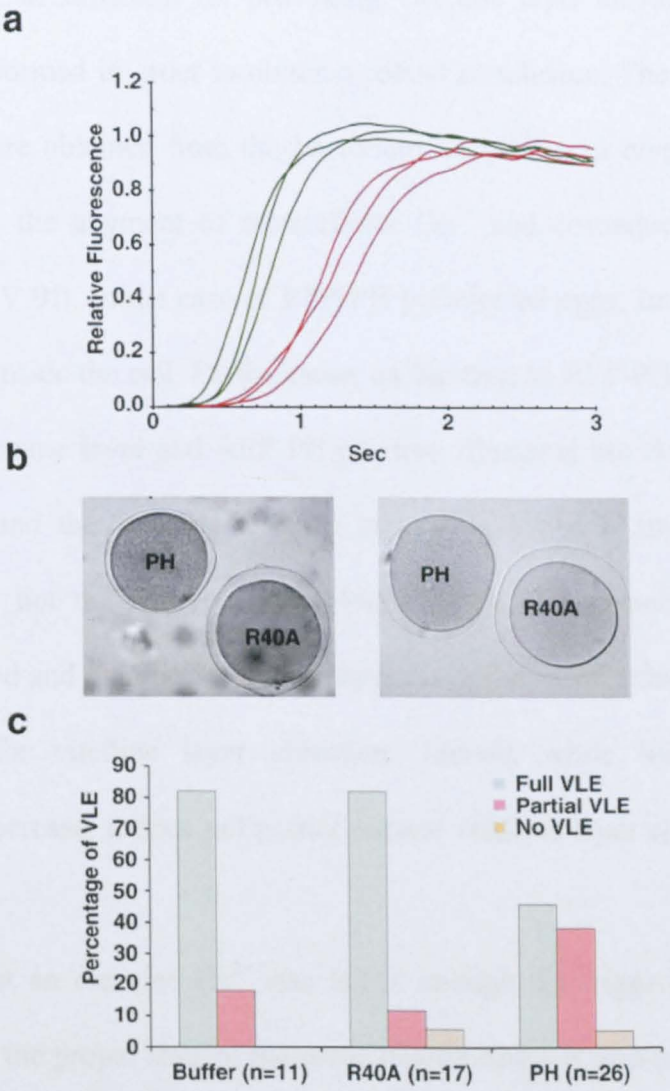

Fig V 8: RFP-PH delays the Ca^{2+} response to $InsP_3$ uncaging and affects vitelline layer elevation. *A. aranciacus* oocytes loaded with Ca^{2+} dye and caged $InsP_3$ were matured for 1hr by 1-MA. Then, they were injected with R40A or RFP-PH and irradiated with UV light. **a**, Ca^{2+} signalling after UV-photoactivation of $InsP_3$. In the case of RFP-PH-injected eggs (red curves), the Ca^{2+} release was delayed when comparing with the control (R40A, green curves). **b**: Bright field images of R40A- and RFP-PH-preinjected eggs, showing the partial vitelline layer elevation in those eggs containing RFP-PH. **c**, the percentages of vitelline layer elevation (VLE) after $InsP_3$ uncaging in the presence of Injection Buffer, R40A or RFP-PH.

The impairment of vitelline layer elevation could be again explained by a Ca^{2+} release lower than that sufficient for provoking vitelline layer elevation. Thus, another experiment was performed in order to obtain a robust conclusion. The drug Ionomycin, a potent Ca^{2+} ionophore obtained from the bacterium *Streptomyces conglobatus* was used. This drug provokes the augment of intracellular Ca^{2+} and consequent cortical granule exocytosis (see Fig V 9f). In the case of RFP-PH preinjected eggs, Ionomycin incubation induces a Ca^{2+} rise inside the cell. Furthermore, an increase in RFP-PH signal is generated at the plasma membrane level and RFP-PH-positive filaments are detected between the plasma membrane and the elevated vitelline layer (Fig V 9a, b and d). However, the vitelline layer does not uniformly elevate (Fig V 9 c). The presence of the RFP-PH provokes an impaired and polarized vitelline layer elevation, confirming that Ca^{2+} increase is not sufficient for vitelline layer elevation. Indeed, while Ionomycin creates a considerable Ca^{2+} increase, it does not permit normal vitelline layer elevation in the RFP-PH presence.

Since it is clear that an elevated Ca^{2+} rise is not enough for triggering cortical granule exocytosis, and that the proper state of the cortical actin fibers is also relevant, the RFP-PH influence on the actin cytoskeleton was important to study.

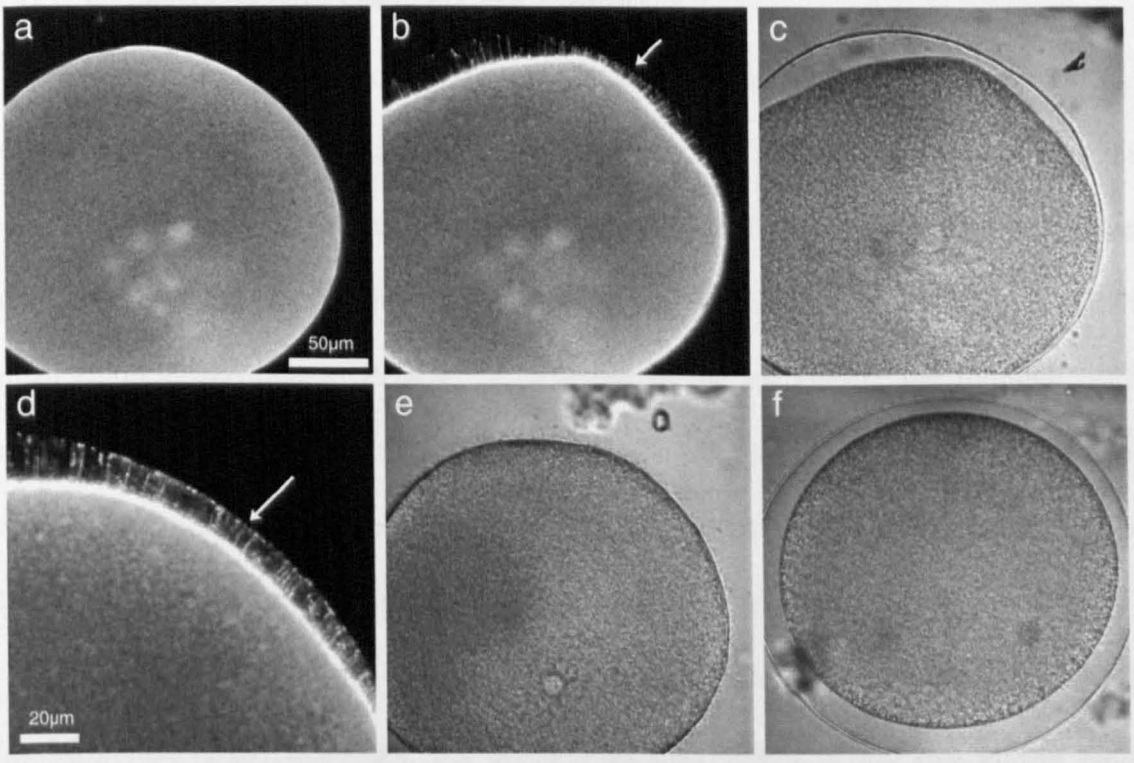

Fig V 9: RFP-PH impedes normal vitelline layer elevation due to Ionomycin incubation. *A. aranciacus* eggs were injected with RFP-PH (9 µg/µl), and Ionomycin (10µM) was added while analyzing under the laser-scanning confocal microscope. **b**, At 4 min after Ionomycin addition (at time 0 min, **a**), the RFP-PH signal at the plasma membrane increases and filaments are seen projecting from the plasma membrane (arrow). The corresponding bright field on the right shows that the vitelline layer elevation has been partially impaired (**c**). A higher magnification of the same egg is shown after 8 min in **d**. In **e**, an egg incubated with DMSO in sea water does not elevate the vitelline layer. A control egg incubated with Ionomycin is shown in **f**, with its vitelline layer normally elevated.

RFP-PH colocalizes with newly formed F-actin.

Mature eggs microinjected with phalloidin show an array of fibers apposed to the plasma membrane, as well as actin fibers resembling 'porcupine spines' in the inner cytoplasm (Fig V 10a). In the unstimulated eggs, PH-GFP stained the PIP_2 in the plasma membrane but not the actin fibers in the inner cytoplasm (Fig V 10c). Lower intensities of green fluorescence due to PH-GFP is detected in the cytoplasm, the rounded profiles suggest that the staining identifies the ER *cisternae*. At these unstimulated or steady-state conditions, the signals emitted by the two probes cannot be said to colocalize, although they share some patterns of distribution in the cortex of the egg.

Surprisingly, when the eggs were subjected to actin-polymerizing drug Jasplakinolide (JAS) treatment, the changes of distribution of the two probes showed remarkable similarities. In Fig V 10b, JAS has hyperpolymerized the F-actin, as expected. Very long and ordered F-actin fibers are seen in the cortical area, perpendicularly to the plasma membrane. Also, the internal region of the cell has been affected but in a different way, undergoing F-actin fibers-depletion. Probably, cytoplasmic actin monomers have been recluted to the cortical area to induce the observed cortical hyperpolimerization, devoiding the inner cytosol of fibers. Indeed, it has been reported that JAS increases the actin fibers adjacent to the plasma membrane in smooth muscle and Madin-Darby canine kidney cells, accompanied by the loss of stress fibers (Bubb et al., 2000). The JAS-induced loss of F-actin labeling in some cellular domains *in vivo* is due to the dual effects of JAS. On one hand, it stimulates G-actin liberation from actin-sequestering proteins, and on the other hand, it induces nucleation and elongation from existing filament ends (Bubb et al., 2000).

Most interesting is the change experienced by the PH-GFP probe after JAS incubation. While the plasma membrane staining was maintained, additional RFP-PH-positive structures were observed in the cortical region. The staining shows a fibrillar nature, just like the phalloidin one. These fibers look more compact and thinner in

structure, and extend to the same thickness from the plasma membrane to the cytoplasm as the phalloidin fibers do (see asterisks in Fig V 10 b and d). Also in this situation, the enhanced staining at the cortical region meant a lowering of the internal fluorescence. These results suggest that the PH-GFP probe could be detecting F-actin containing structures induced by JAS and formed *de novo*, either by direct or indirect binding. In the figure V 10e, the R40A-GFP distribution in a mature egg is shown. Like the case of immature oocytes, the mutant probe does not bind the PIP_2 in the plasma membrane. After JAS incubation, however, fiber-like structures are recognized by the probe in the cortex of the egg. The cytoplasmic staining has undergone some changes as well, but has not been completely abolished (Fig V 10f) as in the RFP-PH case. It is surprising that the mutant analog R40A-RFP, unable to recognize the PIP_2 molecules, is still relocated to the cortex and stains the *de novo* formed actin fiber-candidates.

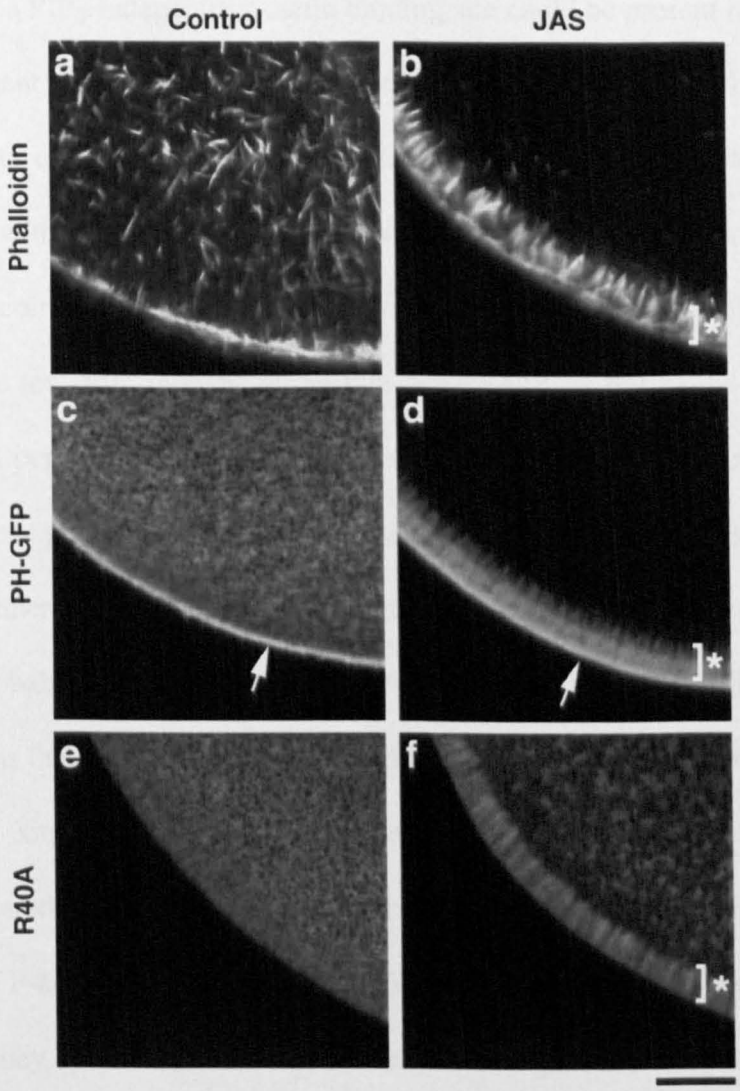

Fig V 10: PH-GFP colocalizes with newly polymerized F-actin. Mature *A. aranciacus* were injected with Alexa Fluor 488-conjugated phalloidin (50 µM, **a** and **b**), with PH-GFP (9 µg/µl, **c** and **d**) or with R40A-GFP (9 µg/µl **e** and **f**). Then, they were incubated with JAS (12 µM, 20 min) or with DMSO. The increased actin filaments polymerized by JAS are signalled by an *, and the PH-GFP stain at the plasma membrane is indicated by arrows. Scale bar: 20 µm.

This suggests that a PIP_2-independent- actin binding site could be present in these proteins.

In agreement with the idea that PH distribution correlates with areas of actin remodeling are the confocal immages of immature *A. aranciacus* oocytes injected with heparin and then with the PH-GFP domain. As discussed in the previous section, heparin can remodel the cortical F-actin. In Fig V 11, PH visualizes *fibers* projecting from the plasma membrane inwardly into the cytoplasm, where PIP_2 is not likely to be located. If the PH and R40A peptides actually have the ability to associate with actin fibers, then the preinjection of these peptides could alter the access of phalloidin and the staining of the F-actin. This experiment has been performed and the results are shown in Fig V 12. In the case of R40A, probably the main difference when compared to the control (just containing Injection Buffer) is that more fibers are detected in the inner cytoplasm. The cortical fibers, as in the control situations, are located perpendicularly to the plasma membrane in a compact and ordered form. In the RFP-PH preinjected eggs though, phalloidin stains a thinner cortex of F-actin. The fibers are not displayed in a palisade perpendicular to the cortex. Instead, they seem to be shorter or arrayed in a parallel direction to the plasma membrane. The net result is the staining of a thinner cortex when the eggs contain RFP-PH, poorer in F-actin.

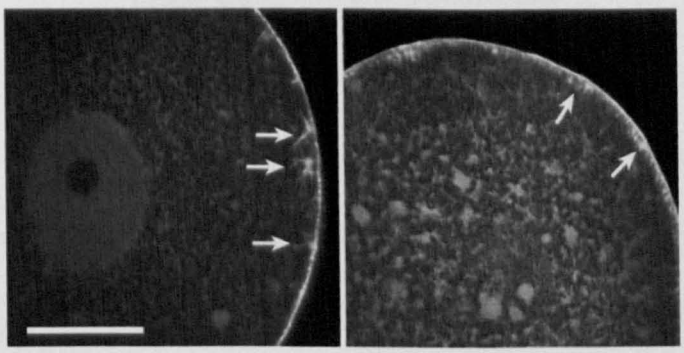

Fig V 11: PH-GFP visualizes fibers induced by heparin injection. *A. aranciacus* oocytes were injected with heparin (50 μg/μl) and then with PH-GFP (9 μg/μl). The confocal observation revealed the presence of fibers in the subplasmalemmal area of the oocytes (arrows). Scale bar = 50 μm.

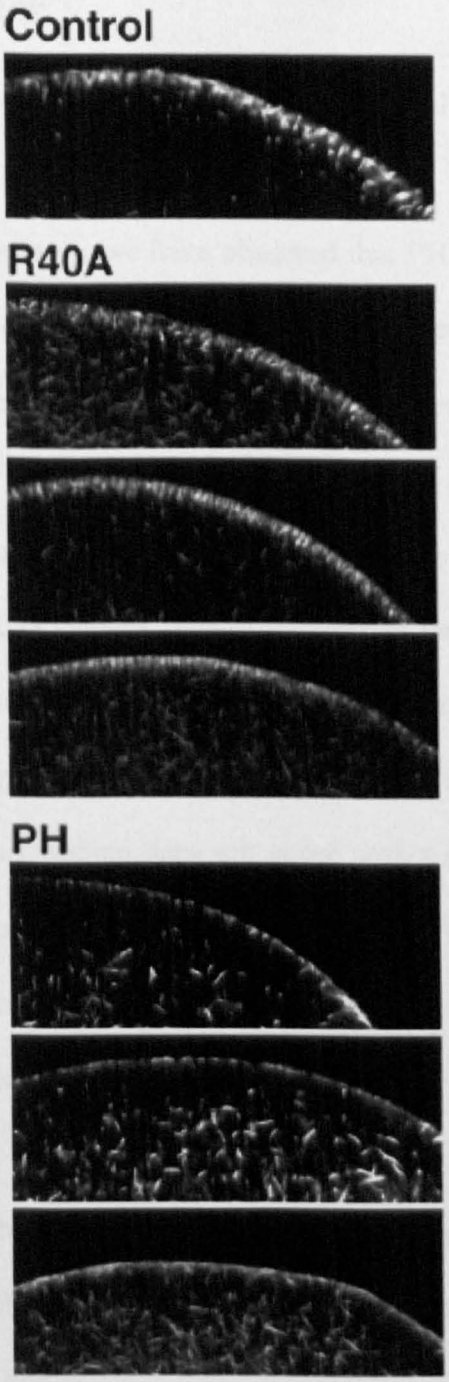

Fig V 12: RFP-PH affects the subplasmalemmal F-actin network. Postmeiotic eggs of *A. aranciacus* were microinjected with either RFP-PH or R40A-RFP (15 µg/µl, pipette concentration) and incubated for 25 min. In the figure, an area of three different treated cells is shown for each condition. The actin cytoskeleton was visualized by Alexa Fluor 488-conjugated phalloidin.

Discussion for Chapter V.

The RFP-PH fusion protein used in this work specifically visualized the PIP_2 at the plasma membrane of starfish oocytes, as was demonstrated in various other cell types (Stauffer et al., 1998). Interestingly, we have observed that PH domain stains short finger-like protrusions present in the surface of starfish oocytes. Since the surface of the oocytes is known to be covered with microvilli, such protrusions were considered microvilli that were visualized thanks to the staining of the PIP_2 present in the plasma membrane.

The changes of plasma membrane PIP_2 levels at the time of fertilization were studied under the cooled CCD camera. The simultaneous measurements registering the changes of RFP-PH (red) and of the Ca^{2+} ions (green fluorescence) showed that RFP-PH decrease, representing PIP_2 hydrolysis, were detected *after* the major part of Ca^{2+} wave had been already propagated. This finding does not agree with a need for $InsP_3$ formation in order to initiate the intracellular Ca^{2+} release. It is known that the PIP_2 turnover is small in comparison to the big PPI turnover at fertilization (Ciapa et al., 1992), and it has been proposed that the degradation is immediately compensated by synthesis (Halet et al., 2002). Thus, if the initial degradation has passed unobserved in our case due to methodological limits, and the PH-staining increase is due to posterior PIP_2 synthesis, the question remains as to the physiological function that PIP_2 may play after the Ca^{2+} wave has already swept across the egg.

We have observed that the PIP_2 level at the plasma membrane is elevated for extended period of time after the Ca^{2+} signal at fertilization. This increase appears to represent the net increase of PIP_2 contents at the plasma membrane. Intuitively, the PIP_2 level at the plasma membrane was expected to decrease as PIP_2 is hydrolyzed to $InsP_3$ to support Ca^{2+} signalling. However, biochemical mass assays indicate that only a small quantity of $InsP_3$ is formed before the Ca^{2+} wave generation, and that the major increase occurs at the time of Ca^{2+} peak (Kuroda et al., 2001). The $InsP_3$ levels may continue to rise even after the Ca^{2+} cytoplasmic concentration is declining (Kuroda et al, 2001). In

accordance with our results, plasma membrane PIP_2 levels increased during fertilization of mouse oocytes (Halet et al., 2002).

A very interesting observation was made in sequential confocal images taken during fertilization. After sperm arrival and during vitelline layer elevation, RFP-PH-stained spikes were observed to protrude from the plasma membrane and invade the perivitelline space. The fluorescence emitted by the filaments, which rest close to the plasma membrane, could contribute to the augmented PH signal observed at fertilization. The filaments extending towards the vitelline layer are observed until 20 min after sperm arrival. A possible function for them would be to keep the vitelline layer in its elevated position, and could play a later role in positioning the daughter cells after the first mitosis and keeping the polarity for the future embryo. Such filaments have been described in sea urchin species, presenting heterogeneous lengths as well (Spiegel et al., 1989). In sea urchin, they are dynamic and "elastic", changing length during cell divisions. The RFP-PH stained filaments in starfish eggs are also F-actin-containing, as shown by phalloidin staining. Thus, they might be formed *de novo* on the microvilli basis by extending the existing actin filaments, or borrowing plasma membrane and cytoskeletal componenets from them.

On the other hand, the fluorescent PH domain proved not to be just a passive reporter for PIP_2 or $InsP_3$ formation. In our hands, the injection of RFP-PH slightly lagged the Ca^{2+} dynamics after fertilization and $InsP_3$ photoliberation, but the point mutant control protein R40A-RFP did not. Although the total amount of liberated Ca^{2+} was similar to the control, the vitelline layer elevation was affected, showing either reduced swelling and elevation of the vitelline layer as well as partial block at one pole of the cell. Then, polyspermy was enhanced in eggs microinjected with RFP-PH. The phenotypes of vitelline layer elevation and polyspermy observed in presence of PH domain resemble those observed in the fertilization experiments carried out with heparin in the previous chapter.

Interestingly, heparin-injected sea urchin eggs showed delayed and reduced PH-GFP translocation at fertilization (Thaler et al., 2004). Due to the $InsP_3R$ antagonist function of heparin, it should not influence the $InsP_3$ formation and thus PH domain translocation. The authors though, taking into consideration the Ca^{2+} sensibility of PLC indicated that the reduced Ca^{2+} amount liberated in the cytosol of heparin-containing eggs would affect PLC activation. As shown in the results, and according to what published by Thaler and Halet, Ca^{2+} increase is necessary for PH-reported changes. However, vitelline layer elevation was also impaired in ionomycin-incubated eggs, indicating that the sequestration of PIP_2 by PH alters vitelline layer elevation.

Affected vitelline layer elevation could result from impaired formation of filaments at fertilization that can not support a normal vitelline layer elevation. As it is known, PIP_2 regulates actin binding proteins that may interfere with the F-actin present in the cortex of the cell (Di Paolo and De Camilli, 2006). Moreover, the PH-stained filaments have been demostrated to be built from actin filaments. Thus, the PH domain could interfere with the PIP_2 in the membranes having a negative impact on the actin rearrangements necessary for filament construction.

Similarly, PH could alter the docking or exocytosis of cortical granules. PIP_2 is known to be directly involved in exocytotic processes (Di Paolo and De Camilli, 2006), and it could in turn affect the cortical actin cytoskeleton via association with ABP. Indeed, Fig V 12 shows that preinjection of PH domain changes the cortical F-actin as visualized by phalloidin staining. After stimulation by sperm, the rearrangements could be even more drastic.

Moreover, it was discovered that PH marks regions where actin has been synthesized *de novo*. When F-actin polymerization was induced by JAS incubation, the pattern of RFP-PH distribution colocalized with that of phalloidin. Even clear fibrous structures are seen with the PH marker (Fig V 10). Enrichment of PIP_2 in actin-rich lamellipodia-like structures has been reported (Watt et al., 2002), as well as colocalization

with microvillus-like protrusions and dynamic ruffles in NIH-3T3 fibroblasts (Tall et al., 2000), which involve areas of continuous reorganization and events of actin hypo and hyperpolarization. It has been proposed that the basically charged ABPs responsible for actin remodelling would create a positively-charged environment, thus building a diffusion barrier for the PIP_2 lipid and making it colocalize with F-actin (Downes et al., 2005). Moreover, the increase in the PH domain signal after fertilization observed in mouse oocytes is inhibited by the addition of the actin-depolymerizing drug Cyto-B (Halet et al, 2002). While the authors assume that the disruption of the cytoskeleton could influence the anchorage of the PIP_2 synthetic machinery in the plasma membrane, it could as well be due to a lack of PH domain staining to the reduced F-actin in the cortex.

RFP-PH has also stained the fertilization cone, as observed in Fig V 5. All the fertilization cone is filled with RFP-PH staining, but as the images were taken in one confocal plane, the fluorescent signal corresponds to the plasma membrane staining as well as the actin fibers from which the fertilization cone is composed of. The negative mutant R40A-RFP also visualizes the fertilization cone interior, but not the plasma membrane. Then, in figure V 10, after JAS treatment it displays almost the same pattern of distribution than phalloidin. Such results indicate a possible direct association with actin that had not previously been reported. Direct binding experiments carried in the Lab have shown that there is indeed a weak direct binding between RFP-PH and R40A-RFP with actin (Chun et al under revision). Such findings pose some doubts on the existence of more non described bindings with other proteins.

In conclusion, it has been observed that the PH domain signal in the cortex of fertilized starfish eggs augments at fertilization, after the Ca^{2+} wave has been generated and propagated. The discovery that the PH domain signal correlates to PIP_2 rich areas *plus* to those with dynamic rearrangement of F-actin, binding via ABPs or due to direct interaction, gave the clues to explain our observations.

Since the decrease in the PH signal was observed seconds after the Ca^{2+} signalling started, the sperm arrival would generate Ca^{2+} release due to generation of second messenger others than $InsP_3$. Indeed, the role of NAADP in the priming of the Ca^{2+} response of starfish eggs has been documented (Moccia et al., 2004). Moreover, actin rearrangements are necessary to ensure monospermy and normal sperm entry, as shown in the previous chapter. Ca^{2+} cytoplasmic increase as well as the actin changes would trigger cortical granule exocytosis. The exocytosis of the granules has two consequences, the increase of the plasma membrane after fusion and the vitelline layer elevation. Further, the granules contain PIP_2 synthetic machinery (Halet et al., 2002) that contributes to PIP_2 formation at the plasma membrane. At this time point, the actin containing and RFP-PH-positive filaments are formed. The increase in PIP_2 would be necessary for directing the actin changes that involve filament formation. Such filaments might play an important mechanical role in the elevation of the vitelline layer, and in membrane disipation that would avoid changes in the volume/surface ratio after the cortical granules fusion.

Our results show that PIP_2 may play diverse roles during fertilization. It is involved in generating Ca^{2+} signals by providing $InsP_3$ due to its hydrolysis. Then, it seems to augment its levels in the plasma membrane in order to concert structural changes necessary for normal fertilization. The PH domain used in the present work could visualize *de novo* synthesized actin filaments induced by JAS incubation, as well as the F-actin present inside the filaments generated at the egg surface after fertilization.

The PIP_2 increase and the subsequent actin spike-formation may provide the mechanical basis for the vitelline layer elevation.

CHAPTER VI: Neomycin affects vitelline layer elevation during fertilization.

Results.

Neomycin is an inhibitor of PIP_2 hydrolysis. Given that PIP_2 cleavage by PLC is a necessary step for $InsP_3$ production, the use of this substance can alter the $InsP_3$-dependent Ca^{2+} signals during fertilization. Fertilization experiments were performed after microinjection of 1M neomycin (pipette concentration) in starfish eggs, since this amount would represent a final cytoplasmic concentration of 10 mM, the one reported to block PIP_2 hydrolysis in sea urcin egg plasma membranes (Swann and Whitaker, 1986). The results indeed showed that the Ca^{2+} release was completely blocked (Fig VI 1) in all cases except only one egg that managed to generate a very low Ca^{2+} response by multiple sperms. In all the neomycin-treated eggs, including the one that generated a reduced Ca^{2+} release, the vitelline layer elevation was blocked (Fig VI 1b). Such a result was expected since cortical granule exocytosis and vitelline layer elevation are Ca^{2+}-dependent. The sperm added to these eggs was stained by incubation with the DNA dye Hoechst. Surprisingly, even if neither vitelline layer elevation nor fertilization cones were detected, many sperm were able to enter the egg as evidenced by the Hoechst fluorescence (Fig. VI 1a).

Then, the neomycin concentration used was diminished in order to find the minimum effective dose. Experiments using just half the concentration first tested and a very much diluted one, applying pipette concentrations of 500 mM and 10 mM neomycin, were performed.

Ca^{2+} peaked at 0.59 ± 0.07 RFU when 500 mM neomycin was injected (n = 7), while control cells peaked at 0.66 ± 0.06 RFU (n = 5), confering statistical non significant results. However, at this concentration the time required for reaching the peak (130.1 ± 24.4 sec) lagged in neomycin-treated eggs compared to the control (98.6 ± 20.1 sec). It might seem like a slight difference, but the neomycin-treated eggs failed to elevate the vitelline envelope (Fig VI 2).

At 10 mM in the pipette, the Ca^{2+} response peaked at 0.51 ± 0.08 RFU (n = 8), and the control at 0.57 ± 0.03 RFU (n = 10). The lag time to the peak was 124.9 ± 57.7 sec versus 121.5 ± 44.5 sec in the control, which were virtually the same.

Despite the subtle differences in the Ca^{2+} dynamics, the presence of neomycin did provoke morphological changes. Transmission-light observations showed that the cortical granule exocytosis in these eggs was slightly impaired (not shown).

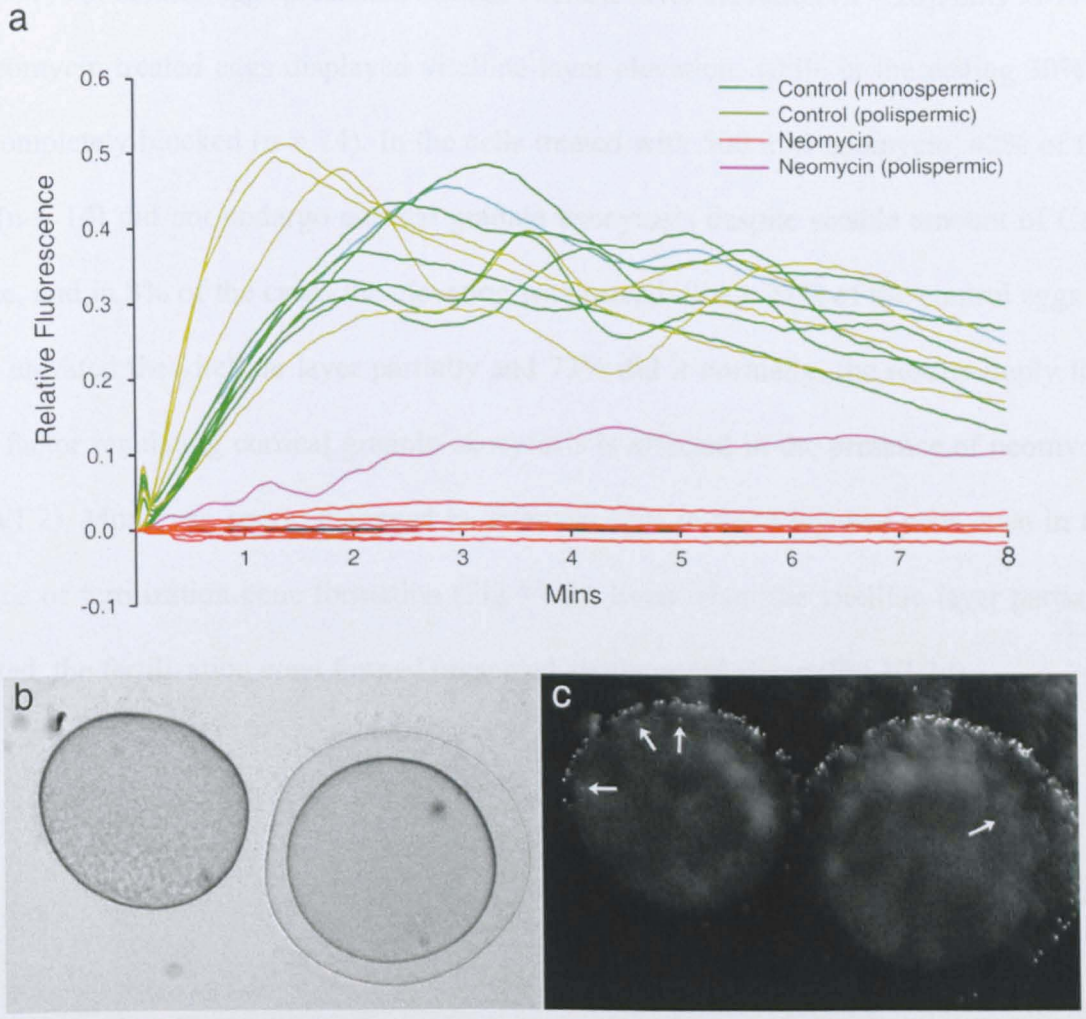

Fig VI 1: Neomycin at high dose completely blocks the Ca^{2+} release at fertilization. Oocytes from *A. aranciacus* loaded with Ca^{2+} dye were matured and subsequently microinjected with neomycin (1M, pipette concentration) before fertilization. **a**, The Ca^{2+} release was measured under CCD camera and shown in the graph. The green curves correspond to the control (injection buffer) eggs that displayed monospermy. The dark green curves correspond to control eggs with polyspermic interactions. The pink curves were obtained from neomycin injected eggs. The violet curve is the result of a polyspermically fertilized neomycin-containing egg. **b**, This same egg is shown in the bright field image below (on the left), next to a control egg. **c**, sperm stained with Hoechst 33342. At least three sperm heads entered the neomycin-treated egg (arrows).

While 97% of control eggs presented normal vitelline layer elevation (n = 20), only 70% of the neomycin-treated eggs displayed vitelline layer elevation, while in the resting 30% it was completely blocked (n = 14). In the cells treated with 500 mM neomycin, 42% of the cells (n = 14) did not undergo cortical granule exocytosis despite sizable amount of Ca^{2+} release, and in 8% of the cases the elevation was partial. Since 27% of the control eggs (n = 11) elevated the vitelline layer partially and 73% did it normally, the results imply that some factor regulating cortical granule exocytosis is affected in the presence of neomycin (Fig VI 2). Moreover, sperm managed to enter the eggs in these injected cells even in the absence of fertilization cone formation (Fig VI 2). Even when the vitelline layer partially elevated, the fertilization cone formed presented an abnormal shape (Fig VI 2d).

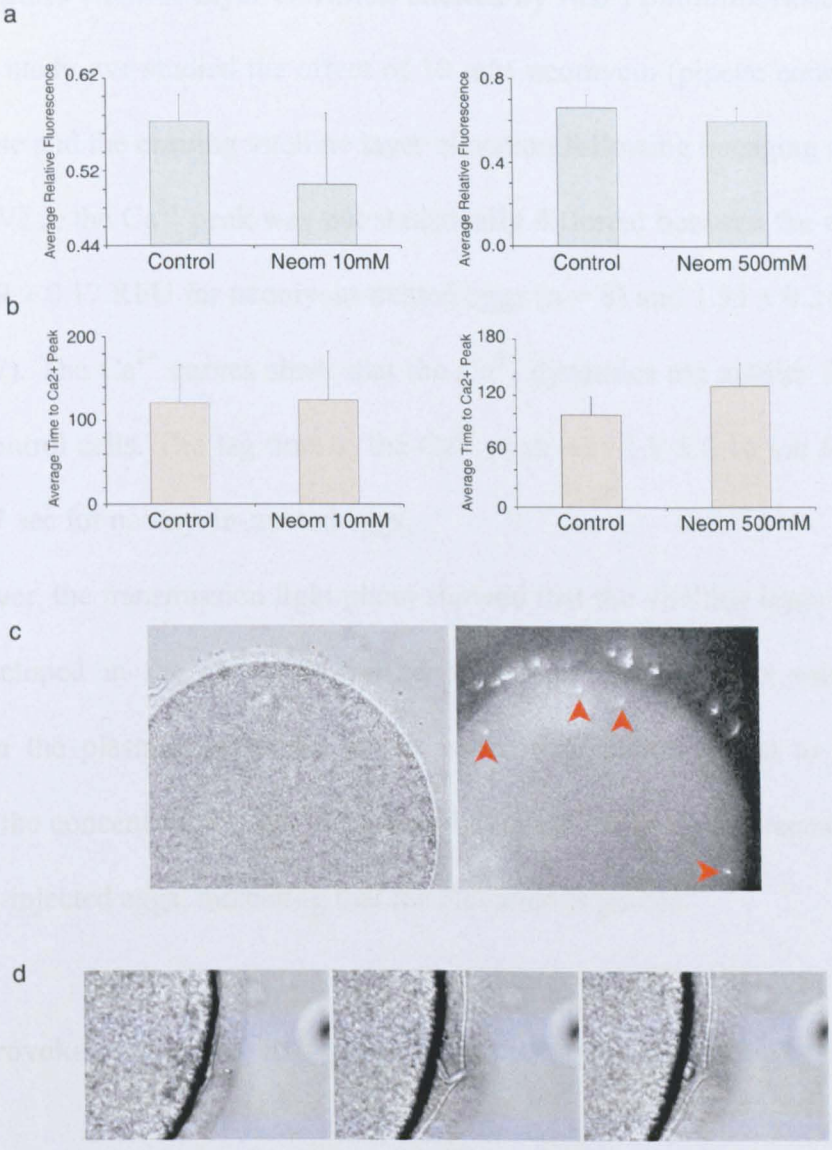

Fig. VI 2: Dose effect of neomycin on the Ca^{2+} waves and vitelline layer elevation. At 10 and 500 mM in pipette, neomycin had little effect on Ca^{2+} signalling at fertilization but drastically affected vitelline layer elevation. *A. aranciacus* oocytes loaded with Ca^{2+} dye were matured and microinjected with either buffer or neomycin (10 mM or 500 mM in pipette). The Ca^{2+} peak (**a**) and the lag time to reach the peak (**b**) are shown in the graphs of bars. **c**, The transmitted light image shows eggs preinjected with 500 mM neomycin (pipette concentration) with blocked vitelline elevation. Several Hoechst-stained sperm have penetrated the egg on the right with no vitelline layer elevation (arrows). No stained sperm head is visible at this focal plane in the oocyte located on the left. **d**, a filamentous abnormal fertilization cone (arrowhead) is produced by a sperm (arrow) fertilizing a neomycin (500 mM) loaded egg.

Neomycin impairs vitelline layer elevation elicited by $InsP_3$ photoliberation.

In this study, we studied the effect of 10 mM neomycin (pipette concentration) on the Ca^{2+} release and the ensuing vitelline layer elevation following uncaging of preinjected $InsP_3$. In Fig VI 3, the Ca^{2+} peak was not statistically different between the two groups of cells with 1.39 ± 0.17 RFU for neomycin-treated eggs (n = 8) and 1.53 ± 0.21 RFU for the control (n = 7). The Ca^{2+} curves show that the Ca^{2+} dynamics are similar for neomycin-treated and control cells. The lag time to the Ca^{2+} peak was 1.8 ± 0.16 sec for the control and 1.8 ± 0.17 sec for neomycin-treated eggs.

However, the transmission light photo showed that the vitelline layer elevation was not well developed in the neomycin-treated egg. The vitelline layer was not equally elevated from the plasma membrane in the entire egg surface failed to hold the egg cytoplasm in the concentric position. This morphological phenotype is repeated in 71% of the neomycin-injected eggs, indicating that the elevation is partial.

Neomycin provokes structural changes in both the cortex and inner cytoplasm of the eggs.

In order to study the effects of neomycin on PIP_2, RFP-PH was microinjected into the eggs. Figure VI 4 shows the results obtained by confocal microscopy. The RFP-PH probe localized preferentially in the plasma membrane, with some minor distribution in the cytoplasm. The neomycin-injected cells instead manifested numerous aggregates stained with RFP-PH in the cytoplasm. Such aggregates were present even in the control experiments, using the RFP reporter protein and the mutant R40A-RFP, suggesting that it may not represent PIP2. Similarly, the area where the germinal vesicle was present is very strongly stained in all groups of cells containing neomycin, invariably localized apposed to the plasma membrane. Thus, it could be inferred that neomycin causes changes in the architecture of the cytoplasm, forming 'islands' that would non-specifically clog the tagged proteins together, resulting in the observed fluorescent patches. The staining at the plasma

membrane level slightly differs whether the neomycin drug has been injected before or after the RFP-PH probe, and between the experimental and control cells. When neomycin is introduced in the cell before the RFP-PH, it seems that the cortical staining is stronger than if the experiment is performed in the opposite order (Fig VI 4). On the other hand, the cortical staining is absent in RFP and R40A-RFP-containing cells. These results very importantly show that in basal conditions, in the absence of any stimulus, neomycin profoundly changes the physical nature of the egg cytoplasm. Although both neomycin and RFP-PH target PIP_2, their effect over the phospholipid is diverse. While the RFP-PH binds reversibly to PIP_2 and enables its hydrolysis by PLC and $InsP_3$ formation (Wang et al., 2005), neomycin inhibits this interaction with the consequent blockage of the $InsP_3$-dependent Ca^{2+} signalling.

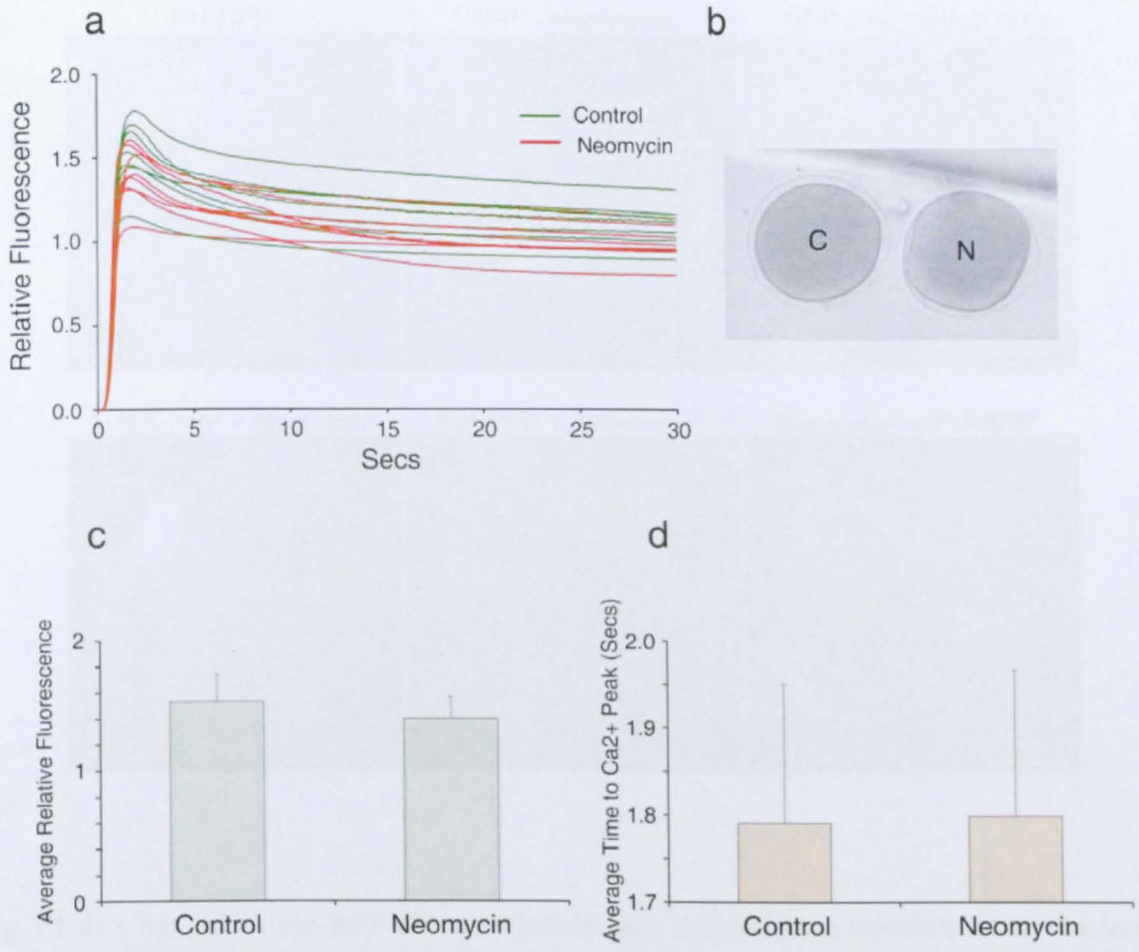

Fig VI 3: Neomycin does not affect the $InsP_3$-dependent Ca^{2+} release but suppresses the vitelline layer elevation. *A. pectinifera* oocytes were loaded with Ca^{2+} dye and caged $InsP_3$ (50 μM). After 1hr incubation with 1-MA, they were microinjected with neomycin (10 mM, pipette concentration). The released Ca^{2+} dynamics after $InsP_3$ photoactivation of control (green curves) and neomycin-containing eggs (red curves) are shown in the graph (**a**). **b**, The bright field image shows a pair of control and neomycin-injected egg after $InsP_3$ activation. The neomycin-injected egg (N) displayed partial vitelline layer elevation. In the histograms, **c** shows the mean values of Ca^{2+} peaks in the control (n = 7) and the neomycin-treated eggs (n = 8), and **d** the average lag time to the Ca^{2+} peak.

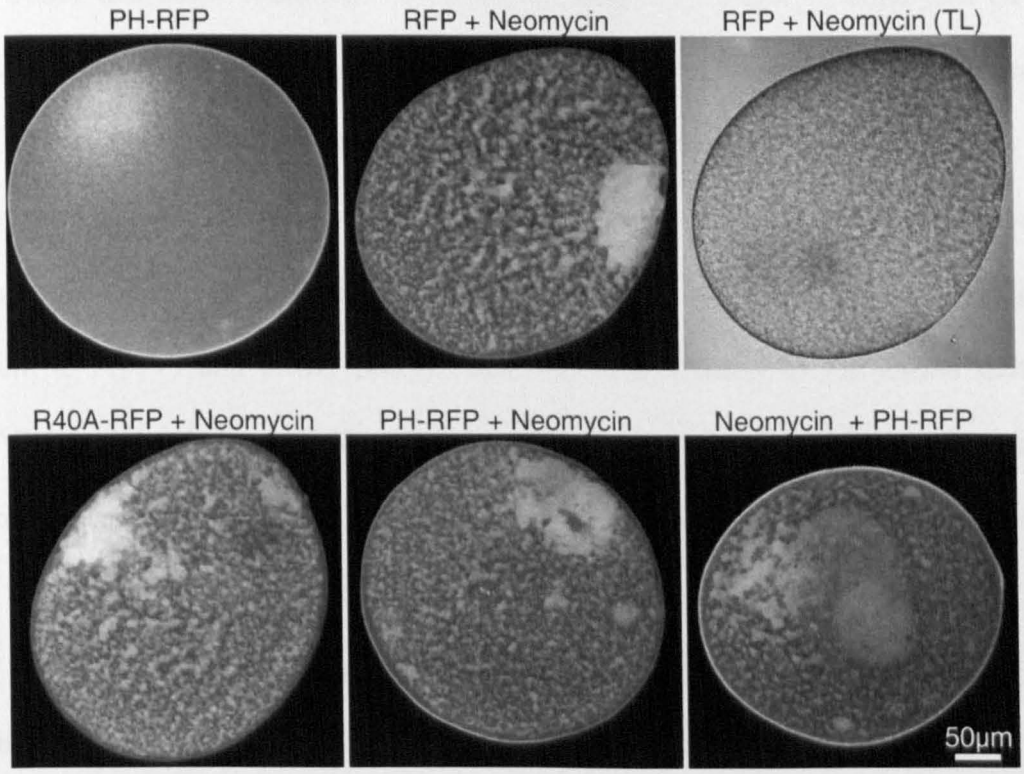

Fig VI 4: Changes in the RFP-PH distribution due to neomycin injection. *A. aranciacus* mature eggs were microinjected with RFP-PH (9 µg/µl), RFP (6 µg/µl), R40A-RFP (9 µg/µl), incubated for 15 min and injected with neomycin 10 mM (pipette concentration) for 10 min. In the last image shown, the order of injection was inverted; neomycin was injected and then RFP-PH was injected 10 min later.

Under this basal condition, however, the inhibitory effect of neomycin on Ca^{2+} signalling looses relevance. Then, the images shown in Fig VI 4 could be indicating the role of the PIP_2 molecule in other cellular pathways. The PIP_2 interaction with actin binding proteins, for instance, could be altered by the neomycin presence, provoking structural changes. Some work however, has reported that PH-GFP blocks the binding of neomycin to PIP_2 (Wang et al., 2005). Then, the interpretation of the results shown in figure VI 4 must be done carefully. Taking this into account, and added to the fertilization data analyzed previously showing the impaired vitelline layer elevation, a study of the effects of the neomycin drug over the state of F-actin filaments was performed.

F-actin distribution is affected by neomycin microinjection.

Live oocytes were microinjected with neomycin (1 M pipette concentration) and then with fluorescent phalloidin. In neomycin-treated eggs, the cortical F-actin was evident, but it contained very few distinct F-actin filaments, unlike the control. The inner cortex below the subplasmalemmal region seemed dark and devoid of fluorescence (Fig VI 5). In the inner cytoplasm, many fluorescent patches or condensed areas of phalloidin-stained material were detected. These phalloidin-stained structure in the inner cytoplasm may correspond to or even be responsible for the corrugated surface visible in the transmission light image. The region where the germinal vesicle material was present is also intensely stained by phalloidin. Similar phalloidin staining patterns were reproduced with fixed eggs treated with neomycin treatment. As shown in Fig VI 5b, the fixed egg presents a phalloidin staining that resembles very much the one observed in living cells. The plain ring devoid of actin fibers below the subplasmalemmal area is more accentuated in the fixed cells.

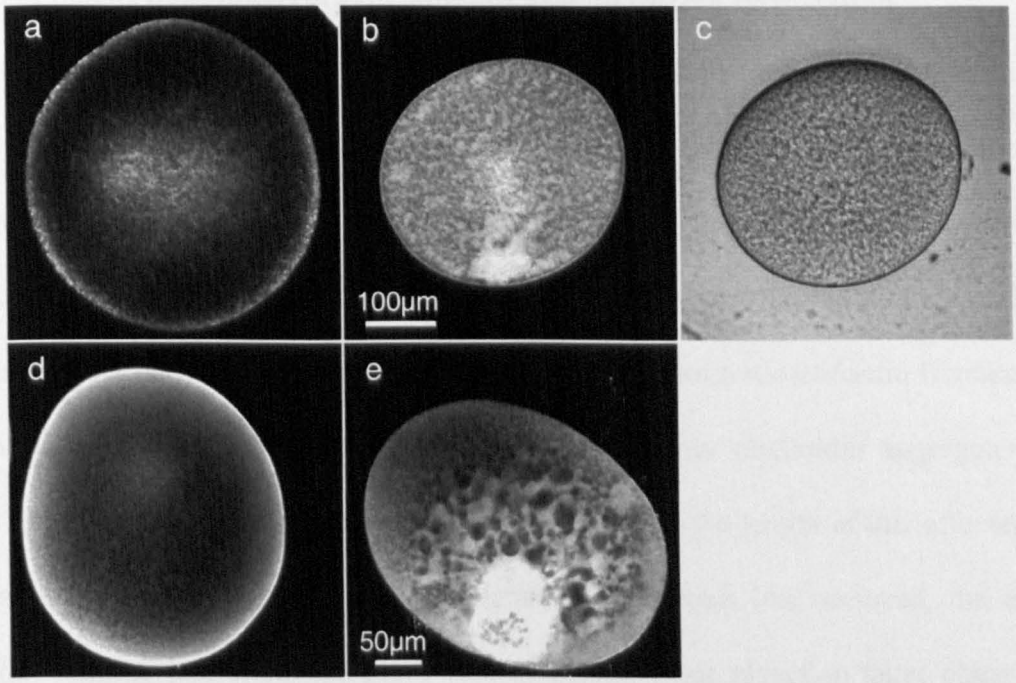

Fig VI 5: Neomycin affects the F-actin distribution. **a**: *A. aranciacus* eggs were microinjected with injection buffer (**a**) or with neomycin (1 M in pipette, **b**) and then microinjected again with Alexa Fluor 488-conjugated phalloidin (50 µM, pipette concentration) and observed by confocal microscopy. **c,** a transmitted light image of an egg injected with neomycin (1 M in pipette) shows its corrugated surface. Eggs preinjected with buffer (**d**) or neomycin (**e**, 1 M in pipette) were fixed with glutaraldehyde 0.5% and probed with fluorescent phalloidin.

Neomycin blocks dynamic reorganization of F-actin during fertilization.

Fertilization is followed by changes in the actin cytoskeleton. We studied how this process is influenced by neomycin in an attempt to understand its effects on the actin dynamics and vitelline layer elevation. Indeed, when the sperm was added to the eggs preinjected with 1 M neomycin, the vitelline layer elevation was partially blocked (Fig VI 6). After interaction with the sperm, there is no centripetal migration of actin filaments that was normally observed in the control eggs. Instead, many phalloidin aggregates were formed in the cortex of the cell (Fig VI 6 at 6'). In most of the length of this affected area, the vitelline layer elevates. After cortical granule exocytosis has occurred, the cortical phalloidin-staining just under the place where vitelline layer elevation takes place is lost (Fig VI 6 at 16'). All the same, some phalloidin patches are maintained in other regions of the plasma membrane where the vitelline layer has not elevated (arrowhead, same figure). In the cases where neomycin was injected in lower concentrations, the vitelline layer elevation was possible (Fig VI 7a). However, even in these cases, the changes in the actin cytoskeleton during fertilization were different between neomycin-treated and control cells (Fig VI 7). While in the control egg injected with phalloidin the cortical ring of fibers migrate to the center of the cell after fertilization, their distribution almost does not change in neomycin-containing eggs. In this latter group of eggs, the F-actin ring is maintained even after sperm entry.

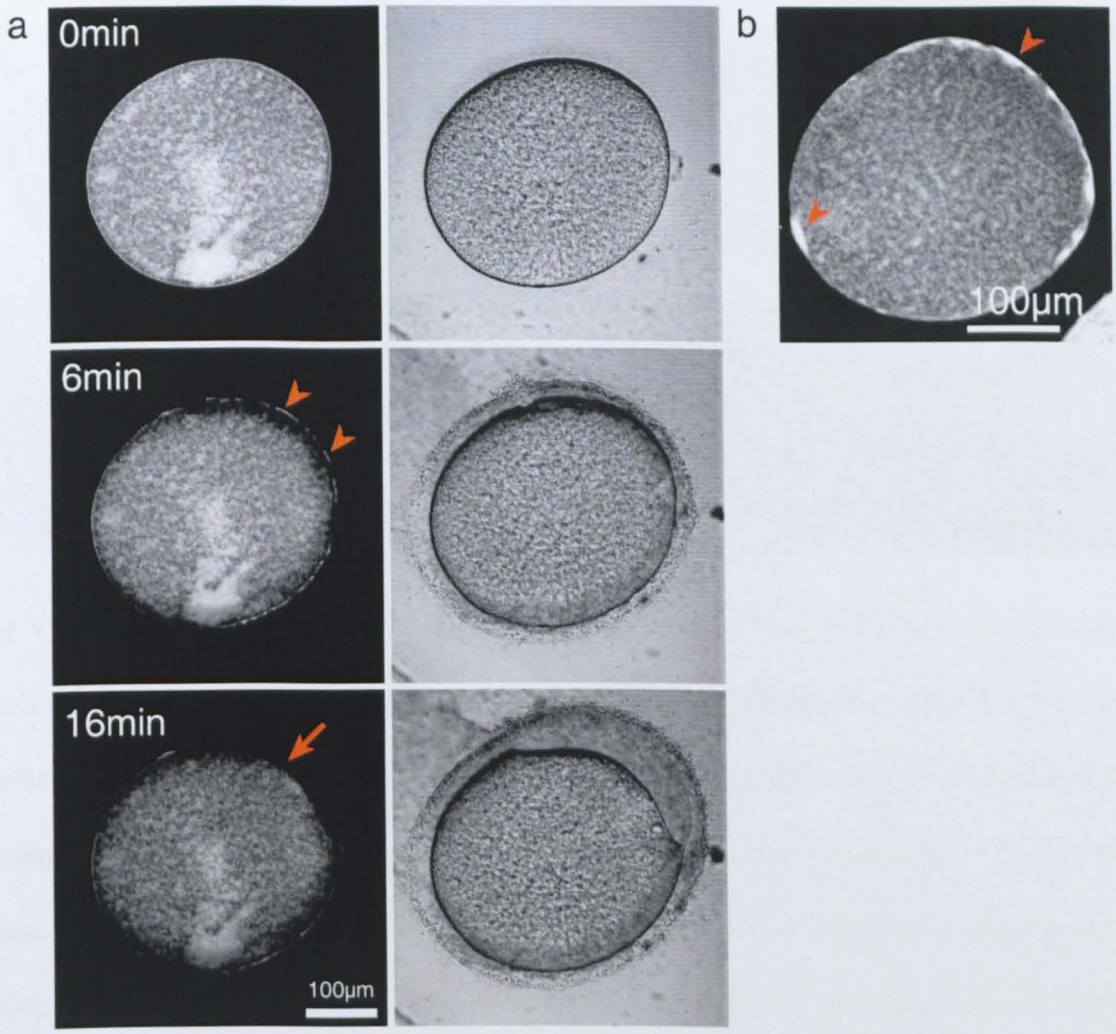

Fig VI 6: Neomycin impairs vitelline layer elevation at fertilization, which occurs only in the areas where F-actin has been remodelled. Eggs from *A. aranciacus* were microinjected with neomycin (1 M, pipette concentration) and with Alexa Fluor 568-conjugated phalloidin (50 µM, pipette concentration). **a**: Sperm were added at 0 min. Confocal images (left panels) show that at 6 min the cortical F-actin ring is disrupted forming discontinued clusters (arrowheads). The bright field images (right panels) show the corrugated surface of the neomycin-injected cell. At 16 min the vitelline layer elevation occurs in the region were the cortical F-actin patches desappeared (arrow). **b**: A confocal image of an *en face* focal plane shows the cortical patches (arrowheads) formed in the cortex of the egg due to neomycin presence.

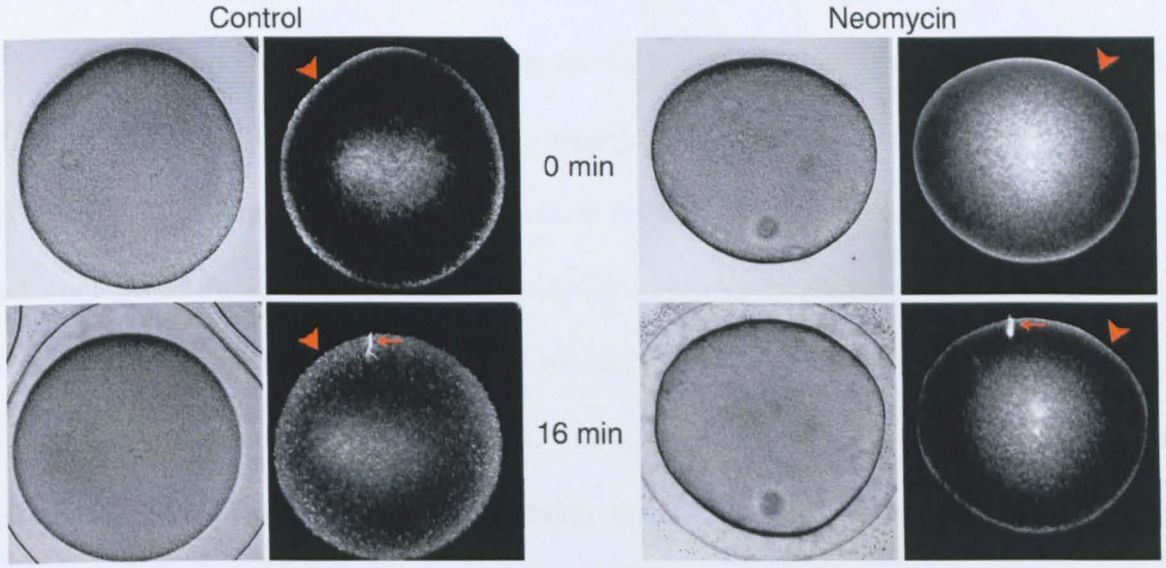

Fig VI 7: Neomycin affects the changes in the cortical actin cytoskeleton at the time of vitelline layer elevation. *A. aranciacus* eggs were microinjected with injection buffer (control) or with neomycin (10 mM, pipette concentration) and then with Alexa Fluor 568-conjugated phalloidin (50 μM, pipette concentration). Sperm were added at time set to 0min. Confocal images show that at 16min the cortical F-actin fibers have migrated to the inside of the egg in the case of control, but not in neomycin-injected eggs (arrowheads). In the two cases, a bunch of actin filaments in the surface of the egg are seen, indicating the sperm entry (arrows). The bright field images show the fertilization envelope formation in both cases.

Neomycin prevents microvilli formation on the surface of the egg at fertilization.

The morphological changes triggered by neomycin are also detectable at the ultrastructural level. Eggs pretreated with neomycin or buffer were analyzed by electron microscopy. The control eggs after fertilization showed an elevated vitelline layer and the dark contents of the exocytosed cortical granules within the perivitelline space, (Fig VI 8). Moreover, emitting from the plasma membrane and into the perivitelline space, many microvilli are present (arrow in Fig VI 8). In the sections taken from neomycin-injected cells, the vitelline layer is elevated, and many cortical granules are observed underneath the plasma membrane, showing that they have failed or delayed to undergo exocytosis after fertilization (arrow in Fig VI 8), probably contributing to an impaired vitelline layer elevation. More importantly, no microvilli are detected on the surface of neomycin-treated eggs (Fig VI 8). Thus, the neomycin binding to PIP_2 in some way modifies the remodeling of the egg cortex at the time of fertilization, preventing microvilli formation.

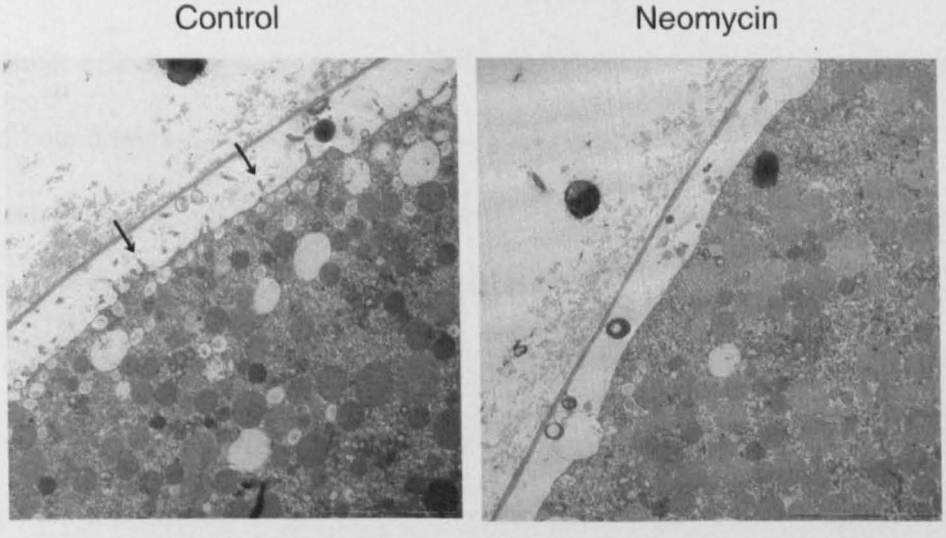

Fig VI 8: Neomycin abolishes microvilli in the surface of fertilized eggs. A transmission electron micrograph from the surface of an *A. aranciacus* egg treated with neomycin (10 mM, pipette concentration) and buffer (control). The arrows indicate the lack of microvilli at the plasma membrane.

Discussion for Chapter VI.

Neomycin is an aminoglycoside antibiotic with six primary amine groups (McLaughlin and Whitaker, 1988). Due to its basic charge, it stabilizes membranes by binding to phospholipids (Crabb and Jackson, 1986). Regarding this theory, neomycin has been shown to reduce the lateral mobility of glicoproteins in erithrocytes membranes, in the absence of changes in the lipid microviscosity and dependent on changes in the actin cytoskeleton (Schindler et al., 1980). Probably because of such alterations, it completely blocks Ca^{2+} release and thus vitelline layer elevation in starfish eggs when injected in high concentrations such as 1 M. At lower concentrations, fertilization was possible. As described, the injection of 500 mM neomycin affected some aspects of fertilization. Whilst the Ca^{2+} amounts released were comparable between neomycin-injected and control cells, the rise time to peak intracellular Ca^{2+} was increased in neomycin containing eggs. Neomycin has been reported to bind to PIP_2 and prevents its hydrolysis by PLC. Thus, one of the indirect effects of neomycin is to increase the PIP_2 pool. However, whether such a neomycin-bound pool is active for interaction with other targets is not certain.

At fertilization of sea urchin eggs, it has been proposed that Ca^{2+} released after sperm arrival further activates PLC and hydrolyse more PIP_2, generating $InsP_3$. Such process would create an autocatalytic wave of Ca^{2+} release and propagation (Swann and Whitaker, 1986). Neomycin, by blocking PIP_2 hydrolysis, would impair the propagation of the wave. The described mechanism could in part explain our results with the 500 mM neomycin concentration. In this case, the time employed to reach the maximum Ca^{2+} peak was delayed, however, the total amount of Ca^{2+} released was not much affected.

Most interesting are the results of experiments carried with neomycin and $InsP_3$ uncaging. In such conditions, $InsP_3$ is released (uncaged by photolysis) at the same time and homogeneously in the whole cytoplasm. In this way, Ca^{2+} is not influenced by the direct inhibitory effect of neomycin on PLC activities. Indeed, the Ca^{2+} quantities and

dynamics are very similar between neomycin-treated and control eggs (Fig. VI 3). However, the vitelline layer elevation in the cells is noticeably impaired.

Although sea urchin egg activation depends on the $InsP_3$ concentration delivered, and low concentrations triggered local and partial fertilization envelope formation (Swann and Whitaker, 1986), this is not the case for our experiments. Partial vitelline layer elevation did not occur due to insufficient amounts of released Ca^{2+}, but as a consequence of structural changes of the cytoplasm. In line with this idea, experiments of $InsP_3$ uncaging in mature eggs treated with the PLC inhibitor U73122 or the polymerizing agent JAS, released the same Ca^{2+} amounts as the control eggs, but the elevation of their vitelline layers was blocked (Kyozuka et al., 2008). It was suggested that the actin hyperpolymerizing effects of these two drugs (JAS and U73121) were linked to the blockade of vitelline layer elevation.

Neomycin alters the vitelline layer elevation not only after $InsP_3$ photoliberation but also at fertilization. At high concentrations, the elevation occurs only in the areas where cortical actin was displaced or rearranged. Such rearrangements could be impaired by the presence of actin patches present in the subplasmalemmal region, as observed in Fig VI 6. Neomycin binds in a cooperative way to PIP_2 (Whitaker and Aitchison, 1985), then it is possible that the local attachment of neomycin to certain pools of PIP_2 may create localized reorganization of F-actin via ABPs, thus creating the phalloidin-positive patches observed. Even in the eggs where the vitelline elevation occurred at entire egg surface with no phalloidin patches formed, the redistribution of F-actin filaments occurred in a diverse form in neomycin-containing and control eggs. Therefore, actin seems to be affected by the presence of neomycin. In support of this idea, TEM showed that neomycin eliminated microfilament-filled microvilli in the neomycin-injected eggs at fertilization.

Neomycin has been reported to inhibit exocytosis from sea urchin egg cortex preparations (Crabb and Jackson, 1986). It was also published that the absence of diacylglycerol production, due to blocked PIP_2 hydrolysis, could help impair exocytosis

since it constitutes an important element mediating membrane bindings (Whitaker and Aitchison, 1985). Moreover, it was proposed that the lack of PIP_2 removal (that would take place via PIP_2 hydrolysis and in this case inhibited by neomycin) would impair membrane fusion, since a diminished negative charge in the membrane is an important event leading to exocytosis (Whitaker and Aitchison, 1985). Previous experiments with sea urchin eggs showed that neomycin blocks vitelline layer elevation (Swann et al., 1992). Electrophysiological measurements showed that even if the fertilization envelope was not formed, the sperm was still capable of generating an inward current. However, sperm did not enter the eggs. Even in non voltage-clamped eggs treated with 5-10 mM neomycin, the sperm was not detected by Hoechst staining (Swann et al., 1992). Although the authors do not mention it, the surface of the neomycin-treated sea urchin eggs was corrugated, just as we observed in starfish eggs. Hence, the observed effect of neomycin could be ascribed not only to inhibition of its PIP_2 hydrolysis but also to its capacity as a polycation to change the plasma membrane surface charge.

In our case, many sperm heads were observed inside the neomycin-treated eggs at fertilization even when the vitelline layer elevation was blocked. This is a very surprising result since vitelline layer elevation is necessary for fertilization cone formation and sperm entry. In previous results it was discussed that heparin provoked polyspermy and fertilization cones of diverse shapes that did not permit entry of sperm in all the cases. In the present case, when neomycin is injected, sperm seems to enter the egg even in the absence of fertilization cones, or as is the case of heparin-injected eggs, abnormal fertilization cones were observed. The sperm did not enter deep into the cytoplasm of the egg when the vitelline layer elevation was blocked, their centripetal migration seemed to stop close to the subplasmalemmal region. This interesting observation certainly deserves further investigations. In these cases, polyspermy may occur due to the lack of vitelline layer elevation, considered as a mechanical block to supernumerary sperm entry.

Finally, it is proposed that neomycin affects the Ca^{2+} release and propagation at fertilization due to its PIP_2-binding function. The binding inhibits its hydrolysis by PLC and $InsP_3$ formation, and alters its interactions with ABPs, thus changing the actin cytoskeleton dynamics. Consequently, vitelline layer elevation was impaired.

CHAPTER VII: Anti-Depactin specifically impairs the actin cytoskeleton and alters Ca^{2+} signalling at fertilization.

Results.

The actin cytoskeleton is a highly dynamic structure, and its monomer-polymer equilibrium is regulated by the action of many actin-binding proteins. Depactin is a 17 kDa protein that has been identified in starfish (Mabuchi, 1981) and specifically binds to actin (Sutoh and Mabuchi, 1989). It has been reported to reduce polymerized actin *in vitro* (Takagi et al., 1988), probably by randomly taking actin proteins from the polymer or detaching them from any of both ends of the filament, and forming a 1 to 1 actin-depactin complex (Mabuchi, 1983). However, depactin has been shown to accelerate the polymerization rate since by chopping the filaments, many nuclei or roots for new filaments formation are generated (Mabuchi, 1983). The depactin protein contains a dodecapeptide region that shows similarity with corresponding sequences in cofilin, ADF and destrin proteins (Yonezawa et al., 1991).

In this section, I have used anti-depactin antibody (a generous gift from Prof. Mabuchi) as a specific function-blocking agent for depactin, a starfish version of cofilin. This antibody is expected to prevent depactin from interacting with its physiological partners, and thereby alter F-actin dynamics. This antibody has been generated against starfish (*Asterias amurensis*) depactin, and was demonstrated to detect a single band of 17 kDa in the western blot analysis of *A. aranciacus* (Nusco et al., 2006). I have used it with the aim of studying the effects of the specific impairment of the actin cytoskeleton in the Ca^{2+} signalling generated during fertilization.

Anti-depactin modifies the cortical and cytoplasmic actin cytoskeleton in immature oocytes.

To test how the F-actin was modified in response to the anti-depactin antibody in starfish oocytes, the antibody was microinjected and after half hour incubation fluorescent phalloidin was delivered to monitor the actin cytoskeleton under confocal microscopy. This procedure carried out in immature oocytes revealed interesting results. To start with, the second microinjection I had to perform in order to introduce the phalloidin inside the cell showed that the oocyte had lost rigidity, and its consistency was much softer and elastic than the control eggs. When observed under the confocal microscope, the continuous ring formed of F-actin at the subplasmalemmal area was disrupted. In the cytoplasm, a network of filaments is present, but many rods and dots were visualized by phalloidin staining (Fig VII 1), indicating that the antibody has shifted the actin polymerization dynamics. The actin filaments around the germinal vesicle (GV) have also been affected, and they do not form a continuous cord in the nuclear membrane perimeter any more. Most impressive, is the presence of actin filaments inside the GV domain.

Actin in its monomeric glomerular form is known to be present inside the nuclear compartment of starfish oocytes at the GV stage, playing diverse roles other than structural, such as regulating transcription and gene expression (Zheng et al., 2009). F-actin has been reported in the nuclear area forming a net that would help bring the chromosomes close to the microtubular spindle during cell division (Lenart et al., 2005), but not only, since F-actin has been reported in interphase-nucleus as well (Gieni and Hendzel, 2009). However, F-actin is usually not evidenced by phalloidin staining in the GV of our model oocytes. The visualization of actin fibers inside the GV after anti-depactin injection clearly demonstrate that this antibody is functional in blocking actin depolymerizing activity of depactin/cofilin in starfish. Another interesting feature is that the fibers present in the GV seem to originate from one point in a pole of the nuclear membrane, and from there form a nest or basket (see Fig VII 1). In the base of this basket

the nucleolus is placed. The described results in the immature oocytes indicate that anti-depactin exerts changes in the actin cytoskeleton.

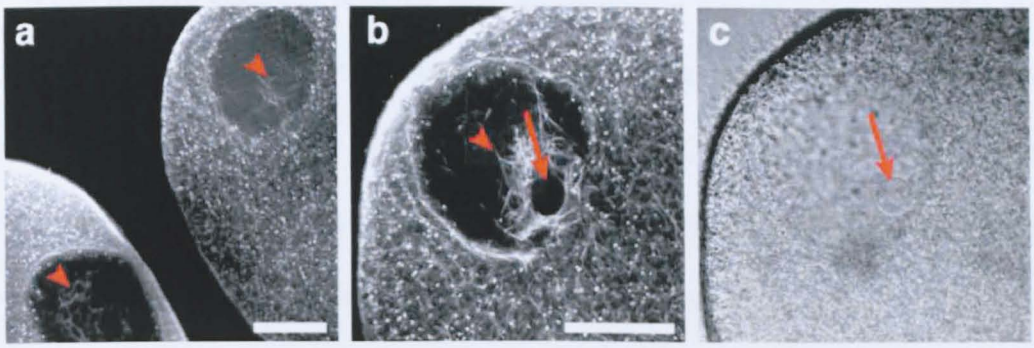

Fig VII 1: Anti-depactin changes the actin cytoskeleton in cytoplasm and germinal vesicle (GV) of oocytes. *A. aranciacus* oocytes were injected with anti-depactin (9 μg/μl in pipette) and then with Alexa Fluor 488-conjugated phalloidin (50 μM in pipette). Confocal images show phalloidin-positive dots in the cytoplasm and fibers inside the GV of two oocytes (**a,** arrowheads), contrary to what observed in control oocytes (see images in Chapter III, specifically Fig III 1). In **b**, a basket-like distribution of actin fibers at one pole of the GV is observed. The nucleolus appears contained in such basket (arrow). **c,** the corresponding bright field of the oocyte in b with an arrow indicating the nucleolus. Scale bars: 50 μm.

Anti-depactin and cofilin modify the actin cytoskeleton of mature eggs in different ways.

When mature eggs are injected with anti-depactin and incubated for half an hour, the posterior phalloidin injection reveals rods and dots in the cytoplasm. In the cortical area, the fibers are few, short and thick (see Figures VII 2 top row). In the surface, microvilli and phalloidin-positive filaments are detected (Fig VII 2). The experiment was also performed with modifications. In this case, anti-depactin is injected at the immature oocyte stage and incubated for half an hour. Then, the oocyte is challenged with the hormone 1-MA and immediately after GVBD phalloidin is injected and observed. The results are shown in Fig VII 2 "Anti-Depactin+1-MA+Phalloidin". The actin filaments present in the cortical region seem to be more numerous than in the previous experiment and thinner in architecture. Similar to what happens in the latter experiment, the cytoplasm is rich in rods and actin microvilli and filaments emmanate from the surface.

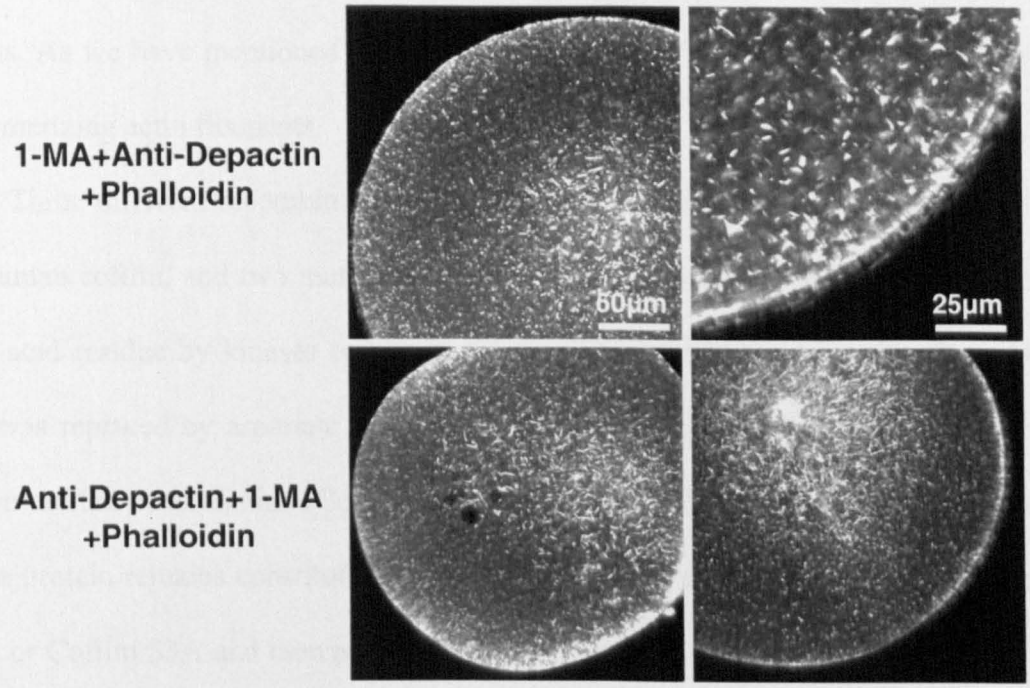

Fig VII 2: Anti-depactin changes the actin cytoskeleton in mature eggs. Top panels: *A. aranciacus* oocytes were matured by 1-MA incubation for 1 hr and injected with anti-depactin (9 µg/µl in pipette). Then, Alexa Fluor 568-conjugated phalloidin (50 µM in pipette) was loaded and eggs were observed by confocal microscope. In the lower panels, anti-depactin (9 µg/µl in pipette) was injected prior to maturation. In this latter case, the actin filaments in the cortex are more hyperpolymerized than in the panels above.

The studies of the actin dynamics were also performed after injection of cofilin proteins. As we have mentioned above, depactin and cofilin have homologous activity in depolymerizing actin filaments.

Three different recombinant cofilin proteins were prepared in the laboratory: wild type human cofilin, and two mutants at Serine 3 (Ser-3) position. Phosphorylation of this amino acid residue by kinases results in the inactivation of the cofilin functions. Hence, Ser-3 was replaced by aspartate to mimick phosphorilation (Cofilin S3D) to serve as an inactive cofilin, or to alanine (Cofilin S3A), in which case there is no phosphorilation site and the protein remains constitutively active. The mature eggs injected with the wild type cofilin or Cofilin S3A and then phalloidin present an enhanced organization of the cortical actin filaments when compared to the blank control (phalloidin only) or the one injected with Cofilin-S3D (Fig VII 3). This results show that the phalloidin staining after cofilin injection is indeed opposite from the one observed after anti-depactin treatment. However, the latter results involving cofilin and phalloidin should be taken carefully since it has been published that cofilin, by cooperatively binding to F-actin changes its helical twist and in this way prevents the phalloidin binding to the fiber (McGough et al., 1997). Previously, we have shown that the fluorescent PH domain probe stains actin filaments formed *de novo* in living cells. Then, cofilin was preinjected into mature eggs along with the PH domain. Fluorescent PH-GFP, instead of staining the plasma membrane in all its perimeter, formed intermitent patches in the cortex when cofilin was present. It is known that PIP_2 (PH domain target) interacts with and regulates the cofilin protein. Moreover, strutural analyses have shown that PIP_2 binding site to cofilin overlaps with the actin binding site on the same protein (Ono, 2007). Thus, the impossibility of cofilin simultaneously binding actin and PIP_2 may explain the results of figure VII 4.

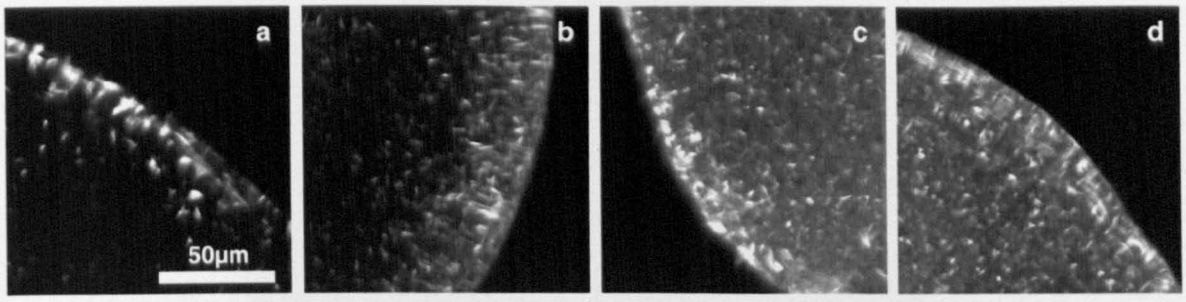

Fig VII 3: Cofilin changes the cortical actin cytoskeleton in mature eggs. Injection Buffer (**a**), Cofilin wild type (5 µg/µl in pipette, **b**), the inactive mutant Cofilin S3D (5 µg/µl in pipette, **c**) and the constitutively active Cofilin S3A (**d**) were injected in *A. aranciacus* eggs. Then, fluorescent phalloidin (50 µM in pipette) was delivered into the eggs and they were observed by confocal microsopy. The organization of the cortical F-actin is enhanced in the case of wild type cofilin and Cofilin S3A injection in comparison to the IB and Cofilin S3D controls.

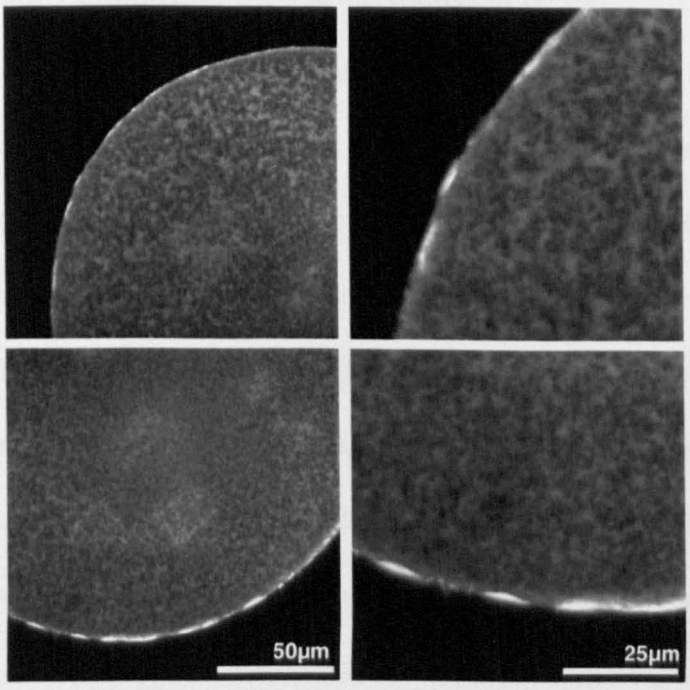

Fig VII 4: Cofilin changes PH-GFP distribution in mature eggs. Cofilin wild type (5 µg/µl in pipette) was injected into *A. aranciacus* eggs. After 20 min incubation, PH-GFP (9 µg/µl in pipette) was delivered into the eggs and they were observed by confocal microsopy. The photos of the two eggs on the left of the figure are shown magnified in the left images. It is clear that cofilin provokes the formation of PH-GFP patches in the cortex of the eggs.

Anti-depactin antibody diminishes the Ca^{2+} response at fertilization.

In the previous work from our laboratory, cofilin enhanced Ca^{2+} responses to fertilizing sperm and second messengers, e.g. $InsP_3$ and NAADP. *A. aranciacus* eggs were microinjected either with anti-depactin antibody or the negative control rabbit serum (9 μg/μl in pipette). In the control eggs receiving preimmune serum, the Ca^{2+} peak reached 0.65 ± 0.07 RFU (n = 3) after fertilization (Fig VII 5). On the other hand, the eggs treated with anti-depactin responded with a lower mean Ca^{2+} amount, peaking at the 0.33 ± 0.01 RFU (n = 8). Hence, anti-depactin suppressed the Ca^{2+} response at fertilization in line with the previous result using microinjection of exogenous cofilin (Nusco et al., 2006).

When more diluted concentrations of rabbit serum and anti-depactin were delivered into the egg, the control and experimental eggs showed diminished differences, although still statistically significant. Hence, the effect was dose-dependent. In Figure VII 5b, eggs containing rabbit serum 3 μg/μl reach the Ca^{2+} maximum at 0.88 ± 0.06 RFU (n = 9), while in those containing anti-depactin 3 μg/μl the mean Ca^{2+} peak value is 0.75 ± 0.07 RFU (n = 7). However, further experiments using even lower concentrations of antibody revealed interesting results.

Control eggs were injected with 0.15 μg/μl rabbit serum, and after fertilization these eggs responded with a Ca^{2+} wave of a 0.80 ± 0.08 RFU peak (Fig VII 6b). Then, eggs were injected with either 0.3 μg/μl or 0.15 μg/μl anti-depactin. In the case of 0.3 μg/μl, fertilization triggered a mean Ca^{2+} response of 0.76 ± 0.07 RFU, non significantly different from the control. In those eggs with 0.15 μg/μl, however, the Ca^{2+} wave peaked at 0.58 ± 0.02 RFU (Fig VII 6), lower than controls with injected serum. These results are intriguing since the most concentrated of these last two antibody dilutions tested generated a higher Ca^{2+} signal. This is contrary to what was expected, considering that in the previous experiments the tendency was that diluted concentrations of antibody provoked also diluted effects over the Ca^{2+} signals. The 0.15 μg/μl dilution is the one in which the time spent to reach the maximum Ca^{2+} peak was longer. While control eggs take 101.5 ± 22.8

sec to reach the Ca^{2+} peak value, the 0.3 μg/μl anti-depactin-containing eggs take 123.4 ± 24.2 sec. Then, the eggs injected with anti-depactin 0.15 μg/μl employed 168.2 ± 35.8 sec to reach the maximum Ca^{2+} peak.

On the other hand, vitelline layer elevation was influenced by the presence of the antibody. While the 100% of the control eggs showed complete vitelline layer elevation (n = 6), in the eggs with 0.3 μg/μl anti-depactin the vitelline layer elevation was partial in 50% of the cases (n = 6), and in those containing 0.15 μg/μl anti-depactin, the partial elevation was observed in 75% of the eggs (n = 5).

Besides the comparison of the Ca^{2+} amounts released in the entire egg, the appearance of the cortical flash has been recorded. In the experiments microinjecting more diluted concentrations, 83% cells containing 0.15 μg/μl rabbit serum presented a cortical flash (n = 6). However, only 50% of cells with 0.3 μg/μl anti-depactin presented a cortical flash (n = 6) and none of the cells containing 0.15 μg/μl anti-depactin (n = 6) produced a cortical Ca^{2+} flash.

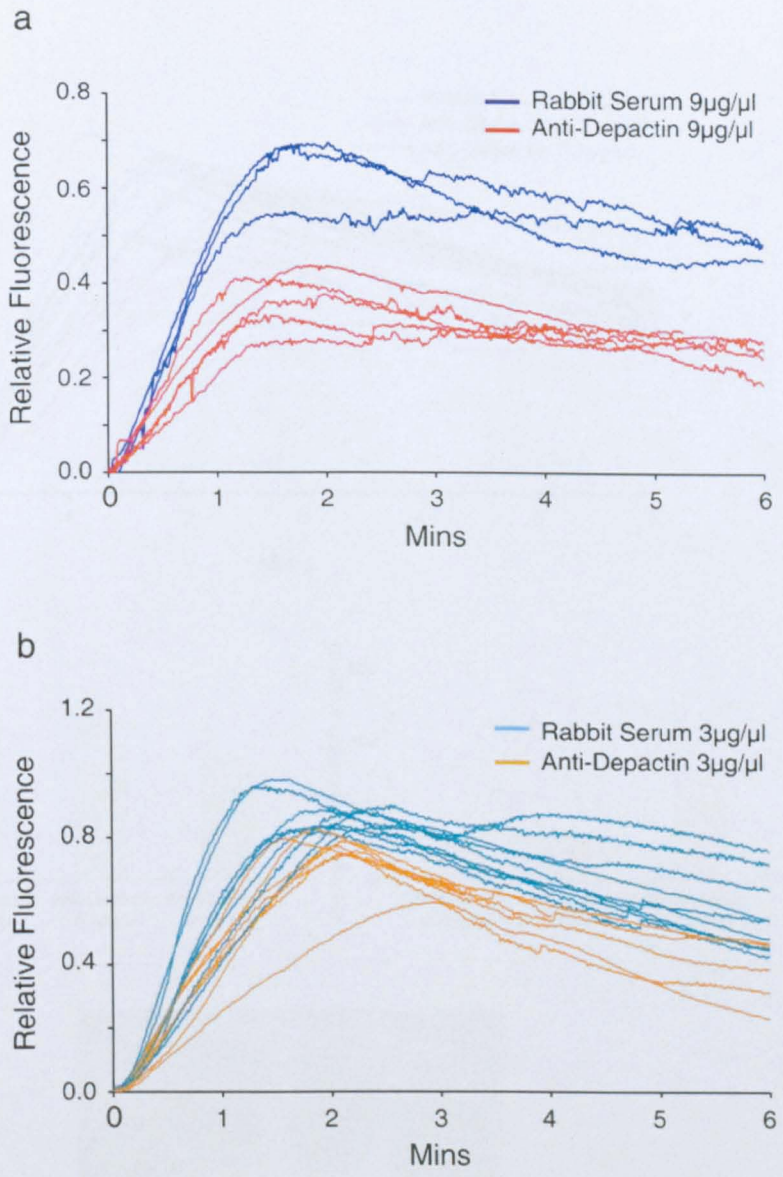

Fig VII 5: Anti-depactin antibody suppresses the fertilization-induced Ca^{2+} response. Oocytes of the *A. aranciacus* species were injected with Ca^{2+} dye and matured. Rabbit-serum was then injected as a negative control, and two different concentrations were tried (9 µg/µl in graph **a** and 3 µg/µl in graph **b**). In another group of eggs, anti-Depactin antibody (9 µg/µl or 3 µg/µl in injection pipette) was injected. The graphs show the Ca^{2+} release kinetics after fertilization. The anti-depactin-injected eggs always released less Ca^{2+} than the rabbit serum-injected eggs.

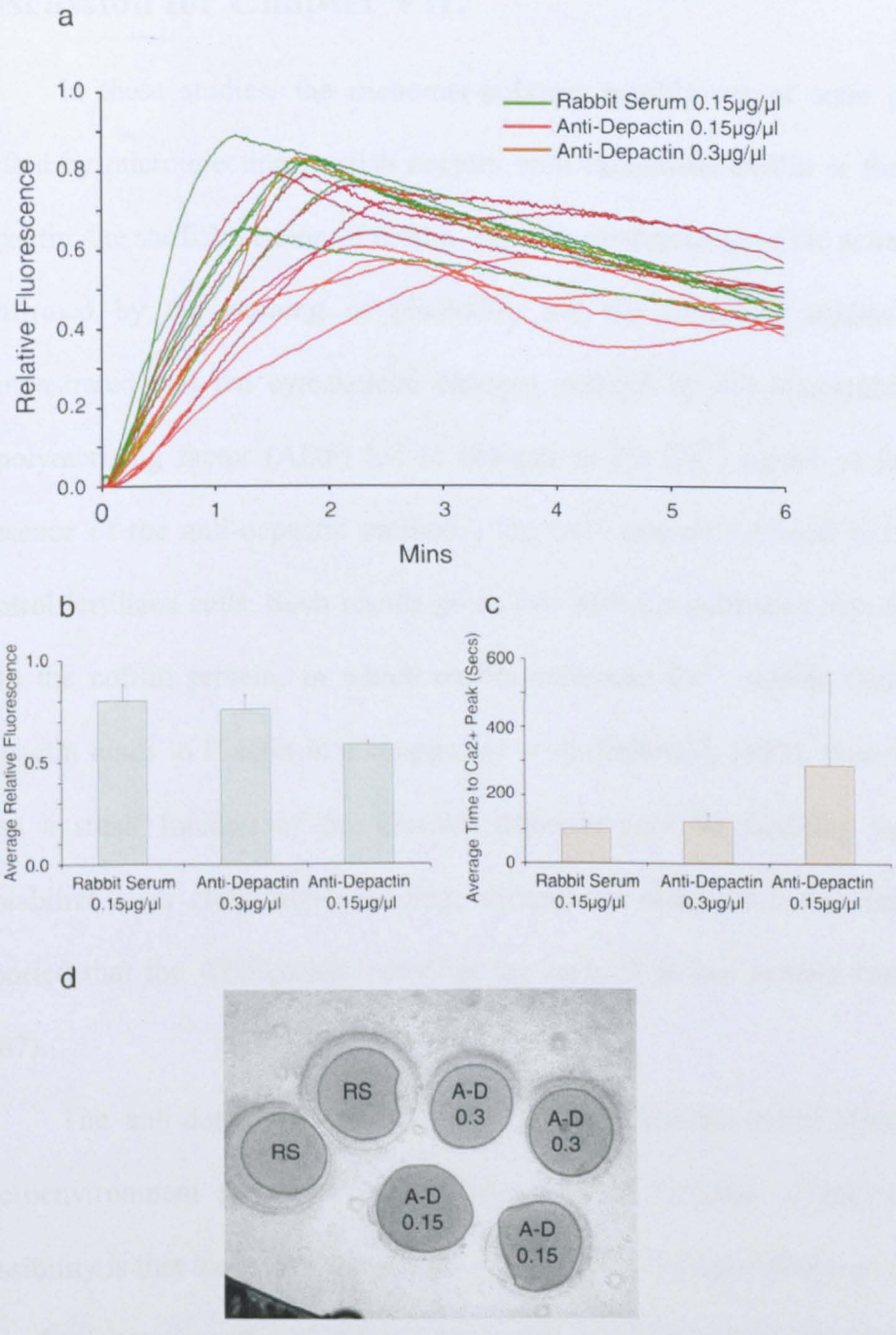

Fig VII 6: Anti-depactin injection at 0.3 µg/µl and 0.15 µg/µl (pipette concentrations) are able to impair Ca^{2+} signals at fertilization. It is interesting to notice that the curves corresponding to 0.15 µg/µl concentration (red curves, n = 4) reach lower Ca^{2+} peaks than the eggs injected with 0.3 µg/µl anti-depactin solution (brown curves, n = 6). The bar histograms compare the average Ca^{2+} peaks for control and experimental cells (**b**), and the average time to reach the peak for the three groups of eggs (c). **d**, The bright field images show the impaired vitelline layer elevation in those eggs treated with the two concentrations of Anti-Depactin (A-D 0.15 µg/µl and A-D 0.3 µg/µl).

Discussion for Chapter VII.

In these studies, the monomer-polymer equilibrium of actin proteins has been shifted by microinjecting starfish oocytes with exogenous cofilin or the antibody against depactin, the starfish version of cofilin. The fine modification of the actin cytoskeleton was confirmed by the staining of phallodin, and the following studies using Ca^{2+} dye demonstrated that the cytoskeletal changes induced by the manupulation of this actin depolymerizing factor (ADF) led to changes in the Ca^{2+} signals at fertilization. In the presence of the anti-depactin antibody, the Ca^{2+} amount released is lower than that of control fertilized cells. Such results go in line with the published experiments carried out with the cofilin protein, in which cofilin enhanced Ca^{2+} signals (Nusco et al., 2006). Depactin binds to F-actin in a cooperative way (Mabuchi, 1983), thus the substraction of even a small fraction of the intrinsic depactin pool by injecting the antibody could destabilize such cooperative binding, altering the actin dynamics. Indeed, it has been reported that the ADF/cofilin activities are optimal at low protein concentrations (Ono, 2007).

The anti-depactin-induced modification of F-actin could create an unfavorable microenvironment for Ca^{2+} channel activation at the time of sperm arrival. Another possibility is that the liberation of Ca^{2+} directly from the actin fibers, as proposed by the F-actin-Ca^{2+} store hypothesis (Lange and Brandt, 1996), has been affected by the presence of the protein. In both cases, the Ca^{2+} liberation and propagation of the wave would deviate from the norm. Few previous works had indicated the effects of cofilin over the Ca^{2+} signalling (Nusco et al., 2006; Redondo et al., 2006; Rueckschloss and Isenberg, 2001), however, the mechanism is unknown since the exact changes that cofilin exerts over the actin cytoskeleton in the particular subcellular domains of living cells is not clear. Although cofilin is reported to be a severing and G-actin-binding protein with a net depolymerizing effect over F-actin *in vitro* (Ono, 2007), experiments *in vivo* with caged cofilin have shown that it induces actin polymerization (Ghosh et al., 2004). The depactin

protein has also been reported to induce actin depolymerization *in vitro*. On the other hand, it produces the secondary effect of augmenting the rate of polymerization. This is possible since depactin severes the filaments without capping them, thus creating new free ends from which the filaments can ellongate (Mabuchi, 1983).

As shown in the present work, the injection of the anti-depactin antibody in mature eggs of starfish provoked the staining of a thin actin cortex, as well as rods and spots in the cytoplasm (Fig VII 2). On the contrary, when cofilin was preinjected into cells, phalloidin revealed that the cortical actin fibers occupied a thicker area apposed to the plasma membrane as seen in the control eggs (Fig VII 3).

In the experiments where fertilization was performed in the presence of actin depolymerizing drugs like Lat-A, the Ca^{2+} signal measured in the entire egg was not enhanced (Puppo et al., 2008). Likewise, in the eggs preinjected with anti-depactin antibody, the Ca^{2+} wave was suppressed and delayed, and the elevation of the vitelline layer elevation was impaired as was the case with JAS or Lat-A-treated eggs. In the eggs injected with anti-depactin antibody, the cortical flash was absent in most of the cases. Similarly, when cofilin is injected into cells and fertilized, the cortical flash is abolished or reduced (Nusco et al., 2006). Hence, studies using cofilin proteins or depactin antibody had many coherent parallel results.

The modification of the actin distribution inside the GV by the presence of the anti-depactin antibody in the cytoplasm strongly suggests that the actin nucleus is under the effect of actin binding factor that prevents polymerization. Nuclear actin is not visualized by phalloidin in starfish oocytes neither in other cell types, indicating that it is mostly present in a monomeric form or that its decoration with ABPs is different from the cytoplasmic (Pendleton et al., 2003). The effect of the depactin antibody in the cytoplasmic actin cytoskeleton could provoke the augment of the G-actin pool. Monomeric actin, although lacks any nuclear localization sequence, is small enough to enter the nucleous by passive diffusion through the nuclear pore complexes. The G-actin increase in the GV

compartment could favour the filament formation. Another hypothesis is that by modifying the cytoplasmic cytoskeleton, the nuclear pore complexes and general GV architecture can be disadjusted, enabling the intermixing of cytoplasmic and nuclear environments. The entry of cytoplasmic actin-binding proteins into the GV area could change the nuclear actin state.

As mentioned above, the vitelline layer elevation is also affected by the presence of anti-depactin antibody, rendering further support to the idea that cortical granule exocytosis requires adequate control of the actin cytoskeleton in the cortex and the suplasmalemmal regions. The vitelline layer elevation has been reported to occur depending on a dynamic cortical actin cytoskeleton in several different cell types (Muallem et al., 1995).

It has been published that cofilin binds preferentially to cofilin-bound fibers; indeed, electron microscopy images show that a population of fibers treated with cofilin present heterogeneous lengths, indicating that the binding has occurred in a fraction of the population (Mabuchi, 1983). When cofilin is injected in cells it binds cooperatively to some actin fibers, modifying them. Posterior injection of PH domain would stain the non cofilin-bound actin fibers, giving the patched-liked distribution of the PH domain (Fig VII 4), instead of the continuous staining of the cortex.

Our results suggest that microinjected anti-depactin antibody specifically modifies the treadmilling of the actin cytoskeleton. The actin modifications caused by the protein influence the Ca^{2+} amounts released at fertilization, as well as the propagation of the Ca^{2+} wave and vitelline layer elevation.

CONCLUSION

Meiotic maturation and fertilization of starfish eggs involve highly dynamic and precisely regulated reorganization of the actin cytoskeleton. This change is spatiotemporally linked to the Ca^{2+} mobilization during these two processes; an interesting idea to test is whether or not the actin reorganization has a regulatory role in shaping the Ca^{2+} response. In this study, as a potential modulator of the Ca^{2+} signalling at meiotic maturation and fertilization, the role of F-actin has been investigated. My initial research task has been to explore the experimental paradigms to alter the actin cytoskeleton and see how these structural changes would affect the intracellular Ca^{2+} signalling pattern.

During the course of this dissertation study, I helped to develop and evaluate the method to visualize the F-actin cytoskeleton in living oocytes by use of a phalloidin microinjection technique. In immature oocytes, treatment with the blockers of the $InsP_3$-dependent Ca^{2+} pathway U73122 and heparin, showed an unexpected striking effect on the cortical F-actin structure even in non-stimulated conditions. A similar effect was found when analogs of heterotrimeric G-proteins were microinjected. They changed the cortical actin cytoskeleton and altered the 1-MA-triggered Ca^{2+} wave that marks the restart of the meiotic maturation process, as well as the Ca^{2+} release generated due to exogenously administrated $InsP_3$. The changes in the cortical actin cytoskeleton were reproduced by drugs that are specific modulators of the microfilaments, just as Lat-A and JAS.

The sequence of morphological and Ca^{2+} release events from the sperm arrival to its entry into the egg were analyzed while studying the fertilization of mature eggs.

In postmeiotic eggs, heparin induced hyperpolymerization in the cortex. This change had negative effects on the Ca^{2+} signalling during egg fertilization, since the cortical flash of Ca^{2+} release was abolished. Although this may be attributed to the inhibitory effect on $InsP_3$ receptors, pharmacological agents producing similar changes in cortical actin had a similar results, e.g. JAS, GDPβS, Lat-A. After treatment, the cortical

flash resulted impaired and vitelline layer elevation was blocked. High levels of polyspermy were detected after JAS application. Furthermore, polyspermic interactions occurred and the treated eggs presented abnormal fertilization cone formation, as well as block of sperm entry and of vitelline layer elevation. Taken together, these results clearly demonstrate that the fine regulation of cortical actin during fertilization is utterly important in producing a proper Ca^{2+} response and the ensuing cortical granule exocytosis.

In this dissertation, the spatiotemporal relationship between the changes of PIP_2 levels at the the plasma membrane and the increase of Ca^{2+} signalling at fertilization were studied. The plasma membrane PIP_2 level did not decrease at fertilization until the initial Ca^{2+} signal propagated well into the cytoplasm, suggesting that the possibility that the initial Ca^{2+} trigger at starfish fertilization might be independent of $InsP_3$. The PIP_2 had a more delayed but prolonged increase at the plasma membrane, and this change was linked to the formation of actin-filled spikes that apparently lifted the elevating vitelline layer at fertilization.

Neomycin microinjection had slight effects on the Ca^{2+} release during the fertilization event, mainly retarding the Ca^{2+} wave front propagation. However, it exerts drastic changes in the cortical actin cytoskeleton, impairing microvilli formation at fertilization, as observed by TEM. In most of the cases vitelline layer elevation is completely or partially blocked, with the formation of aberrant or non fertilization cones, which do not seem to abolish sperm entry.

Finally, the microinjection of the anti-depactin antibody lessens the Ca^{2+} amount released at insemination, which is the clear indication that actin matters in Ca^{2+} signalling.

In conclusion, the results of this dissertation work corroborated and extended the early works from our laboratory that suggested that fine regulation of the actin cytoskeleton is a key player in guiding fertilization because of its involvement in Ca^{2+} signalling and cortical granule exocytosis. Based on the results in this work and what is known in the literature, the emerging consensus on the potential mechanisms of actin-

based regulation of Ca^{2+} signalling is as follows: (1) the local environment of the actin cytoskeleton may modulate the ion channel activities such as $InsP_3$ or cell surface ion channels, (2) In a theory set forth by the pioneering work of K. Lange, the actin assembly and disassembly can serve a mechanism to absorb and release the local Ca^{2+} by directly buffering the Ca^{2+} ions in the actin proteins.

For model 1, actin-dependent modulation has been reported for Na^+/Ca^{2+} exchangers, Na^+/K^+-ATPases, ryanodine receptors and voltage gated Na^+ channels (Rueckschloss and Isenberg, 2001). Moreover, the actin-disrupting drug Cytochalasin D has been demonstrated to inhibit L-type Ca^{2+} channel currents via cofilin protein (Rueckschloss and Isenberg, 2001). A variant of this hypothesis includes not only Ca^{2+} release but Ca^{2+} entry from the extracellular media and refilling of stores as well. Rosado and colls. (Rosado et al., 2000) while studying the store-operated Ca^{2+} entry (SOCE) in human platelets, showed that the cortical actin cytoskeleton plays a crucial role in Ca^{2+} release and entry. The authors suggested that Cytochalasin B and Lat-A treatment generated a biphasic time-dependent behaviour of the Ca^{2+} dynamics: cytosolic Ca^{2+} increase was enhanced after 1 min treatment with the drugs, but blocked after F-actin was depolymerized. The authors believe the *de novo* conformational coupling model to be responsible for the refilling of the internal Ca^{2+} stores. This model suggests that the cortical actin cytoskeleton needs to be disrupted in order to allow the interaction between the ER and the plasma membrane. Then, the drugs-mediated F-actin depolymerization would help and enhance the response while its sustained depolimerization would block SOCE. Moreover, they showed that the actin depolymerization occurred before than the Ca^{2+} release from internal stores, and that it depended on the cofilin protein activity (Redondo et al., 2006). Furthermore, studies of store operated Ca^{2+} channels in rat hepatocytes indicated that disruption of the actin cytoskeleton by cytochalasin D inhibited the Ca^{2+} influx from the extracellular media after induction of internal stores depletion by thapsigargin incubation. Then, although Cytochalasin D did not inhibit the total amount of Ca^{2+}

liberated from the ER in response to thapsigargin, the kinetics of the release were altered, again indicating a possible role for F-actin in internal Ca^{2+} signalling (Wang et al., 2002). Another theory involving the actin cytoskeleton in Ca^{2+} signalling has been proposed in systems presenting stretch-induced Ca^{2+} release. Vascular smooth muscle cells release Ca^{2+} from internal stores after cyclical stretch events in an $InsP_3$, NAADP and cADPr-independent way. The authors have suggested the possibility that the mechanical stress could be transduced from the plasma membrane to the internal stores without the formation of a biochemical mediator. Since the addition of Cytochalasin D (but not nocodazole) inhibited the stretch-induced Ca^{2+} release, it has been suggested that the actin cytoskeleton could be responsible for such mediation (Mohanty and Li, 2002).

For the Model 2 of the actin-based regulation of Ca^{2+} signalling, the possibility that the actin fibers store Ca^{2+} and release it after depolymerization exists. G-actin subunits loaded with ATP present high affinity for binding Ca^{2+}, and once being part of the actin fiber, the exchange rate of Ca^{2+}/Mg^{2+} is 4000- fold lower than for G-actin (Lange and Gartzke, 2006). When F-actin depolymerises, G-actin-ATP subunits represent low affinity binding sites for Ca^{2+}, being rapidly exchanged with Mg^{2+} and thus becoming a free ion (Ca^{2+} release). Cortical F-actin and microvilli that normally undergo threadmilling would serve as a backup reservoir for Ca^{2+} whenever a surge of Ca^{2+} is released in the microdomain. In line with this hypothesis, the F-actin disruption *in vitro* by ultrasounds liberates free Ca^{2+} (Lange and Brandt, 1996), and depolymerization by means of the actin-binding protein profilin can also release Ca^{2+} *in vitro* (Lange, 1999). Experiments carried out in mature starfish eggs *in vivo* demonstrated that disassembly of actin filaments with Lat-A resulted in Ca^{2+} release (Lim et al., 2002).

Since Ca^{2+} signals mediate a vast number of cellular processes and actin is the most abundant protein in eukaryotes (Disanza et al., 2005), as well as one of the most conserved ones, the physiological role of F-actin as a modulator of Ca^{2+} signals might have implications for several cellular systems and organisms.

REFERENCES

Aarhus, R., Dickey, D.M., Graeff, R.M., Gee, K.R., Walseth, T.F. and Lee, H.C. (1996) Activation and inactivation of Ca2+ release by NAADP+. *J Biol Chem*, **271**, 8513-8516.

Ambach, A., Saunus, J., Konstandin, M., Wesselborg, S., Meuer, S.C. and Samstag, Y. (2000) The serine phosphatases PP1 and PP2A associate with and activate the actin-binding protein cofilin in human T lymphocytes. *Eur J Immunol*, **30**, 3422-3431.

Begg, D.A., Wong, G.K., Hoyle, D.H. and Baltz, J.M. (1996) Stimulation of cortical actin polymerization in the sea urchin egg cortex by NH4Cl, procaine and urethane: elevation of cytoplasmic pH is not the common mechanism of action. *Cell Motil Cytoskeleton*, **35**, 210-224.

Berridge, M.J. (2005) Unlocking the secrets of cell signaling. *Annu Rev Physiol*, **67**, 1-21.

Berridge, M.J. (1995) Inositol trisphosphate and calcium signaling. *Ann N Y Acad Sci*, **766**, 31-43.

Berridge, M.J. (1984) Inositol trisphosphate and diacylglycerol as second messengers. *Biochem J*, **220**, 345-360.

Bose, D.D. and Thomas, D.W. (2009) The actin cytoskeleton differentially regulates NG115-401L cell ryanodine receptor and inositol 1,4,5-trisphosphate receptor induced calcium signaling pathways. *Biochem Biophys Res Commun*, **379**, 594-599.

Bubb, M.R., Spector, I., Beyer, B.B. and Fosen, K.M. (2000) Effects of jasplakinolide on the kinetics of actin polymerization. An explanation for certain in vivo observations. *J Biol Chem*, **275**, 5163-5170.

Burgess, D.R. and Schroeder, T.E. (1977) Polarized bundles of actin filaments within microvilli of fertilized sea urchin eggs. *J Cell Biol*, **74**, 1032-1037.

Calcraft, P.J., Ruas, M., Pan, Z., Cheng, X., Arredouani, A., Hao, X., Tang, J., Rietdorf, K., Teboul, L., Chuang, K.T., Lin, P., Xiao, R., Wang, C., Zhu, Y., Lin, Y., Wyatt, C.N., Parrington, J., Ma, J., Evans, A.M., Galione, A. and Zhu, M.X. (2009) NAADP mobilizes calcium from acidic organelles through two-pore channels. *Nature*, **459**, 596-600.

Camps, M., Carozzi, A., Schnabel, P., Scheer, A., Parker, P.J. and Gierschik, P. (1992) Isozyme-selective stimulation of phospholipase C-beta 2 by G protein beta gamma-subunits. *Nature*, **360**, 684-686.

Carafoli, E. (2002) Calcium signaling: a tale for all seasons. *Proc Natl Acad Sci U S A*, **99**, 1115-1122.

Carroll, D.J., Ramarao, C.S., Mehlmann, L.M., Roche, S., Terasaki, M. and Jaffe, L.A. (1997) Calcium release at fertilization in starfish eggs is mediated by phospholipase Cgamma. *J Cell Biol*, **138**, 1303-1311.

Carroll, J., Jones, K.T. and Whittingham, D.G. (1996) Ca2+ release and the development of Ca2+ release mechanisms during oocyte maturation: a prelude to fertilization. *Rev Reprod*, **1**, 137-143.

Chiba, K. (2000) Meiosis reinintiation in starfish oocyte. *Zool Sci*, **17**, 413-417.

Chiba, K., Longo, F.J., Kontani, K., Katada, T. and Hoshi, M. (1995) A periodic network of G protein beta gamma subunit coexisting with cytokeratin filament in starfish oocytes. *Dev Biol*, **169**, 415-420.

Chiba, K., Kado, R.T. and Jaffe, L.A. (1990) Development of calcium release mechanisms during starfish oocyte maturation. *Dev Biol*, **140**, 300-306.

Churchill, G.C., Okada, Y., Thomas, J.M., Genazzani, A.A., Patel, S. and Galione, A. (2002) NAADP mobilizes Ca(2+) from reserve granules, lysosome-related organelles, in sea urchin eggs. *Cell*, **111**, 703-708.

Ciapa, B., Borg, B. and Whitaker, M. (1992) Polyphosphoinositide metabolism during the fertilization wave in sea urchin eggs. *Development*, **115**, 187-195.

Clapham, D.E. (1995) Calcium signaling. *Cell*, **80**, 259-268.

Clapper, D.L., Walseth, T.F., Dargie, P.J. and Lee, H.C. (1987) Pyridine nucleotide metabolites stimulate calcium release from sea urchin egg microsomes desensitized to inositol trisphosphate. *J Biol Chem*, **262**, 9561-9568.

Cooper, J.A. (1987) Effects of cytochalasin and phalloidin on actin. *J Cell Biol*, **105**, 1473-1478.

Crabb, J.H. and Jackson, R.C. (1986) Polycation inhibition of exocytosis from sea urchin egg cortex. *J Membr Biol*, **91**, 85-96.

Davis, L.C., Morgan, A.J., Ruas, M., Wong, J.L., Graeff, R.M., Poustka, A.J., Lee, H.C., Wessel, G.M., Parrington, J. and Galione, A. (2008) Ca(2+) signaling occurs via second messenger release from intraorganelle synthesis sites. *Curr Biol*, **18**, 1612-1618.

De Nadai, C., Cailliau, K., Epel, D. and Ciapa, B. (1998) Detection of phospholipase Cgamma in sea urchin eggs. *Dev Growth Differ*, **40**, 669-676.

Di Paolo, G. and De Camilli, P. (2006) Phosphoinositides in cell regulation and membrane dynamics. *Nature*, **443**, 651-657.

Disanza, A., Steffen, A., Hertzog, M., Frittoli, E., Rottner, K. and Scita, G. (2005) Actin polymerization machinery: the finish line of signaling networks, the starting point of cellular movement. *Cell Mol Life Sci*, **62**, 955-970.

Doree, M., Cavadore, J.C. and Picard, A. (1990) Facts and hypotheses of calcium regulation of MPF activity during meiotic maturation of starfish oocytes. *J Reprod Fertil Suppl*, **42**, 135-140.

Doree, M., Moreau, M. and Guerrier, P. (1978) Hormonal control of meiosis. In vitro induced release of calcium ions from the plasma membrane in starfish oocytes. *Exp Cell Res*, **115**, 251-260.

Doree, M. and Guerrier, P. (1975) Site of action of 1-methyladenine in inducing oocyte maturation in starfish. Kinetic evidence for receptors localized on the cell membrane. *Exp Cell Res*, **91**, 296-300.

Downes, C.P., Gray, A. and Lucocq, J.M. (2005) Probing phosphoinositide functions in signaling and membrane trafficking. *Trends Cell Biol*, **15**, 259-268.

Eddy, E.M. and Shapiro, B.M. (1976) Changes in the topography of the sea urchin egg after fertilization. *J Cell Biol*, **71**, 35-48.

Fissore, R.A. and Robl, J.M. (1994) Mechanism of calcium oscillations in fertilized rabbit eggs. *Dev Biol*, **166**, 634-642.

FitzHarris, G., Marangos, P. and Carroll, J. (2003) Cell cycle-dependent regulation of structure of endoplasmic reticulum and inositol 1,4,5-trisphosphate-induced Ca2+ release in mouse oocytes and embryos. *Mol Biol Cell*, **14**, 288-301.

Foltz, K.R. and Lennarz, W.J. (1993) The molecular basis of sea urchin gamete interactions at the egg plasma membrane. *Dev Biol*, **158**, 46-61.

Franco, L., Guida, L., Bruzzone, S., Zocchi, E., Usai, C. and De Flora, A. (1998) The transmembrane glycoprotein CD38 is a catalytically active transporter responsible for generation and influx of the second messenger cyclic ADP-ribose across membranes. *Faseb J*, **12**, 1507-1520.

Fujimoto, T., Miyawaki, A. and Mikoshiba, K. (1995) Inositol 1,4,5-trisphosphate receptor-like protein in plasmalemmal caveolae is linked to actin filaments. *J Cell Sci*, **108 (Pt 1)**, 7-15.

Fujiwara, T., Nakada, K., Shirakawa, H. and Miyazaki, S. (1993) Development of inositol trisphosphate-induced calcium release mechanism during maturation of hamster oocytes. *Dev Biol*, **156**, 69-79.

Furuichi, T., Yoshikawa, S., Miyawaki, A., Wada, K., Maeda, N. and Mikoshiba, K. (1989) Primary structure and functional expression of the inositol 1,4,5-trisphosphate-binding protein P400. *Nature*, **342**, 32-38.

Galione, A., McDougall, A., Busa, W.B., Willmott, N., Gillot, I. and Whitaker, M. (1993) Redundant mechanisms of calcium-induced calcium release underlying calcium waves during fertilization of sea urchin eggs. *Science*, **261**, 348-352.

Galione, A. (1994) Cyclic ADP ribose, the ADP-ribosyl cyclase pathway and calcium signalling. *Mol Cell Endocrinol*, **98** (2), 125-31.

Genazzani, A.A., Mezna, M., Dickey, D.M., Michelangeli, F., Walseth, T.F. and Galione, A. (1997) Pharmacological properties of the Ca2+-release mechanism sensitive to NAADP in the sea urchin egg. *Br J Pharmacol*, **121**, 1489-1495.

Gerasimenko, O.V., Gerasimenko, J.V., Tepikin, A.V. and Petersen, O.H. (1995) ATP-dependent accumulation and inositol trisphosphate- or cyclic ADP-ribose-mediated release of Ca2+ from the nuclear envelope. *Cell*, **80**, 439-444.

Gerasimenko, O. and Gerasimenko, J. (2004) New aspects of nuclear calcium signalling. *J Cell Sci*, **117**, 3087-3094.

Gerasimenko, J.V., Maruyama, Y., Yano, K., Dolman, N.J., Tepikin, A.V., Petersen, O.H. and Gerasimenko, O.V. (2003) NAADP mobilizes Ca2+ from a thapsigargin-sensitive store in the nuclear envelope by activating ryanodine receptors. *J Cell Biol*, **163**, 271-282.

Ghosh, M., Song, X., Mouneimne, G., Sidani, M., Lawrence, D.S. and Condeelis, J.S. (2004) Cofilin promotes actin polymerization and defines the direction of cell motility. *Science*, **304**, 743-746.

Gieni, R.S. and Hendzel, M.J. (2009) Actin dynamics and functions in the interphase nucleus: moving toward an understanding of nuclear polymeric actin. *Biochem Cell Biol*, **87**, 283-306.

Gilkey, J.C., Jaffe, L.F., Ridgway, E.B. and Reynolds, G.T. (1978) A free calcium wave traverses the activating egg of the medaka, Oryzias latipes. *J Cell Biol*, **76**, 448-466.

Giusti, A.F., Xu, W., Hinkle, B., Terasaki, M. and Jaffe, L.A. (2000) Evidence that fertilization activates starfish eggs by sequential activation of a Src-like kinase and phospholipase cgamma. *J Biol Chem*, **275**, 16788-16794.

Giusti, A.F., Carroll, D.J., Abassi, Y.A., Terasaki, M., Foltz, K.R. and Jaffe, L.A. (1999) Requirement of a Src family kinase for initiating calcium release at fertilization in starfish eggs. *J Biol Chem*, **274**, 29318-29322.

Guse, A.H. and Lee, H.C. (2008) NAADP: a universal Ca2+ trigger. *Sci Signal*, **1**, re10.

Guse, A.H. (2000) Cyclic ADP-ribose. *J Mol Med*, **78**, 26-35.

Halet, G., Tunwell, R., Balla, T., Swann, K. and Carroll, J. (2002) The dynamics of plasma membrane PtdIns(4,5)P(2) at fertilization of mouse eggs. *J Cell Sci*, **115**, 2139-2149.

Hamaguchi, Y. and Mabuchi, I. (1982) Effects of phalloidin microinjection and localization of fluorescein-labeled phalloidin in living sand dollar eggs. *Cell Motil*, **2**, 103-113.

Heil-Chapdelaine, R.A. and Otto, J.J. (1996) Characterization of changes in F-actin during maturation of starfish oocytes. *Dev Biol*, **177**, 204-216.

Higgs, H.N. and Pollard, T.D. (1999) Regulation of actin polymerization by Arp2/3 complex and WASp/Scar proteins. *J Biol Chem*, **274**, 32531-32534.

Hilpela, P., Vartiainen, M.K. and Lappalainen, P. (2004) Regulation of the actin cytoskeleton by PI(4,5)P2 and PI(3,4,5)P3. *Curr Top Microbiol Immunol*, **282**, 117-163.

Hinchliffe, K.A., Irvine, R.F. and Divecha, N. (1996) Aggregation-dependent, integrin-mediated increases in cytoskeletally associated PtdInsP2 (4,5) levels in human platelets are controlled by translocation of PtdIns 4-P 5-kinase C to the cytoskeleton. *Embo J*, **15**, 6516-6524.

Hirose, K., Kadowaki, S., Tanabe, M., Takeshima, H. and Iino, M. (1999). Spatiotemporal dynamics of inositol 1,4,5-trisphosphate that underlies complex Ca2+ mobilization patterns. *Science,* **284**, 1527-1530.

Hokin, L.E. (1985) Receptors and phosphoinositide-generated second messengers. *Annu Rev Biochem*, **54**, 205-235.

Ikegami, S., Tamura, S. and Kanatani, H. (1967) Starfish gonad: action and chemical identification of spawning inhibitor. *Science*, **158**, 1052-1053.

Iwasaki, H., Chiba, K., Uchiyama, T., Yoshikawa, F., Suzuki, F., Ikeda, M., Furuichi, T. and Mikoshiba, K. (2002) Molecular characterization of the starfish inositol 1,4,5-trisphosphate receptor and its role during oocyte maturation and fertilization. *J Biol Chem*, **277**, 2763-2772.

Jaffe, L.A. and Terasaki, M. (1994) Structural changes in the endoplasmic reticulum of starfish oocytes during meiotic maturation and fertilization. *Dev Biol*, **164**, 579-587.

Jaffe, L.A., Gallo, C.J., Lee, R.H., Ho, Y.K. and Jones, T.L. (1993) Oocyte maturation in starfish is mediated by the beta gamma-subunit complex of a G-protein. *J Cell Biol*, **121**, 775-783.

Jaffe, L.A., Turner, P.R., Kline, D., Kado, R.T. and Shilling, F. (1988) G-proteins and egg activation. *Cell Differ Dev*, **25 Suppl**, 15-18.

Jaffe, L.F. (1991) The path of calcium in cytosolic calcium oscillations: a unifying hypothesis. *Proc Natl Acad Sci U S A*, **88**, 9883-9887.

Janmey, P.A. (1998) The cytoskeleton and cell signaling: component localization and mechanical coupling. *Physiol Rev*, **78**, 763-781.

Kanatani, H. and Hiramoto, Y. (1970) Site of action of 1-methyladenine in inducing oocyte maturation in starfish. *Exp Cell Res*, **61**, 280-284.

Kanatani, H. (1969). Induction of spawning and oocyte maturation by 1-methyladenine in starfishes. *Exp. Cell Res.* **57**, 333–337.

Kishimoto, T. (1999) Activation of MPF at meiosis reinitiation in starfish oocytes. *Dev Biol*, **214**, 1-8.

Kishimoto, T. (1998) Cell cycle arrest and release in starfish oocytes and eggs. *Semin Cell Dev Biol*, **9**, 549-557.

Kline, D. (2000) Attributes and dynamics of the endoplasmic reticulum in mammalian eggs. *Curr Top Dev Biol*, **50**, 125-154.

Kline, D., Mehlmann, L., Fox, C. and Terasaki, M. (1999) The cortical endoplasmic reticulum (ER) of the mouse egg: localization of ER clusters in relation to the generation of repetitive calcium waves. *Dev Biol*, **215**, 431-442.

Kuroda, R., Kontani, K., Kanda, Y., Katada, T., Nakano, T., Satoh, Y., Suzuki, N. and Kuroda, H. (2001) Increase of cGMP, cADP-ribose and inositol 1,4,5-trisphosphate preceding Ca(2+) transients in fertilization of sea urchin eggs. *Development*, **128**, 4405-4414.

Kyozuka, K., Chun, J.T., Puppo, A., Gragnaniello, G., Garante, E. and Santella, L. (2009) Guanine nucleotides in the meiotic maturation of starfish oocytes: regulation of the actin cytoskeleton and of Ca(2+) signaling. *PLoS One*, **4**, e6296.

Kyozuka, K., Chun, J.T., Puppo, A., Gragnaniello, G., Garante, E. and Santella, L. (2008) Actin cytoskeleton modulates calcium signaling during maturation of starfish oocytes. *Dev Biol*, Vol. 320, pp. 426-435.

Lange, K., Gartzke, J. (2006) F-actin based Ca signaling-a critical comparison with the current concept of Ca signaling. *J Cell Physiol,* **209** (2), 270-87.

Lange, K. (1999) Microvillar Ca++ signaling: a new view of an old problem. *J Cell Physiol,* **180** (1), 19-34.

Lange, K. and Brandt, U. (1996) Calcium storage and release properties of F-actin: evidence for the involvement of F-actin in cellular calcium signaling. *FEBS Lett*, **395**, 137-142.

Lawrence, Y., Whitaker, M. and Swann, K. (1997) Sperm-egg fusion is the prelude to the initial Ca2+ increase at fertilization in the mouse. *Development*, **124**, 233-241.

Lee, H.C. (2004) Multiplicity of Ca2+ messengers and Ca2+ stores: a perspective from cyclic ADP-ribose and NAADP. *Curr Mol Med*, **4**, 227-237.

Lee, H.C. (1999) A unified mechanism of enzymatic synthesis of two calcium messengers: cyclic ADP-ribose and NAADP. *Biol Chem*, **380**, 785-793.

Lee, H.C., Aarhus, R. and Graeff, R.M. (1995) Sensitization of calcium-induced calcium release by cyclic ADP-ribose and calmodulin. *J Biol Chem*, **270**, 9060-9066.

Lee, H.C., Aarhus, R. and Walseth, T.F. (1993) Calcium mobilization by dual receptors during fertilization of sea urchin eggs. *Science*, **261**, 352-355.

Lemmon, M.A., Ferguson, K.M., O'Brien, R., Sigler, P.B. and Schlessinger, J. (1995) Specific and high-affinity binding of inositol phosphates to an isolated pleckstrin homology domain. *Proc Natl Acad Sci U S A*, **92**, 10472-10476.

Lenart, P., Bacher, C.P., Daigle, N., Hand, A.R., Eils, R., Terasaki, M. and Ellenberg, J. (2005) A contractile nuclear actin network drives chromosome congression in oocytes. *Nature*, **436**, 812-818.

Lim, D., Ercolano, E., Kyozuka, K., Nusco, G.A., Moccia, F., Lange, K. and Santella, L. (2003) The M-phase-promoting factor modulates the sensitivity of the Ca2+ stores to inositol 1,4,5-trisphosphate via the actin cytoskeleton. *J Biol Chem*, **278**, 42505-42514.

Lim, D., Lange, K. and Santella, L. (2002) Activation of oocytes by latrunculin A. *Faseb J*, **16**, 1050-1056.

Lim, D., Kyozuka, K., Gragnaniello, G., Carafoli, E. and Santella, L. (2001) NAADP+ initiates the Ca2+ response during fertilization of starfish oocytes. *Faseb J*, **15**, 2257-2267.

Longo, F.J., So, F., Schueltz, A.W. (1982) Meiotic Maturation And The Cortical Granule Reaction in Starfish Eggs. *Biol. Bull.*, **163**, 465-476.

Lupu, V.D., Kaznacheyeva, E., Krishna, U.M., Falck, J.R. and Bezprozvanny, I. (1998) Functional coupling of phosphatidylinositol 4,5-bisphosphate to inositol 1,4,5-trisphosphate receptor. *J Biol Chem*, **273**, 14067-14070.

Ma, L., Cantley, L.C., Janmey, P.A. and Kirschner, M.W. (1998) Corequirement of specific phosphoinositides and small GTP-binding protein Cdc42 in inducing actin assembly in Xenopus egg extracts. *J Cell Biol*, **140**, 1125-1136.

Mabuchi, I. (1983) An actin-depolymerizing protein (depactin) from starfish oocytes: properties and interaction with actin. *J Cell Biol*, **97**, 1612-1621.

Mabuchi, I. (1981) Purification from starfish eggs of a protein that depolymerizes actin. *J Biochem*, **89**, 1341-1344.

Masui, Y. and Markert, C.L. (1971) Cytoplasmic control of nuclear behavior during meiotic maturation of frog oocytes. *J Exp Zool*, **177**, 129-145.

McAvey, B.A., Wortzman, G.B., Williams, C.J. and Evans, J.P. (2002) Involvement of calcium signaling and the actin cytoskeleton in the membrane block to polyspermy in mouse eggs. *Biol Reprod*, **67**, 1342-1352.

McDougall, A., Shearer, J. and Whitaker, M. (2000) The initiation and propagation of the fertilization wave in sea urchin eggs. *Biol Cell*, **92**, 205-214.

McGough, A., Pope, B., Chiu, W. and Weeds, A. (1997) Cofilin changes the twist of F-actin: implications for actin filament dynamics and cellular function. *J Cell Biol*, **138**, 771-781.

McLaughlin, S. and Whitaker, M. (1988) Cations that alter surface potentials of lipid bilayers increase the calcium requirement for exocytosis in sea urchin eggs. *J Physiol*, **396**, 189-204.

Meijer, L. and Guerrier, P. (1981) Calmodulin in starfish oocytes. I. Calmodulin antagonists inhibit meiosis reinitiation. *Dev Biol*, **88**, 318-324.

Moccia, F., Nusco, G.A., Lim, D., Kyozuka, K. and Santella, L. (2006) NAADP and InsP3 play distinct roles at fertilization in starfish oocytes. *Dev Biol*, **294**, 24-38.

Moccia, F., Lim, D., Kyozuka, K. and Santella, L. (2004) NAADP triggers the fertilization potential in starfish oocytes. *Cell Calcium*, **36**, 515-524.

Moccia, F., Lim, D., Nusco, G.A., Ercolano, E. and Santella, L. (2003) NAADP activates a Ca2+ current that is dependent on F-actin cytoskeleton. *Faseb J*, **17**, 1907-1909.

Mohanty, M.J. and Li, X. (2002) Stretch-induced Ca(2+) release via an IP(3)-insensitive Ca(2+) channel. *Am J Physiol Cell Physiol*, **283**, C456-462.

Mohri, T., Ivonnet, P.I. and Chambers, E.L. (1995) Effect on sperm-induced activation current and increase of cytosolic Ca2+ by agents that modify the mobilization of [Ca2+]i. I. Heparin and pentosan polysulfate. *Dev Biol*, **172**, 139-157.

Monkawa, T., Miyawaki, A., Sugiyama, T., Yoneshima, H., Yamamoto-Hino, M., Furuichi, T., Saruta, T., Hasegawa, M. and Mikoshiba, K. (1995) Heterotetrameric complex formation of inositol 1,4,5-trisphosphate receptor subunits. *J Biol Chem*, **270**, 14700-14704.

Moreau, M., Guerrier, P., Doree, M. and Ashley, C.C. (1978) Hormone-induced release of intracellular Ca2+ triggers meiosis in starfish oocytes. *Nature*, **272**, 251-253.

Morisawa, M., and Kanatani, H. (1978) Oocyte-surface factor responsible for 1-methyladenine-induced oocyte maturation in starfish. *Gamete Res,* 1: 157-164.

Muallem, S., Kwiatkowska, K., Xu, X. and Yin, H.L. (1995) Actin filament disassembly is a sufficient final trigger for exocytosis in nonexcitable cells. *J Cell Biol*, **128**, 589-598.

Nakahara, M., Shimozawa, M., Nakamura, Y., Irino, Y., Morita, M., Kudo, Y. and Fukami, K. (2005) A novel phospholipase C, PLC(eta)2, is a neuron-specific isozyme. *J Biol Chem*, **280**, 29128-29134.

Nakamura, S. and Hiramoto, Y. (1978) Mechanical properties of the cell surface in starfish eggs. *Dev Growth Differ*, **24**, 429-442.

Nash, M. S., Young, K. W., John Challiss, R. A. and Nahorski, S. R. (2001). Receptor-specific messenger oscillations. *Nature,* **413**, 381-382.

Nemoto, S.-I. (1982) Nature of the 1-methyladenine-requiring phase of starfish oocytes. *Dev Growth Differ*, **24**, 429-442.

Nemoto, S-I., Yoneda, M. and Uemura, I. (1980) Marked decrease in the rigidity of starfish oocytes induced by 1-methyladenine. *Dev Growth Differ*, **22**, 315-325.

Niwa, R., Nagata-Ohashi, K., Takeichi, M., Mizuno, K. and Uemura, T. (2002) Control of actin reorganization by Slingshot, a family of phosphatases that dephosphorylate ADF/cofilin. *Cell*, **108**, 233-246.

Noh, D.Y., Shin, S.H. and Rhee, S.G. (1995) Phosphoinositide-specific phospholipase C and mitogenic signaling. *Biochim Biophys Acta*, **1242**, 99-113.

Nuccitelli, R., Yim, D.L. and Smart, T. (1993) The sperm-induced Ca2+ wave following fertilization of the Xenopus egg requires the production of Ins(1, 4, 5)P3. *Dev Biol*, **158**, 200-212.

Nusco, G.A., Chun, J.T., Ercolano, E., Lim, D., Gragnaniello, G., Kyozuka, K. and Santella, L. (2006) Modulation of calcium signalling by the actin-binding protein cofilin. *Biochem Biophys Res Commun*, **348**, 109-114.

Nusco, G.A., Lim, D., Sabala, P. and Santella, L. (2002) Ca(2+) response to cADPr during maturation and fertilization of starfish oocytes. *Biochem Biophys Res Commun*, **290**, 1015-1021.

Okumura, E., Fukuhara, T., Yoshida, H., Hanada Si, S., Kozutsumi, R., Mori, M., Tachibana, K. and Kishimoto, T. (2002) Akt inhibits Myt1 in the signalling pathway that leads to meiotic G2/M-phase transition. *Nat Cell Biol*, **4**, 111-116.

Ono, S. (2007) Mechanism of depolymerization and severing of actin filaments and its significance in cytoskeletal dynamics. *Int Rev Cytol*, **258**, 1-82.

Ookata, K., Hisanaga, S., Okumura, E. and Kishimoto, T. (1993) Association of p34cdc2/cyclin B complex with microtubules in starfish oocytes. *J Cell Sci*, **105 (Pt 4)**, 873-881.

Parrington, J., Davis, L.C., Galione, A. and Wessel, G. (2007) Flipping the switch: how a sperm activates the egg at fertilization. *Dev Dyn*, **236**, 2027-2038.

Parrington, J., Brind, S., De Smedt, H., Gangeswaran, R., Lai, F.A., Wojcikiewicz, R. and Carroll, J. (1998) Expression of inositol 1,4,5-trisphosphate receptors in mouse oocytes and early embryos: the type I isoform is upregulated in oocytes and downregulated after fertilization. *Dev Biol*, **203**, 451-461.

Patel, R., Holt, M., Philipova, R., Moss, S., Schulman, H., Hidaka, H. and Whitaker, M. (1999) Calcium/calmodulin-dependent phosphorylation and activation of human Cdc25-C at the G2/M phase transition in HeLa cells. *J Biol Chem*, **274**, 7958-7968.

Payrastre, B., Missy, K., Giuriato, S., Bodin, S., Plantavid, M. and Gratacap, M. (2001) Phosphoinositides: key players in cell signalling, in time and space. *Cell Signal*, **13**, 377-387.

Pendleton, A., Pope, B., Weeds, A. and Koffer, A. (2003) Latrunculin B or ATP depletion induces cofilin-dependent translocation of actin into nuclei of mast cells. *J Biol Chem*, **278**, 14394-14400.

Picard, A., Giraud, F., Le Bouffant, F., Sladeczek, F., Le Peuch, C. and Doree, M. (1985) Inositol 1,4,5-triphosphate microinjection triggers activation, but not meiotic maturation in amphibian and starfish oocytes. *FEBS Lett*, **182**, 446-450.

Pinton, P., Pozzan, T. and Rizzuto, R. (1998) The Golgi apparatus is an inositol 1,4,5-trisphosphate-sensitive Ca2+ store, with functional properties distinct from those of the endoplasmic reticulum. *Embo J*, **17**, 5298-5308.

Puppo, A., Chun, J.T., Gragnaniello, G., Garante, E. and Santella, L. (2008) Alteration of the cortical actin cytoskeleton deregulates Ca2+ signaling, monospermic fertilization, and sperm entry. *PLoS ONE*, **3**, e3588.

Redondo, P.C., Harper, M.T., Rosado, J.A. and Sage, S.O. (2006) A role for cofilin in the activation of store-operated calcium entry by de novo conformational coupling in human platelets. *Blood*, **107**, 973-979.

Rhee, S.G. (2001) Regulation of phosphoinositide-specific phospholipase C. *Annu Rev Biochem*, **70**, 281-312.

Rosado, J.A., Jenner, S. and Sage, S.O. (2000) A role for the actin cytoskeleton in the initiation and maintenance of store-mediated calcium entry in human platelets. Evidence for conformational coupling. *J Biol Chem*, **275**, 7527-7533.

Rueckschloss, U. and Isenberg, G. (2001) Cytochalasin D reduces Ca2+ currents via cofilin-activated depolymerization of F-actin in guinea-pig cardiomyocytes. *J Physiol*, **537**, 363-370.

Runft, L.L., Carroll, D.J., Gillett, J., Giusti, A.F., O'Neill, F.J. and Foltz, K.R. (2004) Identification of a starfish egg PLC-gamma that regulates Ca2+ release at fertilization. *Dev Biol*, **269**, 220-236.

Runge, K.E., Evans, J.E., He, Z.Y., Gupta, S., McDonald, K.L., Stahlberg, H., Primakoff, P. and Myles, D.G. (2007) Oocyte CD9 is enriched on the microvillar membrane and required for normal microvillar shape and distribution. *Dev Biol*, **304**, 317-325.

Sadler, K.C. and Ruderman, J.V. (1998) Components of the signaling pathway linking the 1-methyladenine receptor to MPF activation and maturation in starfish oocytes. *Dev Biol*, **197**, 25-38.

Santella, L., Puppo, A. and Chun, J.T. (2008) The role of the actin cytoskeleton in calcium signaling in starfish oocytes. *Int J Dev Biol*, **52**, 571-584.

Santella, L., Lim, D. and Moccia, F. (2004) Calcium and fertilization: the beginning of life. *Trends Biochem Sci*, **29**, 400-408.

Santella, L., Kyozuka, K., Genazzani, A.A., De Riso, L. and Carafoli, E. (2000) Nicotinic acid adenine dinucleotide phosphate-induced Ca(2+) release. Interactions among distinct Ca(2+) mobilizing mechanisms in starfish oocytes. *J Biol Chem*, **275**, 8301-8306.

Santella, L., De Riso, L., Gragnaniello, G. and Kyozuka, K. (1999) Cortical granule translocation during maturation of starfish oocytes requires cytoskeletal

rearrangement triggered by InsP3-mediated Ca2+ release. *Exp Cell Res*, **248**, 567-574.

Santella, L., De Riso, L., Gragnaniello, G. and Kyozuka, K. (1998) Separate activation of the cytoplasmic and nuclear calcium pools in maturing starfish oocytes. *Biochem Biophys Res Commun*, **252**, 1-4.

Santella, L. and Kyozuka, K. (1997) Effects of 1-methyladenine on nuclear Ca2+ transients and meiosis resumption in starfish oocytes are mimicked by the nuclear injection of inositol 1,4,5-trisphosphate and cADP-ribose. *Cell Calcium*, **22**, 11-20.

Santella, L. and Kyozuka, K. (1994) Reinitiation of meiosis in starfish oocytes requires an increase in nuclear Ca2+. *Biochem Biophys Res Commun*, **203**, 674-680.

Sardet, C., Prodon, F., Dumollard, R., Chang, P. and Chenevert, J. (2002) Structure and function of the egg cortex from oogenesis through fertilization. *Dev Biol*, **241**, 1-23.

Saunders, C.M., Larman, M.G., Parrington, J., Cox, L.J., Royse, J., Blayney, L.M., Swann, K. and Lai, F.A. (2002) PLC zeta: a sperm-specific trigger of Ca(2+) oscillations in eggs and embryo development. *Development*, **129**, 3533-3544.

Schindler, M., Koppel, D.E. and Sheetz, M.P. (1980) Modulation of membrane protein lateral mobility by polyphosphates and polyamines. *Proc Natl Acad Sci U S A*, **77**, 1457-1461.

Schroeder, T.E. and Otto, J.J. (1991) Snoods: a periodic network containing cytokeratin in the cortex of starfish oocytes. *Dev Biol*, **144**, 240-247.

Schroeder, T.E. and Otto, J.J. (1984) Assembly-disassembly of actin bundles in starfish oocytes: An analysis of actin-associated proteins in the isolated cortex. *Dev. Biol.* **101**, 263–273.

Schroeder, T.E. and Stricker, S.A. (1983) Morphological changes during maturation of starfish oocytes: surface ultrastructure and cortical actin. *Dev Biol*, **98**, 373-384.

Schroeder, T.E. (1981) Microfilament-mediated surface change in starfish oocytes in response to 1-methyladenine: implications for identifying the pathway and receptor sites for maturation-inducing hormones. *J Cell Biol*, **90**, 362-371.

Schuel, H. (1978). Secretary functions of egg cortical granules in fertilization and development: a critical review. *Gamete Res*, **1**, 299-382

Sechi, A.S. and Wehland, J. (2000) The actin cytoskeleton and plasma membrane connection: PtdIns(4,5)P(2) influences cytoskeletal protein activity at the plasma membrane. *J Cell Sci*, **113 Pt 21**, 3685-3695.

Shida, H. and Shida, M. (1976) Inhibitory effect of alpha-(1 leads to 6)-heterogalactan on oocyte maturation of starfish induced by 1-methyladenine. *Nature*, **263**, 77-79.

Shilling, F., Chiba, K., Hoshi, M., Kishimoto, T. and Jaffe, L.A. (1989) Pertussis toxin inhibits 1-methyladenine-induced maturation in starfish oocytes. *Dev Biol*, **133**, 605-608.

Sitsapesan, R., McGarry, S.J. and Williams, A.J. (1995) Cyclic ADP-ribose, the ryanodine receptor and Ca2+ release. *Trends Pharmacol Sci*, **16**, 386-391.

Spector, I., Shochet, N.R., Blasberger, D. and Kashman, Y. (1989) Latrunculins--novel marine macrolides that disrupt microfilament organization and affect cell growth: I. Comparison with cytochalasin D. *Cell Motil Cytoskeleton*, **13**, 127-144.

States, D.J., Walseth, T.F. and Lee, H.C. (1992) Similarities in amino acid sequences of Aplysia ADP-ribosyl cyclase and human lymphocyte antigen CD38. *Trends Biochem Sci*, **17**, 495.

Stauffer, T.P., Ahn, S. and Meyer, T. (1998) Receptor-induced transient reduction in plasma membrane PtdIns(4,5)P2 concentration monitored in living cells. *Curr Biol*, **8**, 343-346.

Streb, H., Irvine, R.F., Berridge, M.J. and Schulz, I. (1983) Release of Ca2+ from a nonmitochondrial intracellular store in pancreatic acinar cells by inositol-1,4,5-trisphosphate. *Nature*, **306**, 67-69.

Stricker, S., and Schatten, G. (1991). The cytoskeleton and nuclear disassembly during germinal vesicle breakdown in starfish oocytes. *Dev. Growth Differ.* **33,** 163–171.

Strickland, L., von Dassow, G., Ellenberg, J., Foe, V., Lenart, P. and Burgess, D. (2004) Light Microscopy of Echinoderm Embryos. Methods in Cell Biology. Vol 74. Elsevier Inc.

Sun, H.Q., Yamamoto, M., Mejillano, M. and Yin, H.L. (1999) Gelsolin, a multifunctional actin regulatory protein. *J Biol Chem*, **274**, 33179-33182.

Sutoh, K. and Mabuchi, I. (1989) End-label fingerprintings show that an N-terminal segment of depactin participates in interaction with actin. *Biochemistry*, **28**, 102-106.

Swann, K., McCulloh, D.H., McDougall, A., Chambers, E.L. and Whitaker, M. (1992) Sperm-induced currents at fertilization in sea urchin eggs injected with EGTA and neomycin. *Dev Biol*, **151**, 552-563.

Swann, K. and Whitaker, M. (1986) The part played by inositol trisphosphate and calcium in the propagation of the fertilization wave in sea urchin eggs. *J Cell Biol*, **103**, 2333-2342.

Takagi, T., Konishi, K. and Mabuchi, I. (1988) Amino acid sequence of starfish oocyte depactin. *J Biol Chem*, **263**, 3097-3102.

Takai, Y., Kishimoto, A., Kikkawa, U., Mori, T. and Nishizuka, Y. (1979) Unsaturated diacylglycerol as a possible messenger for the activation of calcium-activated, phospholipid-dependent protein kinase system. *Biochem Biophys Res Commun*, **91**, 1218-1224.

Tall, E.G., Spector, I., Pentyala, S.N., Bitter, I. and Rebecchi, M.J. (2000) Dynamics of phosphatidylinositol 4,5-bisphosphate in actin-rich structures. *Curr Biol*, **10**, 743-746.

Thaler, C.D., Kuo, R.C., Patton, C., Preston, C.M., Yagisawa, H. and Epel, D. (2004) Phosphoinositide metabolism at fertilization of sea urchin eggs measured with a GFP-probe. *Dev Growth Differ*, **46**, 413-423.

Tosuji, H., Miyaji, K., Fusetani, N. and Nakazawa, T. (2000) Effect of calyculin A on the surface structure of unfertilized sea urchin eggs. *Cell Motil Cytoskeleton*, **46**, 129-136.

Turvey, M.R., Fogarty, K.E. and Thorn, P. (2005) Inositol (1,4,5)-trisphosphate receptor links to filamentous actin are important for generating local Ca2+ signals in pancreatic acinar cells. *J Cell Sci*, **118**, 971-980.

Varnai, P. and Balla, T. (1998) Visualization of phosphoinositides that bind pleckstrin homology domains: calcium- and agonist-induced dynamic changes and relationship to myo-[3H]inositol-labeled phosphoinositide pools. *J Cell Biol*, **143**, 501-510.

Ville, C.A., Walker, W.F. and Barnes, R.D. (1978) Zoologia Generale, 5th edn. Editoriale Grasso pp. 851-859.

Voronina, E. and Wessel, G.M. (2004) betagamma subunits of heterotrimeric G-proteins contribute to Ca2+ release at fertilization in the sea urchin. *J Cell Sci*, **117**, 5995-6005.

Wang, C., Du, X.N., Jia, Q.Z. and Zhang, H.L. (2005) Binding of PLCdelta1PH-GFP to PtdIns(4,5)P2 prevents inhibition of phospholipase C-mediated hydrolysis of PtdIns(4,5)P2 by neomycin. *Acta Pharmacol Sin*, **26**, 1485-1491.

Wang, Y.J., Gregory, R.B. and Barritt, G.J. (2002) Maintenance of the filamentous actin cytoskeleton is necessary for the activation of store-operated Ca2+ channels, but not other types of plasma-membrane Ca2+ channels, in rat hepatocytes. *Biochem J*, **363**, 117-126.

Watt, S.A., Kular, G., Fleming, I.N., Downes, C.P. and Lucocq, J.M. (2002) Subcellular localization of phosphatidylinositol 4,5-bisphosphate using the pleckstrin homology domain of phospholipase C delta1. *Biochem J*, **363**, 657-666.

Weiss, A. (1993) T cell antigen receptor signal transduction: a tale of tails and cytoplasmic protein-tyrosine kinases. *Cell*, **73**, 209-212.

Whitaker, M. (2006) Calcium at fertilization and in early development. *Physiol Rev*, **86**, 25-88.

Whitaker, M. and Aitchison, M. (1985) Calcium-dependent polyphosphoinositide hydrolysis is associated with exocytosis in vitro. *FEBS Lett*, **182**, 119-124.

Yonezawa, N., Nishida, E., Iida, K., Kumagai, H., Yahara, I. and Sakai, H. (1991) Inhibition of actin polymerization by a synthetic dodecapeptide patterned on the sequence around the actin-binding site of cofilin. *J Biol Chem*, **266**, 10485-10489.

Yonezawa, N., Nishida, E., Iida, K., Yahara, I. and Sakai, H. (1990) Inhibition of the interactions of cofilin, destrin, and deoxyribonuclease I with actin by phosphoinositides. *J Biol Chem*, **265**, 8382-8386.

Zheng, B., Han, M., Bernier, M. and Wen, J.K. (2009) Nuclear actin and actin-binding proteins in the regulation of transcription and gene expression. *Febs J*, **276**, 2669-2685.

Legatoria - Tipografia - Stampa Digitale RICCO - Via Mezzocannone, 105 Napoli
Tel./Fax 081.551.66.55 - e-mail: tipografiaricco@libero.it
Premiata con Medaglia d'oro "Premio Minerva 1988"